MAX-PLANCK-INSTITUT
FÜR METEOROLOGIE

Response of the summer North Atlantic Oscillation to global warming

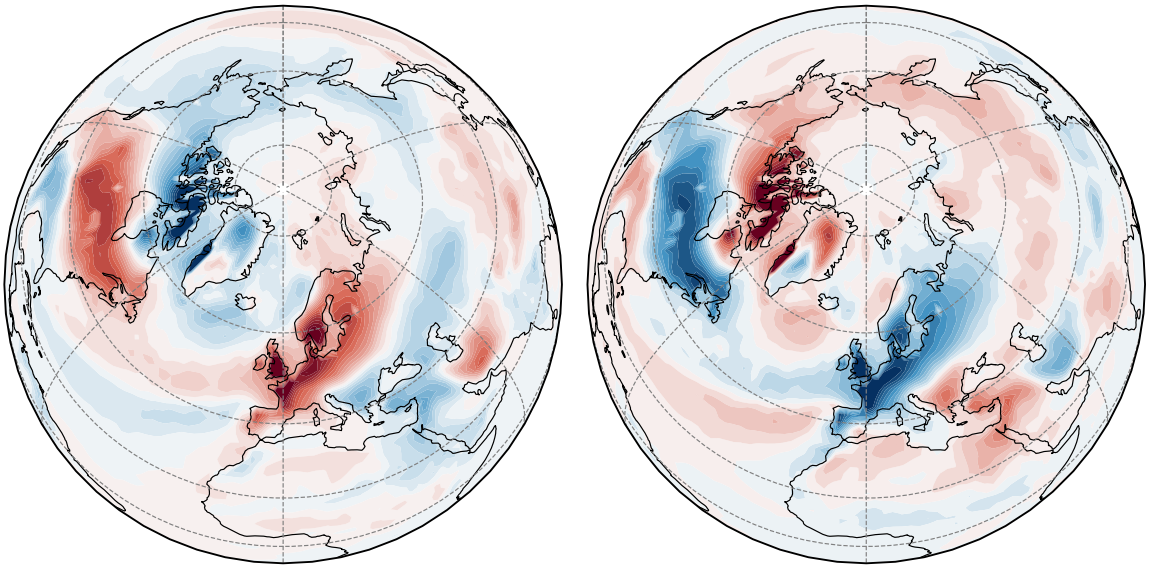

Quan Liu

Hamburg 2026

Berichte zur Erdsystemforschung
Reports on Earth System Science

295
2026

Hinweis

Die Berichte zur Erdsystemforschung werden vom Max-Planck-Institut für Meteorologie in Hamburg in unregelmäßiger Abfolge herausgegeben.

Sie enthalten wissenschaftliche und technische Beiträge, inklusive Dissertationen.

Die Beiträge geben nicht notwendigerweise die Auffassung des Instituts wieder.

Die "Berichte zur Erdsystemforschung" führen die vorherigen Reihen "Reports" und "Examensarbeiten" weiter.

Anschrift / Address

Max-Planck-Institut für Meteorologie
Bundesstrasse 53
20146 Hamburg
Deutschland

Tel./Phone: +49 (0)40 4 11 73 - 0
Fax: +49 (0)40 4 11 73 - 298

name.surname@mpimet.mpg.de
www.mpimet.mpg.de

Notice

The Reports on Earth System Science are published by the Max Planck Institute for Meteorology in Hamburg. They appear in irregular intervals.

They contain scientific and technical contributions, including PhD theses.

The Reports do not necessarily reflect the opinion of the Institute.

The "Reports on Earth System Science" continue the former "Reports" and "Examensarbeiten" of the Max Planck Institute.

Layout

Bettina Diallo and Norbert P. Noreiks
Communication

Copyright

Response of the summer North Atlantic Oscillation to global warming

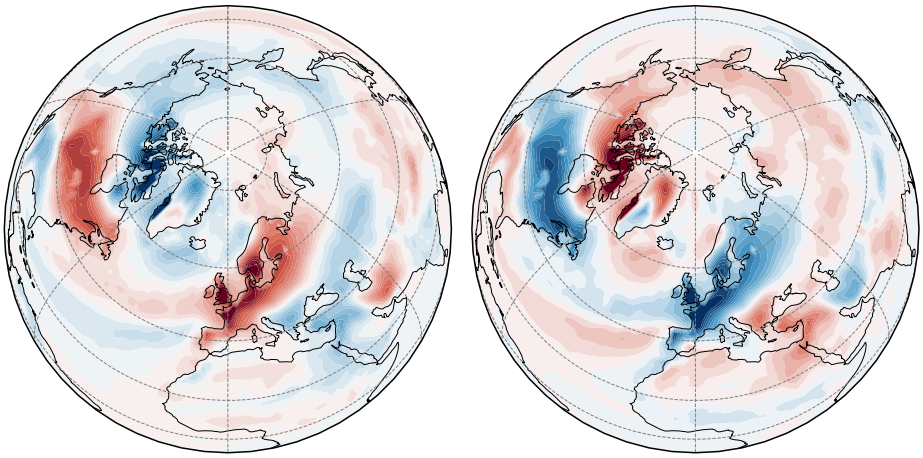

Quan Liu

Hamburg 2026

Quan Liu
aus Gansu, China

Max-Planck-Institut für Meteorologie
The International Max Planck Research School on Earth System Modelling
(IMPRS-ESM)
Bundesstrasse 53
20146 Hamburg

Tag der Disputation: 28. Oktober 2025
Folgende Gutachter empfehlen die Annahme der Dissertation:
Prof. Dr. Jochem Marotzke
Dr. Johann Jungclaus

Vorsitzender des Promotionsausschusses:
Prof. Dr. Hermann Held

Dekan der MIN-Fakultät:
Prof. Dr.-Ing. Norbert Ritter

Titelgrafik:
Difference between the average temperature of summertime North Atlantic Oscillation extremes (left for positive, right for negative) and the average summer temperature of the whole decade (2090-2099) in the Max Planck Institute Earth System Model (MPI-ESM) climate change simulations following the Representative Concentration Pathway 8.5 (RCP8.5), which describes a future with continuing, high emissions of greenhouse gases, resulting in significant climate change by 2100.

Berichte zur Erdsystemforschung / Max-Planck-Institut für Meteorologie 295
Reports on Earth System Science / Max Planck Institute for Meteorology 2026

ISSN 1614-1199 - doi: 10.17617/2.3688001

Quan Liu

Response of the summer North Atlantic Oscillation to global warming

ABSTRACT

The North Atlantic Oscillation (NAO) is the leading mode of large-scale atmospheric circulation variability that steers weather patterns across Europe. In summer, its positive phase is associated with above-average temperatures in northwest Europe and below-average temperatures in the Mediterranean, whereas the negative phase is associated with the opposite pattern. *Background*

Recent increases in the occurrence of contrasting weather events across different parts of Europe have prompted hypotheses that global warming may be altering the variability of the NAO. While climate change simulations generally project a positive trend in the NAO index through the 21st century, this trend reflects changes in the mean state rather than in the variability. Furthermore, most studies examining the NAO response to global warming have focused on winter. To date, no study has examined how variability — particularly extreme states of the NAO — responds to global warming in summer. *Question/issue*

To close this gap, I use transient climate change simulations with a large ensemble size. The ensemble spread of these simulations at each time step measures the internal variability, and its temporal evolutions reveal how this internal variability changes in response to transient climate change. In the first study, I use monthly outputs, both because data at this timescale are available from multiple Earth system models to assess the robustness and because the NAO is a low frequency phenomenon. This low-frequency characteristic does not exclude fast synoptic processes for playing a role. In my second study, I leverage daily output from a single model to investigate the role of Rossby wave breaking events and eddy fluxes in driving the summer NAO variability. I also compare the findings from climate simulations with historical reanalysis data. *Approach*

I find a robust enhancement of summer NAO variability, superimposed on the previously identified long-term trend, in response to global warming. This enhancement is evident as a widening of the summer NAO index distribution, and an increase in the occurrence of both positive and negative phases of summer NAO extremes. I also show that the impact of these summer NAO extreme events on the surface temperature is amplified over northwestern Europe. The signal of increasing occurrence and intensifying impacts of the summer NAO extremes is also emerging in the reanalysis data. *Findings of the first study*

I show that the increased occurrence of summer NAO extremes under global warming is driven by more frequent wave breaking events, which are associated with enhanced variability of upper-level eddy momentum convergence. This momentum forcing is primarily *Findings of the second study*

contributed by transient eddies that are generated from lower-level baroclinicity. The baroclinicity is sustained by heat flux carried by quasi-stationary eddies. As global warming amplifies the land-ocean temperature contrast, the variability of these heat flux increases. This increase ultimately contributes to changes in the occurrence of summer NAO extremes.

Conclusion/implication

In my thesis, I established that the mean state of the summer NAO becomes more positive, meanwhile, both positive and negative phases of the summer NAO extremes become more likely due to an amplified variability under global warming. I attributed the increase in the occurrence of summer NAO extremes to changes in the statistics of their eddy forcing. My finding highlights the effects of climate change on the variability of the atmospheric flow, and thus has important implications for extreme weather attribution and adaptation.

ZUSAMMENFASSUNG

Hintergrundinformation

Die Nordatlantische Oszillation (NAO) ist der dominierende Modus der großräumigen atmosphärischen Zirkulation, der die Wettermuster in Europa steuert. Im Sommer ist eine positive NAO-Phase mit überdurchschnittlichen Temperaturen in Nordwesteuropa und unterdurchschnittlichen Temperaturen im Mittelmeerraum verbunden, während die negative Phase das gegenteilige Muster erzeugt.

Frage/Problem

Die jüngste Zunahme gegensätzliche Wetterereignisse in verschiedenen Teilen Europas hat zu der Hypothese geführt, dass die globale Erwärmung die Variabilität der NAO verändern könnte. Während Simulationen des Klimawandels im Allgemeinen einen positiven Trend des NAO-Indexes für das 21. Jahrhundert voraussagen, spiegelt dieser Trend eher Veränderungen im Mittelwert als in der Variabilität wider. Darüber hinaus konzentrierten sich die meisten Studien, die sich mit der Reaktion der NAO auf die globale Erwärmung befassten, auf den Winter. Bislang wurde in keiner Studie untersucht, wie die Variabilität - insbesondere die extremen Zustände der NAO - im Sommer auf die globale Erwärmung reagiert.

Ansatz

Um diese Lücke zu schließen, verwende ich Simulationen des Klimawandels mit großer Ensemblegröße. Die Ensemblestreuung dieser Simulationen bei jedem Zeitschritt ist ein Maß für die interne Variabilität, und ihre zeitliche Entwicklung zeigt, wie sich diese interne Variabilität als Reaktion auf vorübergehende Klimaänderungen verändert. In der ersten Studie verwende ich monatliche Daten von mehreren Erdsystemmodellen, um die Robustheit der Ergebnisse zu bewerten und, weil die NAO ein niederfrequentes Phänomen ist. Die Tatsache, dass es sich bei der NAO eher um ein niederfrequentes Phänomen handelt, schließt nicht aus, dass auch schnelle synoptische Prozesse eine Rolle spielen. In der zweiten Studie verwende

ich Tagesdaten aus einem einzigen Modell, um die Rolle von Rossby-Wellenbrechungsereignissen und die Rolle von Wärme- und Impulsflüssen durch Störungen bei der Steuerung der sommerlichen NAO-Variabilität zu untersuchen. Die in den Simulationen des Klimawandels ermittelten Veränderungen werden werden mit denen eines Reanalysedatensatz für historische Zeiträume verglichen.

Ergebnisse der ersten Studie

Ich finde eine robuste Verstärkung der sommerlichen NAO-Variabilität als Reaktion auf die globale Erwärmung, die den zuvor ermittelten langfristigen Trend überlagert. Diese Verstärkung zeigt sich in einer Verbreiterung der Verteilung des Sommer-NAO-Indexes und in einer Zunahme der positiven und negativen Phasen der Sommer-NAO-Extreme. Ich zeige auch, dass die Auswirkungen dieser extremen Ereignisse auf die Oberflächentemperatur über Nordwesteuropa verstärkt werden. Das Signal für das zunehmende Auftreten und die sich verstärkenden Auswirkungen sommerlicher NAO-Extreme ist auch in den Reanalysedaten erkennbar.

Ergebnisse der zweiten Studie

In meiner Dissertation habe ich festgestellt, dass der mittlere Zustand der sommerlichen NAO positiver wird, während gleichzeitig sowohl positive als auch negative Phasen der sommerlichen NAO-Extreme aufgrund einer verstärkten Variabilität unter dem Einfluss der globalen Erwärmung wahrscheinlicher werden. Ich habe die Zunahme des Auftretens sommerlicher NAO-Extreme auf Veränderungen in ihrem Antrieb durch atmosphärische Störungen zurückgeführt. Meine Ergebnisse unterstreichen die Auswirkungen des Klimawandels auf die Variabilität der atmosphärischen Strömung und haben daher wichtige Implikationen für die Zuordnung extremer Wetterereignisse und die Anpassung daran.

Schlussfolgerung/Implikation

In meiner Dissertation habe ich festgestellt, dass der mittlere Zustand der sommerlichen NAO positiver wird, während gleichzeitig sowohl positive als auch negative Phasen der sommerlichen NAO-Extreme aufgrund einer verstärkten Variabilität unter dem Einfluss der globalen Erwärmung wahrscheinlicher werden. Ich habe die Zunahme des Auftretens sommerlicher NAO-Extreme auf Veränderungen in ihrem Antrieb durch atmosphärische Störungen zurückgeführt. Meine Ergebnisse unterstreichen die Auswirkungen des Klimawandels auf die Variabilität der atmosphärischen Strömung und haben daher wichtige Implikationen für die Zuordnung extremer Wetterereignisse und die Anpassung daran.

PUBLICATIONS

APPENDIX A

Liu, Q., Bader, J., Jungclaus, J.H., Matei, D. More extreme summertime North Atlantic Oscillation under climate change. Commun Earth Environ 6, 474 (2025). https://doi.org/10.1038/s43247-025-02422-x

APPENDIX B

Liu, Q., Bader, J., Jungclaus, J.H., Matei, D. Changes in atmospheric eddies contribute to more summertime North Atlantic Oscillation extremes. Manuscript in preparation. 2025.

ACKNOWLEDGMENTS

Thanks: firstly to Dr. *Johann Jungclaus*, Dr. *Daniela Matei*, and Dr. *Jürgen Bader*, for their enormous contributions to this project, and for stepping in at the right moments whenever I was heading in the wrong direction; to Prof. Dr. *Jochem Marotzke* for his insightful perspectives in my panel meetings and his feedback in group meetings; to Dr. *Arjun Kumar*, *Giada Cerato*, and *Mikael Karvinen*, who have read through this thesis and their detailed feedback has greatly improved the writing; to *Arim Yoon*, who read almost all of my academic writing and attended all of my test talks for presentations; to Dr. *Moritz Epke* and Dr. *Lara Wallberg* for their generous support with coding and writing while we shared an office; to Dr. *Tianyan Li*, Dr. *Aruhasi*, and many other colleagues in the writing club who have provided important feedback to the manuscript of my first study; to Dr. *Antje Weitz*, Dr. *Florian Mundt*, *Cornelia Kampmann*, and *Michaela Born* in IMPRS-ESM office, who have provided the best administrative support; to the German Climate Computing Center (DKRZ) for providing the necessary computational resources; to Clara Bayley, Lucas Casaroli, and Maria-Jesus Rapanague for their friendship during my PhD; and to my family, for everything.

CONTENTS

LIST OF TABLES

Part I

UNIFIED ESSAY

风起于青萍之末
Winds rise from the tips of duckweeds.
— 战国·宋玉《风赋》
Song Yu, *Fu on Wind*, 298–222 BC

1 INTRODUCTION

Traveling synoptic low- and high-pressure systems, or transient eddies, govern surface weather conditions in mid-latitudes. They are associated with inherent instability of atmospheric flow, and feed circulation patterns of large-scale in which they are embedded [38, 89]. These large-scale circulation patterns are spatially well defined and limited in numbers. They vary in low frequencies [1, 3], and are usually associated with persistent weather conditions [34, 73]. Recently, certain types of severe weather have been occurring more frequently [37, 69, 91], raising concerns that global warming may be altering the variability of these large-scale circulation patterns. However, evidence for such changes remains elusive.

Over the North Atlantic, the leading mode of the large-scale circulation patterns is the North Atlantic Oscillation (NAO). The NAO is a dipole-like pattern in the atmospheric pressure anomaly field that swings over a wide range of time scales. This pattern and the amplitude of its variability are well simulated in atmospheric general circulation models forced with climatological annual cycles of solar insolation and sea surface temperature [71]. This provides strong evidence that much of the NAO variability arises from processes internal to the atmosphere [36].

Meanwhile, the anthropogenic forced changes in North Atlantic circulation projects strongly onto the NAO pattern [21, 63]. This NAO-like response would manifest as a long-term trend in the NAO index, which has been well established by previous studies (e.g, [57, 64]). However, this long-term trend represents changes in the mean state of the NAO, changes in the variability of the NAO in a transient warming climate, on the other hand, remains a knowledge gap. Quantifying such changes is essential for effective risk management of extreme weather in Europe [32]. This thesis aims to fill this gap, with a focus on the NAO in summer.

1.1 NAO VARIABILITY AND EXTREME WEATHER

The NAO variability steers the surface weather over much of Europe and North America. In fact, the NAO was firstly identified from temperature field rather than atmospheric pressure field. During his

An earlier description of the NAO

stay in Greenland between 1770-78, the missionary *Hans Egede Saabye* made the following observation in his diary [70]:

> *"In Greenland all winters are severe, yet they are not alike. The Danes have noticed that when the winter in Denmark was severe, as we perceive it, the winter in Greenland in its manner was mild, and conversely. " - Hans Egede Saabye (1770-78)*

Such a dipole pattern in the temperature field has been linked to the NAO over one century later by *Walker* and *Bliss* (1932 [92]). In their words, the NAO is *"the tendency for pressure to be low near Iceland in winter when it is high near the Azores and south-west Europe; ... this distribution of course is associated with high temperature in north-west Europe and low temperature off the Labrador coast"*.

The difference of the anomalous pressure between the Icelandic Low and the Azores High adopted by *Walker* and *Bliss* remains a standard method to define the NAO index [36]. Meanwhile, pattern decomposition methods, such as the Empirical Orthogonal Function (EOF) analysis, are also widely adopted [2, 93].

Although firstly identified in winter, the NAO is actually a pattern persistent throughout all seasons. I focus on the NAO in summer, as it plays a key role in driving heat waves, droughts, and floods during this season [22, 23, 46, 84]. The pattern of the summer NAO is shown in Figure. 1a. As its winter counterpart, the summer NAO index that measures the strength of this pattern exhibits strong variability over a wide range of time scales (Figure. 1b).

NAO in summer

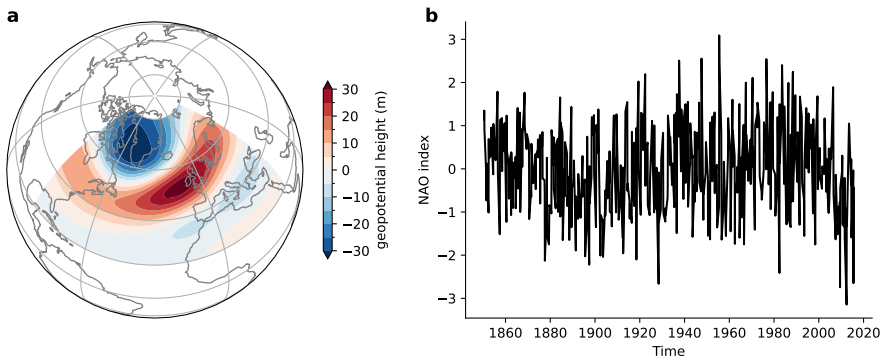

Figure 1: **The summertime North Atlantic Oscillation. a**, Spatial pattern of the summer NAO at mid troposphere (500 hPa). **b**, The corresponding temporal index of the summer NAO. The pattern and the index are decomposed with EOF analysis. The index is normalized with its temporal standard deviation. Data comes from NOAA-CIRES-DOE Twentieth Century Reanalysis (20CR) [11].

summer NAO and extreme weather

Extreme states of the summer NAO, arising from this strong variability, trigger the occurrence of certain severe weather events. For instance, the Russian heatwave and the severe floods in Pakistan in summer 2010 are associated with a persistent negative phase of the

summer NAO [22, 74]. The European hot summer in 2018 is associated with a series of consecutive positive NAO events [46, 84]. From a statistical view point, much of the observed extreme precipitation and temperature over Europe in individual seasons is associated with the NAO [73].

The tight link between the NAO variability and the surface weather, and particularly the important role of the summer NAO in causing severe weather, indicates that any changes in the NAO variability due to global warming would have profound impacts on society and ecosystems. In the remainder of this section, I firstly review the correspondence between the phases of the NAO and the state of the atmospheric mean flow (section 1.2). Then I show how the associated mean flow changes in response to global warming (section 1.3). To provide a dynamical framework for explaining changes in the NAO variability, I review the "eddy-mean-flow" interactions (section 1.4). This is followed by an introduction to the main tool used to investigate changes in the NAO variability—the large ensemble simulations (section 1.5). Finally, I outline the research gap and pose the research questions to be answered in this thesis (section 1.6).

a preview

1.2 NAO VARIABILITY AND LARGE-SCALE MEAN FLOW

The atmospheric flow over the North Atlantic exhibits multiple equilibrium states, known as flow regimes [8]. They arise due to multiple equilibria of the nonlinear equations that govern the atmospheric dynamics [8, 87]. For instance, a quasi-geostrophic β-plane model of barotropic flow over topography exhibits two stable flow regimes: one is a 'high-index' flow with a weak wave component and a relatively stronger zonal component; the other is a 'low-index' flow with a strong wave component and relatively weaker zonal component. Similarly, the observed atmosphere over North Atlantic also exhibits two preferred flow regimes, a zonal flow regime and a blocked flow regime [99]. Transitions between the two flow regimes are associated with the NAO variability [98].

flow regimes

The positive phase of the NAO corresponds to the zonal flow regime, while the negative phase of the NAO corresponds to the blocked flow regime [98]. Regime shifts between these flow regimes are associated with the location of the westerly jet stream. There are two jet streams over the North Atlantic, namely the subpolar jet and the subtropical jet [61]. The subpolar jet is essentially eddy-driven, and the subtropical jet is related to the upper branch of the Hadley Cell [61]. During the zonal flow regime, the subpolar jet diverts northward and separates from the subtropical jet (Figure. 2a). Whereas during the blocked flow regime, the subpolar jet shifts southward and merges with the subtropical jet, which is accompanied with a strengthened Greenland blocking [65] (Figure. 2b).

jet stream

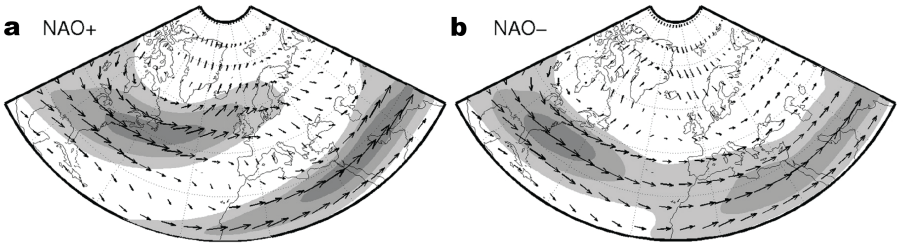

Figure 2: **The NAO is associated with zonal and blocked flow regimes. a** Composite mean of the 300 hPa wind field during positive phase of the winter (DJF) NAO. Isotachs are shaded at 20, 30, and 40 $m\ s^{-1}$. Arrows show the wind vector. **b** Same as **a**, but for negative phase of the NAO. Plot is adapted from ref [98]. Data are from 40-yr ECMWF Reanalysis (ERA-40) [88]

Rossby wave breaking

The physical processes that induce the meridional displacement of the jet stream include Rossby wave breaking. The Rossby waves are large-scale wavelike disturbances that arise under the effects of potential vorticity (PV) gradient. In the barotropic flow, the potential vorticity is the absolute voricity that increases monotonically poleward [89]. Because the PV of air parcels is conserved, meridional displacements of the air parcels would therefore change the PV gradient and lead to Rossby wave breaking. Both a poleward displacement (Figure. 3a) or a equator-ward displacement (Figure. 3b) may reduce the PV gradient [94]. Depending on the sign of the momentum flux ($u'v'$) associated with the waves, the Rossby wave breaking can be classified into anticyclonic wave breaking ($u'v' > 0$, Figure. 3a)) and cyclonic wave breaking ($u'v' < 0$, Figure. 3b) [67]. The anticyclonic wave breaking, which predominantly occurs at the equator flank of the jet stream, acts to push the jet stream poleward (Figure. 3a). The cyclonic wave breaking, which predominantly occurs at the poleward flank of the jet stream, acts to push the jet stream equatorward (Figure. 3b). Therefore, the anticyclonic wave breaking is regarded as a precursor of the positive NAO, and the cyclonic wave breaking is regarded as a precursor of the negative NAO.

To conclude, the variability of the NAO is associated with transitions between flow regimes over the North Atlantic. Such transitions are connected to the meridional displacement of the subpolar jet, which is aided by Rossby wave breaking events. In this thesis, I will show that changes in the variability of the NAO under global warming are consistent with changes in the large-scale atmospheric mean flow.

1.3 CHANGES IN THE NORTH ATLANTIC MEAN FLOW

Changes in flow regimes

The North Atlantic mean flow changes in both the zonal and blocked regimes. On the one hand, the zonal component of the upper-level

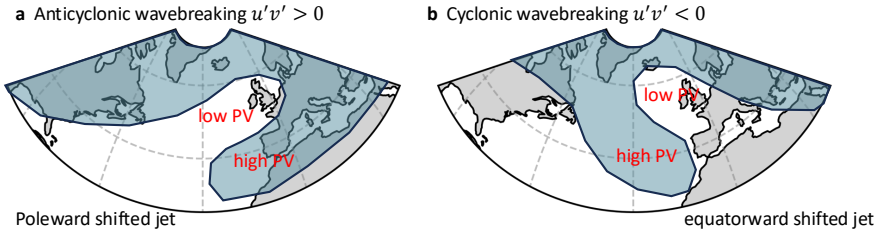

Figure 3: **Wave breaking events drive meridional displacement of the jet stream. a** Schematic plot of anticyclonic wave breaking on a isentropic surface. Blue color shows the stratospheric air with high potential vorticity (PV). White color shows the tropospheric air with low PV. $u'v'$ represents eddy momentum flux. **b**, Same as **a**, but for the cyclonic wave breaking.

jet stream winds accelerates with simulated global warming, with its mean location shifting poleward [76] (lines, Figure. 4a-c). A similar acceleration is also emerging in the reanalysis during the historical period [96]. On the other hand, the Greenland blocking has enhanced in the past 40 years [65], and the waviness of the jet has increased in summer at lower altitudes [13]. The concurrent changes in both the zonal and the blocked flow regimes in midlatitudes manifest themselves as changes in the variability of the zonal jet stream winds (lines, Figure. 4d-f), a pattern that overlap with the NAO (Figure. 4g-h).

Theories seeking to explain changes in the atmospheric mean flows under global warming include thermal wind balance. Using pressure (p) as vertical coordinates, the thermal wind balance is given by:

$$-\frac{\partial \overline{u}}{\partial p} = -\frac{R}{fp}\frac{\partial \overline{T}}{\partial y} \tag{1}$$

where R is the specific gas constant for dry air, f is Coriolis parameter, u is zonal wind, and T is air temperature. Any processes that change the temperature field must be compensated for by adjusting the wind field to maintain the thermal wind balance [38]. For instance, at the upper level, the meridional temperature is strengthening due to the upper troposphere warming over the tropics and the stratosphere cooling over the North pole, and the upper-level zonal jet stream winds accelerate and shift northward in response (contours, Figure. 4a-c) [45]. Studies also argued that the zonal mean flow at the lower-level is weakening in response to the weakening meridional temperature gradient due to Arctic Amplification [13]. However, whether this change is an externally forced signal or the internal variability remains inconclusive [61].

effects of temperature gradient

Apart from the temperature gradient, the effect of changes in water vapor on atmospheric response can also be interpreted through the thermal wind balance [76, 77]. This effect includes changes in both the density (adding water vapor to an air parcel at same temperature

effects of water vapor

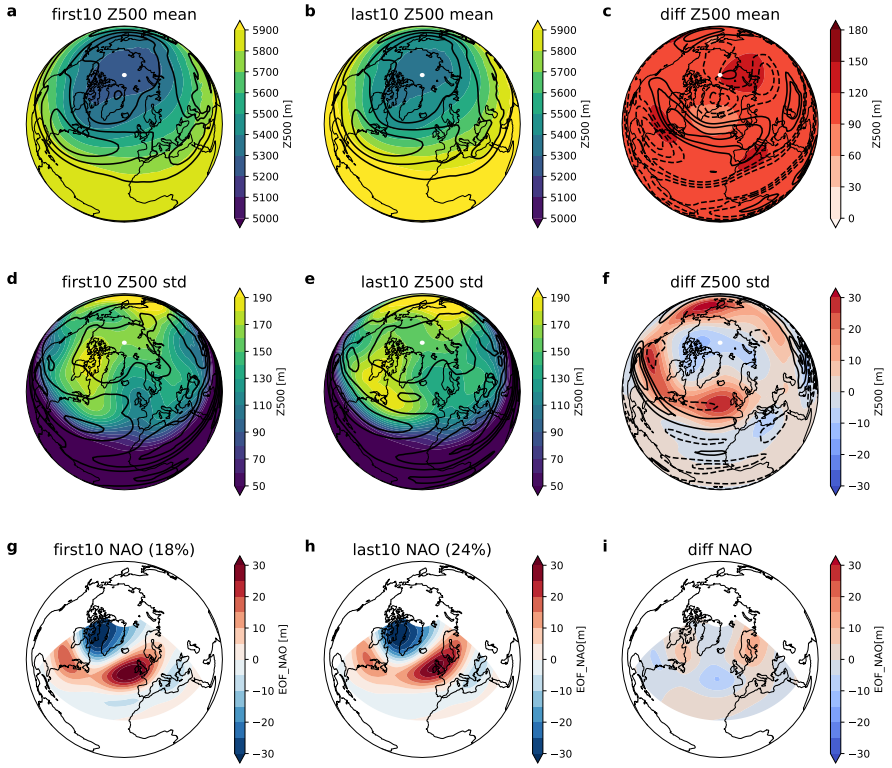

Figure 4: **North Atlantic atmospheric circulation changes in response to global warming. a**, Shading shows the mean of the 500 hPa geopotential height in meters for 1850-1859 in the Max Planck Institute for meteorology Grand Ensemble (MPI_GE) [51]. Contours show the mean of the zonal wind (u) at 500 hPa for 1850-1859 in MPI_GE. Contours are drawn at intervals of 5 m/s, ranging from 0 - 20 m/s. **b**, Same as (**a**), but for years 2090-2099. **c**, The difference between **b** and **a**. Contours are drawn at intervals of 0.5 m/s, ranging from -1.5 - 1.5 m/s, eliminating 0 m/s contour. **d**, Shading shows the standard deviation of the 500 hPa geopotential height for years 1850-1859 in MPI_GE. Contours show the standard deviation of the zonal wind (u) at 500 hPa pressure level for 1850-1859 in MPI_GE. Contours are drawn at intervals of 2 m/s, ranging from 0 - 10 m/s. **e**, Same as (**d**), but for 2090-2099. **f**, The difference between **e** and **d**. The same contour levels are shown as **c**. **g**, The spatial pattern of the NAO for 1850-1859 in MPI_GE. The percentage in the brackets shows the explained variance. **h**, Same as **g**, but for 2090-2099. **i**, The difference between **h** and **g**.

and pressure makes it lighter) and temperature (latent heat release after condensation) of the air. The decrease in the air density due to more water vapor is greater in the tropics than in the polar regions. Meanwhile, latent heat release is also stronger for rising air parcels in tropics than in polar regions. Together, they change the meridional density and temperature gradient, and affect the thermal wind and jet stream.

In summary, the upper-level zonal jet stream winds accelerate in response to the the enhancement in the meridional temperature gradient at upper troposphere to maintain the thermal wind balance. As has been projected by most climate models, this acceleration would correspond to a positive trend in the NAO index [52]. However, the thermal wind balance is built on the equilibrium state [89]. Such an interpretation doesn't rule out any changes that may occur in the transient states. Nevertheless, potential changes in the NAO variability require a different dynamical framework to be explained. In this thesis, I will show that "eddy–mean-flow" interactions provide one such framework.

1.4 NAO VARIABILITY AND EDDY-MEAN-FLOW INTERACTIONS

Eddies in the atmosphere are wave-like departures from the mean flow. In the midlatitudes, the eddies are large and the fluxes of momentum and heat they carry are a major part of the atmospheric circulation. In this section, I will outline how the eddies, although of a smaller scale than the NAO pattern, generate the variability of the NAO.

1.4.1 *Transient eddies and quasi-stationary eddies*

Two types of eddies

Generally, the eddies are characterized by (i) transient eddies that are familiar with fast-traveling low- and high pressure systems, and (ii) quasi-stationary eddies, which are pronounced departures from symmetry in seasonal mean flow. The transient eddies arise from the lower-level baroclinic instability, normally with temporal periods of several days and with zonal wave numbers typically larger than 6 [67, 89]. The quasi-stationary eddies are an atmospheric response to the asymmetric thermal and orographic forcing, with normally smaller wave numbers [13, 38]. The North Atlantic sector experiences both a maximum of the transient eddy kinetic energy (Figure. 5a) and a trough of quasi-stationary eddies with wavenumber 3 (Figure. 5b). In summer, the fluxes of momentum and heat carried by the transient eddies and the quasi-stationary eddies are of comparable magnitude in Northern Hemisphere [38], but they play different roles in forcing the mean flow.

1.4.2 *Eddy momentum forcing of the upper-level subpolar jet*

The momentum flux carried by transient eddies essentially maintains the upper-level zonal mean flow in summer. This eddy momentum forcing can be diagnosed from the momentum equation of quasi-geostrophic flow. By neglecting dissipation and vertical advection, and by approximating the Coriolis parameter by a constant value f_0,

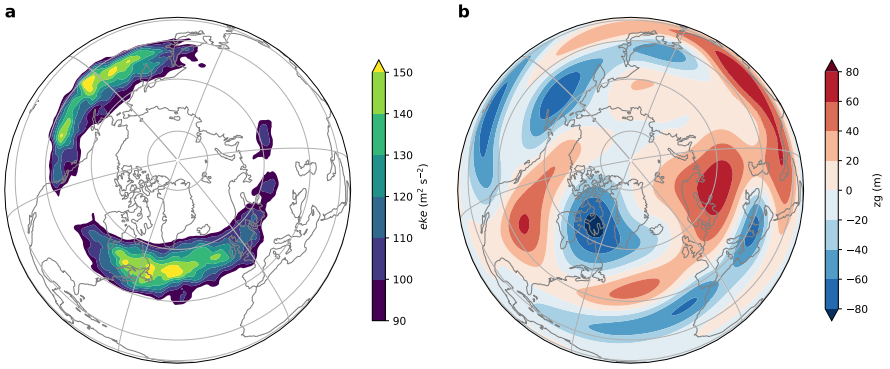

Figure 5: **Transient eddies and quasi-stationary eddies over the Northern Hemisphere in summer. a,** The climatology of the eddy kinetic energy of the transient eddies at 250 hPa during 1979-2024. The transient eddies are extracted based on band-pass filter of 2-12 days according to ref [67]. **b**, Wavenumber 3 quasi-stationary eddies in high latitudes at 250 hPa during the same period. The quasi-stationary eddies are computed from the zonal anomaly of the monthly data of 250 hPa geopoential height according to ref [47]. Data comes from ECMWF Reanalysis v5 (ERA5) [33].

the zonal mean of the zonal momentum for a non divergent flow can be written as [89]:

$$\frac{\partial \overline{u}}{\partial t} = f_0 \overline{v} - \frac{\partial}{\partial y} \overline{u'v'} + \overline{F} \tag{2}$$

where (u, v) is the horizontal velocity, $\overline{F}$ represents frictional term. Hats and primes denote respectively the zonal mean and eddy components of the flow. The $\overline{u'v'}$ is called eddy momentum flux.

eddy momentum forcing

Therefore, the eddies exert forcing to the zonal mean flow via convergence of their momentum flux. This eddy momentum forcing by transient eddies is comparable to that by quasi-stationary eddies in winter, but becomes much stronger in summer [38]. It is what essentially maintains the upper-level subpolar jet [38, 68]. Given the correspondence between the location of the subpolar jet and the phase of the NAO (section 1.2), the anomalous convergence of the eddy momentum flux by transient eddies has been proposed as the key mechanism driving the NAO variability [90].

1.4.3 *Eddy thermal forcing of the lower-level baroclinicity*

Apart from the momentum forcing, eddies also modulate the NAO variability by changing the low-level baroclinicity. The baroclinicity describes a form of unstable states where the fluid, although statically stable, is able to release available energy when parcels move along a sloping path due to perturbations [89]. It can be approximated with the Eady growth rate [35], which is defined as:

$$\sigma_E \approx 0.31 \cdot \frac{f}{N} \left| \frac{\partial \mathbf{v}}{\partial z} \right| \tag{3}$$

where σ_E is the Eady growth rate, f is the Coriolis parameter, N is the Brunt–Väisälä frequency, defined as $N = \sqrt{\frac{g}{\theta}\frac{\partial \theta}{\partial z}}$, where g is gravitational acceleration and θ is the potential temperature, $\frac{\partial \mathbf{v}}{\partial z}$ is the vertical shear of the wind, z is the vertical height, $\mathbf{v}$ is the horizontal wind vector. From this definition, the baroclinicity is linked to the vertical shear of the horizontal wind, which is, in turn, connected to the horizontal temperature gradient via the thermal wind balance (The vertical shear in equation 1 is expressed in pressure coordinates but can be readily converted to height coordinates).

The variation of the meridional component of this temperature gradient under the quasi-geostrophic approximation is given by the meridional derivative of the zonal-mean thermodynamic equation [38, 58]:

$$\frac{\partial}{\partial t}\left(-\frac{\partial}{\partial y}\overline{T}\right) = \frac{\partial^2}{\partial y^2}\overline{v'T'} - \frac{\partial}{\partial y}\left(\Gamma\,\overline{\omega}\right) - \mathcal{R} \tag{4}$$

where T stands for air temperature, $\Gamma = -T\frac{\partial \ln \theta}{\partial p}$ is the static stability parameter; ω represents vertical velocity; $\mathcal{R}$ represents diabatic heating; the $\overline{v'T'}$ represents eddy heat flux. By transporting warm air poleward and cold air equatorward, eddies act to reduce the meridional temperature gradient.

eddy thermal forcing.

Therefore, by altering the meridional temperature gradient, eddies exert forcing to the lower-level baroclinicity. However, the sign of this thermal forcing depends on the distribution of the eddies' critical line. Based on a beta-plane multilayer quasigeostrophic channel model, one study has indicated that while high-frequency eddies act to reduce the baroclinicity, low-frequency eddies act to reinforce it [102]. This contrast arises because the high-frequency eddies experience their critical line at the center of the jet, where their thermal forcing weakens the baroclinicity. In contrast, low-frequency eddies encounter low-level critical line at the poleward of the jet, and their thermal forcing maintain the baroclinicity at the jet core [58, 102]. Hence, transient eddies and quasi-stationary eddies—given their distinct frequencies—may have contrast eddy thermal forcing on the NAO variability.

1.4.4 *Fluctuation of the eddy forcing and the variability of the NAO*

Taken all together, it seems reasonable to draw the following implications: eddies drive the NAO variability by changing the subpolar jet

at upper levels. The variations of the upper-level subpolar jet is primarily driven by transient eddies, which accelerate the zonal mean flow at the jet core via anomalous convergence of their momentum flux. These transient eddies arise from lower-level baroclinicity. The variations of the lower-level baroclinicity is primarily driven by quasi-stationary eddies, which modulate the meridional temperature gradient at the jet core via their heat flux.

positive eddy feedback

Furthermore, the relative low-frequency variability of the NAO can be generated by the high-frequency fluctuations of the eddies via positive eddy feedback. During positive phase of the NAO, the subpolar jet shifts poleward (section 1.2), and the transient eddy generation follows [102]. The eddy momentum forcing at the jet core by these transient eddies reinforces this northerly shifted jet — momentum aspect of the positive eddy feedback. Although the thermal forcing by these transient eddies weakens the lower-level baroclinicity in the process, that by quasi-stationary eddies maintains the baroclinicity at the center of the jet — thermal aspect of the positive eddy feedback. A similar positive eddy feedback can be inferred for the negative phase of the NAO. Therefore, much of the NAO variability is internally generated by the atmospheric circulation via “eddy-mean-flow" interactions.

1.5 QUANTIFYING THE INTERNAL VARIABILITY USING LARGE ENSEMBLE SIMULATIONS

why SMILEs?

The observed atmospheric flow is composed of internal variability superimposed on the anthropogenically forced signal. Examining changes in the internal variability of the NAO over time requires a method to extract this internal variability at each time step. A current approach in climate modeling is to run a large number of simulations (30–100) with the same coupled model and the same protocol for transient radiative forcing (historical and/or future scenario), but with different initial conditions [18, 19]. Because the temporal sequences of internal variability evolve differently in the various ensemble members, once the memory of the initial conditions has been lost, the forced component at each time step (at each location) can be estimated by averaging the members, provided that the ensemble size is sufficiently large. The internal component in each ensemble member is then determined as the residual from the ensemble mean. The spread across all ensemble members after removing the ensemble mean at each time step thus measures the internal variability, and changes in this spread over time show how the internal variability — beyond the mean state — change in response to global warming [54, 62].

SMILEs used in this study

Using a collection of such SMILEs from various Earth system models further ensures the robustness of the results by accounting for the potential bias in individual models. Moreover, since extremes occur

MODELING CENTER	MODEL NAME	SIZE	YEARS
Max Planck Institute for Meteorology	MPI_GE [51]	100	1850–2100
Canadian Centre for Climate Modelling and Analysis	CanESM2 [42]	50	1950–2100
National Center for Atmospheric Research	CESM1_CAM5 [41]	40	1920–2100
Commonwealth Scientific and Industrial Research Organisation	MK3.6 [39]	30	1850–2100
Geophysical Fluid Dynamics Laboratory	GFDL_CM3 [86]	20	1920–2100
Max Planck Institute for Meteorology	MPI_GE_onepct [51]	100	100 years
Max Planck Institute for Meteorology	MPI_GE_CMIP6 [59]	50	1850-2100

Table 1: **SMILEs used in this thesis**. In the first study, I use monthly outputs (the first six rows), in the second study, I use daily outputs (the last row).

very rarely by definition, a sufficiently large database from SMILEs enable a robust investigation of extreme cases of the summer NAO. In this thesis, I use monthly outputs of five SMILEs forced by historical and representative concentration pathway (RCP) 8.5 future scenarios and one SMILEs driven by a forcing where the concentration of the CO_2 increase by 1% per year from 1850 (MPI_GE_onepct) are used (Table 1). To interprate changes in the internal variability of the NAO from perspective of the "eddy-mean-flow" interactions, I use daily output of the CMIP6 version of the Max Planck Institute for meteorology Grand Ensemble forced by historical and Shared Socioeconomic Pathways 585 (SSP5-85) (MPI_GE_CMIP6, Table 1).

why not abrupt CO_2 experiments?

In principle, the internal variability of the NAO can also be estimated from pre-industrial control runs of climate simulations [55, 98], and changes under anthropogenic forcing can be inferred by comparing these with abrupt CO_2 runs (for example, $2\times CO_2$ experiments) [55]. However, experiments with abrupt CO_2 reveal the equilibrium climate response to a stabilized CO_2 concentration, which includes the adjustment of the ocean. Changes in the NAO variability in these abrupt CO_2 runs [55], therefore, would differ from that diagnosed in transient warming scenarios, as the latter capture only the changes in NAO variability that are internally generated within the atmosphere.

1.6 RESEARCH QUESTIONS

Gaps remain in our understanding of the NAO response to global warming:

1. Previous studies have primarily focused on changes in the mean state of the NAO, while changes in its variability — especially its extreme states — remain unexplored in a transient warming climate.

2. Thermal wind balance has been widely used to explain circulation changes under global warming, but it cannot account for changes in the NAO variability, for which a driving mechanism is yet to be understood.

3. Most previous studies have investigated NAO response to global warming in winter, little has been done for the NAO in summer.

To fill the above gaps, I seek to answer the following research questions:

QUESTION 1 *How does the variability, particularly the extreme states of the summer NAO, change in response to global warming?*

QUESTION 2 *What are the physical processes driving such changes?*

2

MORE EXTREME SUMMERTIME NORTH ATLANTIC OSCILLATION UNDER CLIMATE CHANGE

In this chapter, I answer the question of *How does the summer NAO change in response to global warming?* As has been demonstrated in the introduction, such changes can be partitioned into two distinct aspects: (i) changes in the mean state of the NAO, and (ii) changes in the variability of the NAO. The former is well documented; Hints of the latter are emerging.

Changes in the mean state of the NAO are reflected as a long-term trend in the NAO index and have been extensively studied, especially for the winter NAO. In winter, the climate models within the frame of the Coupled Model Intercomparison Project (CMIP) show a large spread in the trends of the NAO [14, 52], with most models agreeing on a positive trend til late 21 century (2080-2099) under high-emissions scenarios [52]. A robust long-term trend in the winter NAO index remains virtually undetectable in observations [64, 82]. In summer, climate models tend to simulate a positive trend of the NAO index during the historical period, which is also subject to a large model dispersion and deviation from observations [5, 27, 37]. Nevertheless, a positive NAO trend is expected as most climate models predict a northward shift of the jet stream under global warming [29, 50, 61, 76].

Studies about changes in the mean state of the NAO.

Although changes in the variability of the summer NAO have not yet been studied, hints of such changes are emerging in studies of the prediction and impact of the NAO. Recent advances in the NAO prediction shows that the predictive skill of NAO variability is beyond the deterministic timescales of weather forecasting [10, 24, 83]. This skillful prediction suggests that some fraction of the NAO variability is driven by predictive boundary conditions, such as the sea surface temperature that changes with global warming [61]. Indeed, a major source of the predictive skill for NAO variability in the late 20th century is external forcing [43]. A recent study shows that the impact of the atmospheric variability modes such as the NAO in winter expands with global warming [62]. Therefore, studies about the NAO suggest that its variability may also undergo changes with global warming.

Hints of changes in the NAO variability

In this study, we examine changes in the variability of the summer NAO using SMILEs and the 20CR data. Compared to the multi-model large ensembles from CMIP, SMILEs not only provides a large sample size to study extreme events of the summer NAO, but also differentiate the uncertainties from the internal variability and uncertainties

The data used in this study

from model bias. The 20CR dataset is used because, compared with other reanalysis datasets, it assimilates only sea-level pressure and sea surface temperature fields rather than utilizing all available observations in the troposphere, making it less sensitive to temporal inhomogeneities in the observations [7] and less constrained so that it includes some of the variability due to internal atmospheric processes [81].

2.1 INCREASED OCCURRENCE OF SUMMER NAO EXTREMES

Widening in the summer NAO index distribution

The Max Planck Institute for Meteorology Grand Ensemble (MPI_GE) simulations [51] project that both the mean state and the variability of the summer NAO change with global warming. The change in the mean state of the summer NAO is evident as the mean of the summer NAO index distribution shifts towards positive values (Figure. 6a). After removing this shift in the mean state, the distribution of the summer NAO index is wider under the simulated ~ 4K warmer climate than under the pre-industrial climate (Figure. 6b). This enhancement of the summer NAO variability is statistically significant based on bootstrapping (asterisk, Figure 6b), and therefore represents a secondary response of the summer NAO to global warming.

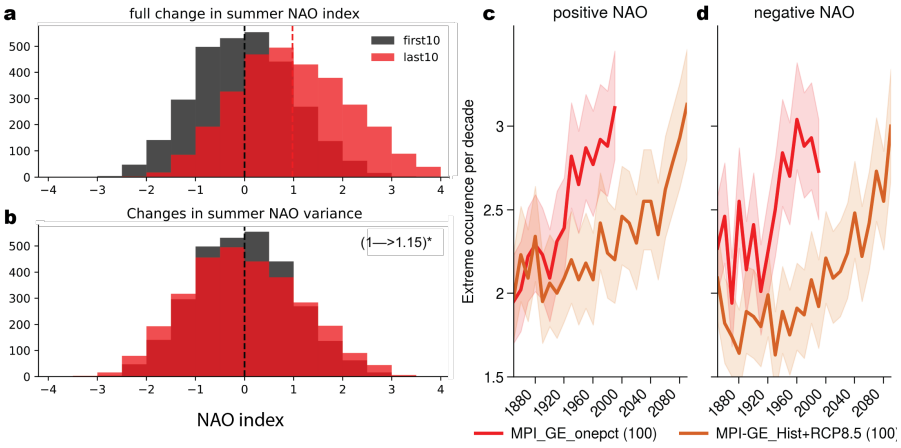

Figure 6: **Summer NAO response to global warming. a**, The summer NAO index distribution in Max Planck Institute for Meteorology Grand Ensemble (MPI_GE) during the first 10 years (1850-1859) and the last 10 years (2090-2099) of the simulations. **b**, Same as **a**, but with the mean of the index removed. Numbers in the brackets show changes in the standard deviation, with a asterisk indicating significance at 95 % confidence level based on bootstrapping. **c** The occurrence of the positive summer NAO extremes in MPI_GE forced by historical and the RCP8.5 scenarios (orange curves), as well as a forcing where the concentration of the CO_2 increases by 1% per year (red curves). The extreme events are identified when the NAO index exceeds or falls below 1.5 standard deviation.

As a consequence of the enhanced summer NAO variability, the occurrence of summer NAO extremes, for both the positive and negative phases, increases. In MPI_GE forced by both the historical and RCP8.5 further scenarios (red curve, Figure 6c, d), and an idealized scenario in which the carbon dioxide content of the atmosphere increases by 1% per year (brown curve, Figure 6c, d), this increase is statistically significant (shadings, Figure. 6c, d).

Increase in summer NAO extremes

2.2 AMPLIFIED IMPACT OF SUMMER NAO EXTREMES

Not only does the occurrence of summer NAO extremes increase, but their impacts on surface temperature also amplify. The positive summer NAO extremes have warming a effect over northwestern Europe and central North America, and a cooling effect over Greenland and the Mediterranean (Figure. 7a, b). Conversely, the negative summer NAO extremes have a cooling effect over northwestern Europe and central North America, and a warming effect over Mediterranean (Figure. 7d, e). Under global warming, the average impacts of such extremes on surface temperature significantly increases over Northwest Europe (Figure. 7c, f).

impact on surface temperature.

We have also examined changes in the impacts of the summer NAO extremes on precipitation. Although an amplified impact on the precipitation over Europe is also indicated by all the climate models used in this study, none of them show that such a change is statistically significant.

impact on the precipitation

2.3 CHANGES IN THE ASSOCIATED FLOW REGIMES

Since the variability of the summer NAO is tightly associated with transitions between the zonal and blocked flow regimes, changes in summer NAO variability may be accompanied by changes in both regimes. In this study, since we use monthly data to ensure the availability of simulations from multiple models, the zonal flow regime is identified by a more northerly shifted eddy-driven jet stream [97], and the blocked flow regime is represented by high values of the Greenland blocking index [30].

Figure. 8a depicts the density of the occurrence of summer NAO extremes against the location of the eddy driven jet stream and the index of the Greenland blocking in MPI_GE. Under the pre-industrial climate, the negative and positive phases of the summer NAO extremes lie correspondingly in the second and fourth quadrant of the coordinate plane defined by these two indexes (Blue shades and contour lines, Figure 8a), confirming the link between the summer NAO variability and the flow regimes. Under the simulated $\sim$ 4K warmer climate, the zonal flow shifts northward (vertical dashed lines, Figure 8a), and the Greenland blocking enhances (horizontal dashed lines,

changes in flow regimes

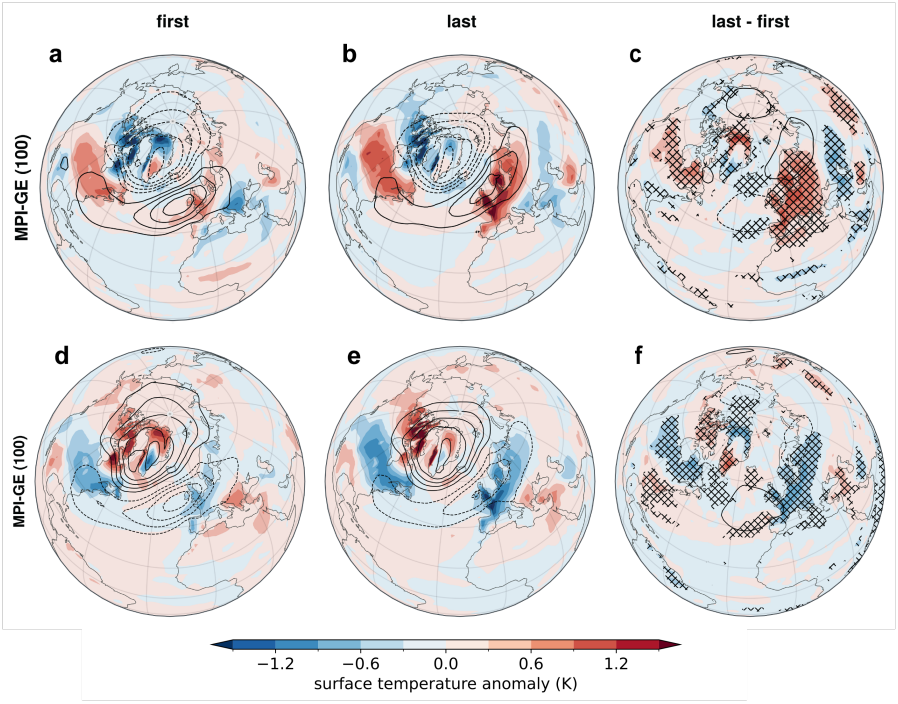

Figure 7: **Amplified impact of the summer NAO extremes on surface temperature.** **a**, Composite mean of the surface temperature (colors) and sea level pressure (contours) during positive summer NAO extremes in the first 10 years of simulations (1850-1859). Contours are drawn at intervals of 1 hPa, ranging from −5 to 5 hPa, with 0 contour omitted. **b**, Same as **a**, but for the last 10 years of simulations (2090-2099). **c** The difference between **b** and **a**. The crossed patches represents areas where the difference is significant at the 95 % confidence level. **d-f**, Same as **a-c**, but for the negative summer NAO extremes.

Figure 8a). Meanwhile, the occurrence of the summer NAO extremes increases, for both the positive phase (solid lines, Figure 8a) and the negative phase (shades, Figure 8a). We further show that increasing negative summer NAO extremes are linked to increasing number of extreme episodes of Greenland blocking (crosses, Figure 8b), and increasing positive summer NAO extremes are linked with increasing extreme episodes of both northward diverting eddy-driven jet and the enhancing Greenland blocking (circles, Figure 8b).

2.4 EMERGENCE OF ENHANCING SUMMER NAO VARIABILITY IN HISTORICAL PERIODS

summer NAO variability enhances during historical periods

It is possible, albeit with large uncertainties, to examine changes in the summer NAO variability using reanalysis data. I compare the temporal variability of the summer NAO between the first 40 years (1850-1889) and the last 40 years (1976-2015) of the 20CR data. The summer NAO variability during the last 40 years is indeed signifi-

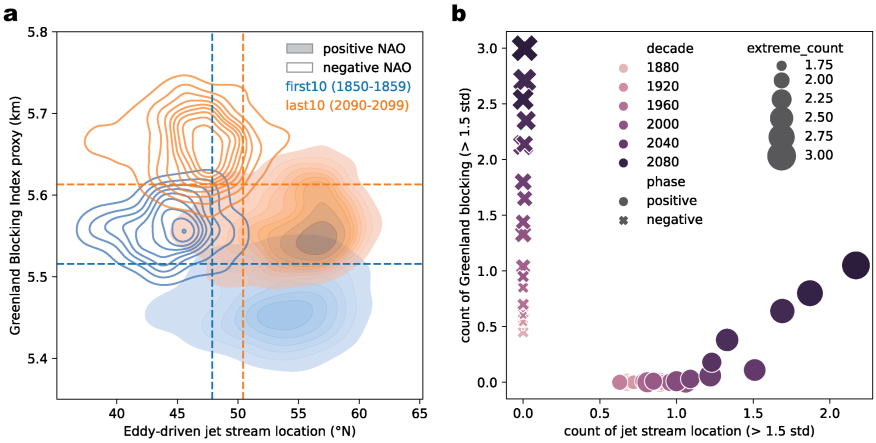

Figure 8: **Changes in the summer NAO extremes coincide with changes in the frequency of flow regimes. a**, Density plot of occurrence of summer NAO extremes as a function of eddy-driven jet stream location and Greenland blocking index. Line contours represent the negative summer NAO extremes, and contours with shading represent the positive summer NAO extremes. Blue colors for the first 10 years of the simulations, and orange colors for the last 10 years. Dashed lines show the climatology. **b** Scatter plot of occurrence of summer NAO extremes every decade as a function of occurrence of different flow regimes. The zonal flow regime is identified when the eddy-driven jet stream location is more north than 1.5 standard deviation of the first 10 years. The blocked flow regime is identified when the Greenland blocking index higher than 1.5 standard deviation of the first 10 years.

cantly larger than the first 40 years (Figure. 9a), consistent with the projections of the MPI_GE (Figure. 6b). Accordingly, the occurrence of summer NAO extremes increases for both the positive (Figure. 9b) and negative phase (Figure. 9c). Although this increase is not statistically significant using bootstrapping based method, the consistence between the 20CR and the SMILEs strengthen our confidence that the signal of increasing summer NAO variability likely emerges in the historical period.

impacts amplify during historical periods

An amplified impact of the summer NAO extremes on the surface temperature is also evident in the 20CR. The warming effect of the positive summer NAO extremes over Northwest Europe is amplified (Figure. 9d-f). This amplification is consistent with the findings in the MPI_GE. Moreover, we found a strong amplification of the warming effect over the Mediterranean during the negative phase of the summer NAO extremes. The amplified impact on the surface temperature is consistent with the enhanced low over the Arctic during the positive phase, and reduced high over north Europe during the negative phase (Contours, Figure. 9).

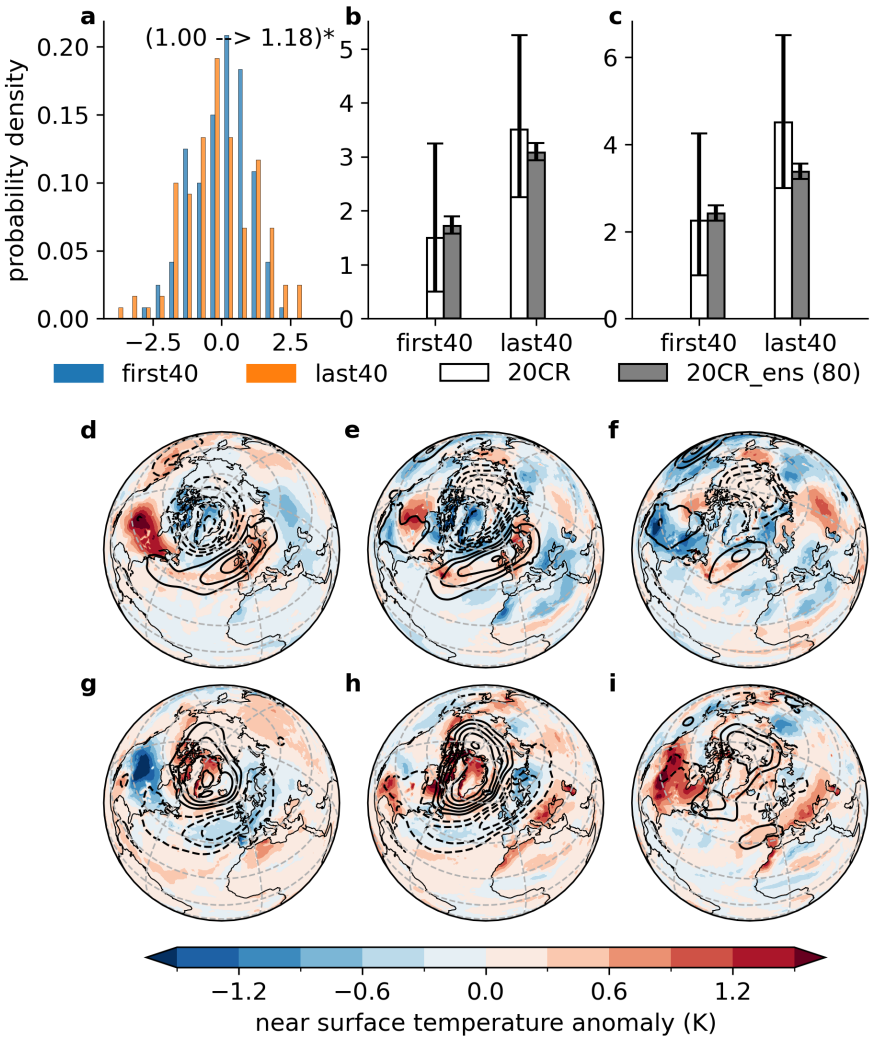

Figure 9: **Hints of enhanced summer NAO variability emerge in historical periods. a**, Distribution of the normalized NAO index in the 20CR. The first 40 years represent 1850-1889, the last 40 years represent 1976-2015. Numbers in the top parentheses indicate changes in the standard deviation, with an asterisk indicating significance at the 95 % confidence level. **b**, The occurrence of positive summer NAO extremes in the 20CR and 20CR with all the ensemble members (20CR_ens). Error bars represent the 95 % confidence interval based on bootstrapping. **c**, Same as **b**, but for the negative summer NAO extremes. **d**, Composite mean of the 10-meter air temperature (shading) and sea level pressure (contours) during the positive phase of the summer NAO extremes in the first 40 years. Contours are drawn at intervals of 1 hPa, ranging from −5 to 5 hPa, with the 0 contour omitted. **e**, Same as **d**, but for the last 40 years. **f**, The difference between **e** and **d**. **g-i**, Same as **d-f**, but for the negative summer NAO extremes.

2.5 ROBUSTNESS OF THE FINDINGS

The summer NAO in this study is decomposed using the Empirical Orthogonal Function (EOF) analysis. EOF is a standard method for

different configurations of the EOF

calculating the spatial pattern and the time series of the NAO. We have shown that the results remain quantitatively similar for changes in various configurations of this approach. For example, we have decomposed the NAO pattern for every non-overlapping 10-year period and generated the NAO index seperately for each decade by projecting the geopotential field data onto the corresponding NAO pattern. The conclusions drawn from the NAO index generated using a temporally fixed pattern are similar to that generated using temporally varying patterns. Indeed, changes in the spatial patten of the summer NAO under global warming are modest (Fig. 4g-i), which is consistent with a relatively local enhancement rather than a spatial shift of the jet variability (Fig. 4d-f).

different approaches for index generation

In addition, we have calculated the summer NAO index using a second, different method. The other classic method to calculate the NAO index apart from the EOF analysis is based on the pressure difference between Iceland and the Azores. Similarly, we have calculated the summer NAO index using the difference in 500 hPa geopotential height between these two boxes. This box difference based method shows a weaker, but still significant increase in the summer NAO variability.

different climate models

We have examined various large ensemble simulations carried out with different Earth system models (Table 1). All models support an increase in the occurrence of negative summer NAO extremes. An increase in positive extremes is found in MPI_GE, CESM1_CAM5, and MK3.6, but not in GFDL_CM3 and CanESM2. By downsampling the MPI_GE to match the smaller ensemble sizes of the other models, we attribute the discrepancy in GFDL_CM3 to its five-times-smaller ensemble size compared to the MPI_GE. On the other hand the different behavior of the CanESM2 might stem from its weak representation of the link between the phase of summer NAO extremes and the position of the eddy-driven jet.

different approach for impact examination

The amplified impacts of the summer NAO extremes on the surface temperature have been investigated using composite analysis. We show that the same conclusion can be drawn from Singular Value Decomposition (SVD) analysis. Based on SVD analysis with one month of lead/lag, we further ensure that the spatial pattern shown in Figure 7 is an effect of the summer NAO extremes rather than of other processes like the soil moisture variability.

3

CHANGES IN ATMOSPHERIC EDDIES CONTRIBUTE TO MORE SUMMERTIME NAO EXTREMES

In this chapter, I answer the question of: *What are the physical processes driving changes in summer NAO extremes in response to global warming?* On the one hand, the increase in the occurrence of summer NAO extremes under a transient warming climate is robust to the choices of Earth System models and approaches used [48]. On the other hand, our understanding of atmospheric response to global warming at regional scale is of low confidence [37, 75, 79, 80]. Such a finding thus requires physical reasoning to be persuasive.

role of eddies in the NAO variability

Previous studies have shown that the thermal wind balance (equation 1) can be used to explain the changes in the upper-level zonal jet-stream winds [45, 76] (section 1.3), but it cannot be used to explain changes in the variability of the summer NAO. This is because the thermal wind balance is built on the equilibrium states rather than transient states. The physical processes driving the NAO variability include Rossby wave breaking (section 1.2), which is associated with the eddy momentum forcing at upper levels (section 1.4). Therefore, the enhancement of the summer NAO variability may be related to changes in the eddy forcing of the mean flow.

approach overview

I use daily output from MPI_GE_CMIP6 to extract the eddy component of atmospheric flow. Transient eddies are obtained by applying a 2–12 day band-pass filter to the daily data [67]. Quasi-stationary eddies are obtained from the zonal anomaly of the 30-day running mean of the daily data [47]. The eddy momentum forcing of the upper-level subpolar jet is quantified by the convergence of eddy momentum flux ($-\frac{\partial}{\partial y}\overline{u'v'}$ in equation 5). Since eddies also provide feedback to the lower-level baroclinicity via eddy heat flux (section 1.4.3), I examine this eddy thermal forcing by the second meridional derivative of eddy heat flux ($\frac{\partial^2}{\partial y^2}\overline{v'T'}$ in equation 6). The effect of eddy forcing on the NAO variability are examined using composite analysis across different phases of the summer NAO extremes. Finally, I demonstrate how changes in the statistics of this eddy forcing contribute to the increase in the summer NAO extremes.

3.1 SUMMER NAO VARIABILITY, UPPER-LEVEL JET, AND LOWER-LEVEL BAROCLINICITY.

I begin by showing that the summer NAO is associated with zonal jet stream winds at upper level. During positive summer NAO extremes, the subpolar jet stream at 250 hPa tilts northeast-southwest towards

upper-level jet

Northern Europe, separating from the subtropical jet (Figure. 10a). Conversely, during negative summer NAO extremes, the subpolar jet merges with the subtropical jet, forming a continuous zonal belt of a single jet stream (Figure. 10b). Therefore, similar to its winter counterpart [98], the variability of the summer NAO is essentially linked to the meridional displacement of upper-level subpolar jet (Figure. 10c).

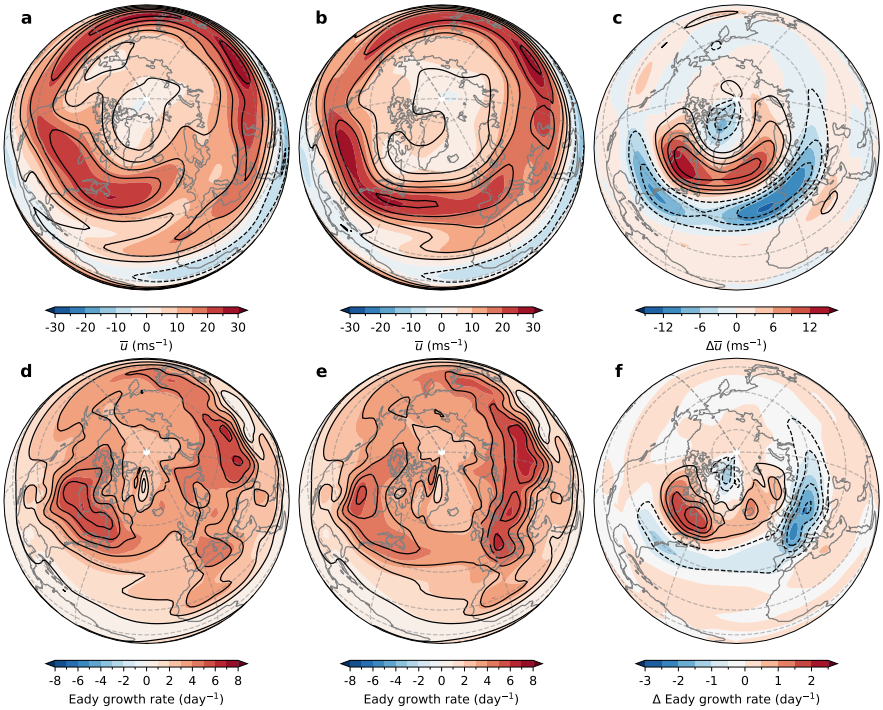

Figure 10: **The variability of the summer NAO is associated with the variability of the upper-level jet and lower-level baroclinicity. a**, Composite mean of the zonal wind (unit: ms^{-1}) at 250 hPa for the positive summer NAO extremes. Shadings show the first 10 years (1850-1859), contours show the last 10 years (2090-2099). Contours share the same intervals as the shadings, eliminating 0 m/s. **b**, Composite mean of the zonal wind at 250 hPa for the negative summer NAO extremes. **c**, The difference between **b** and **a**. **d**, Composite mean of the Eady growth rate (unit: day^{-1}) at 850 hPa for the positive summer NAO extremes. shadings for the first 10 years, and contours for the last 10 years. Contours share the same intervals as the shadings, eliminating 0 day^{-1}. **e**, Composite mean of the Eady growth rate at 850 hPa for the negative summer NAO extremes. **f**, Difference between **e** and **d**.

lower-level baroclinicity

Similarly, the summer NAO is associated with the baroclinicity at lower level. Here, the baroclinicity at 850 hPa is approximated with the Eady growth rate at 850 hPa (equation 7) [35]. During positive NAO extremes, there is a local maximum of the Eady growth rate over the North America continent between [50 - 70 °N] (Figure. 10d), coinciding with the local maximum of the zonal jet stream wind at upper level (Figure. 10d). Conversely, during negative summer NAO

extremes, the Eady growth rate over the North America between [50 - 70 °N] decreases, and that over North Europe between [40-60 °N] increases (Figure. 10e), coinciding with the extension of the zonal jet stream at the upper-level (Figure. 10e). Therefore, the NAO variability is also linked to the fluctuations in the lower-level baroclinicity (Figure. 10f).

The similarity between the pattern of the upper-level jet stream and lower-level baroclinicity associated with the summer NAO variability reveals a positive eddy feedback: transient eddies generation follows the shift of the upper-level jet. However, as discussed in (section 1.4.3), the transient eddies exert a negative eddy thermal feedback. The positive eddy feedback must therefore come from a third process, which i will explain in more details below.

3.2 ROLE OF THE EDDY MOMENTUM FORCING OF THE UPPER-LEVEL JET

eddy momentum forcing

To establish the link between the anomalous eddy momentum forcing and the occurrence of the summer NAO extremes, I plot its spatial average over high latitudes ([50 - 70 ° N]) as a function of time relative to the onset of the summer NAO extremes (Figure. 11a, b). The eddy momentum forcing is indeed a direct driver in the occurrence of the summer NAO extremes, as it starts to diverge from its climatological state roughly 10 days prior to the onset of the positive and negative phases (Figure. 11a, b).Moreover, the transient eddies are playing the leading role (Figure. 11a), and the quasi-stationary eddies are playing the secondary role (Figure. 11b).

3.3 ROLE OF THE EDDY THERMAL FEEDBACK OF THE LOWER-LEVEL BAROCLINICITY

negative feedback of transient eddies

Eddies also modulate the summer NAO variability by changing the lower-level baroclinicity via heat flux they carry. However, by transporting warm air poleward and cold air equatorward, transient eddies, or these low- and high-pressure systems, weaken the meridional temperature gradient and reduce the lower-level baroclinicity in the process (Figure. 11c), forming a negative thermal feedback. For instance, the positive summer NAO extremes require poleward shifted baroclinicity and eddy generation (Figure. 10f). However, as the extreme events develop, the thermal feedback from transient eddies drop below zero (solid lines, Figure. 11c). Similarly, negative summer NAO extremes require equatorward shifted baroclinicity (Figure. 10f), but the transient eddies exert a positive thermal feedback to the lower-level baroclinicity at higher-latitude (dashed lines, Figure. 11c), restricting the southward shift of the lower-level baroclinicity. There-

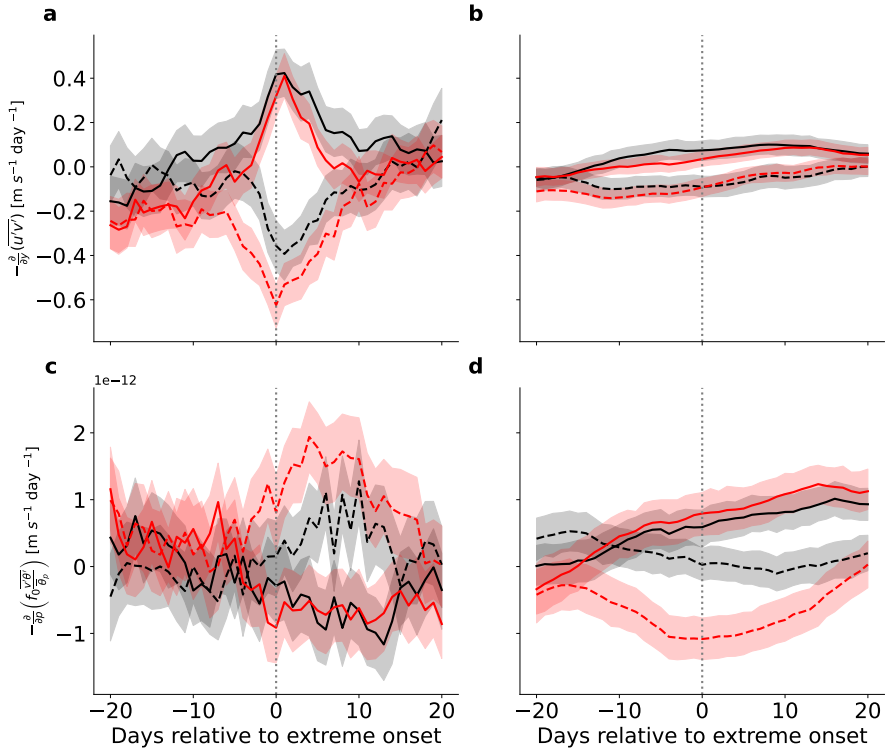

Figure 11: **Role of the upper-level eddy momentum forcing and the lower-level eddy thermal feedback in modulating the summer NAO variability. a**, Spatial mean (averaged over [-180, 180, 50, 70 °N]) of the composite anomalies of the upper-level (250 hPa) eddy momentum forcing from transient eddies as a function of time relative to the onset of the summer NAO extremes. **b**, Same as **a**, but for the quasi-stationary eddies. **c** Spatial mean (averaged over [-180, 180, 50, 70 °N]) of the composite anomalies of the lower-level (850 hPa) eddy thermal feedback from transient eddies as a function of time relative to the onset of the summer NAO extremes. **d** Same as **c**, but for the quasi-stationary eddies.

fore, the thermal forcing by transient eddies acts to dampen the development of the summer NAO extremes.

positive feedback of quasi-stationary eddies

To support a sustained generation of transient eddies during the prolonged summer NAO extremes, the lower-level baroclinicity must be maintained. I show that it is the quasi-stationary eddies that fulfill this role. About 15 days earlier the onset of the positive summer NAO extremes, the quasi-stationary eddies start to exert a positive forcing on the lower-level baroclinicity (solid lines, Figure. 11d). The anomalous positive forcing by the quasi-stationary eddies prevails over the anomalous negative forcing from the transient eddies. As a result, there is a net positive anomaly of the eddy thermal forcing prior to the onset of the positive summer NAO extremes, that maintains the transient eddy generation. Conversely, for negative phase of the summer NAO extremes, the upper-level jet weakens and shifts equatorward (Figure. 10c), in response to a reduced eddy generation

at high latitudes (Figure. 10f). This reduction is mainly contributed by an anomalous negative thermal forcing by quasi-stationary eddies, which begins roughly 15 days prior to the onset (dashed lines, Figure. 11d).

Under global warming, the average upper-level eddy momentum forcing and the lower-level eddy thermal feedback for each extreme events enhance (compare black lines with red lines, Figure. 11). This explains why the intensity of the summer NAO extremes increase with global warming (section 2.2). Below, I demonstrate why the occurrence of these extreme events increase with global warming.

3.4 MORE SUMMER NAO EXTREMES ROOTED IN ENHANCED EDDY MOMENTUM FORCING AND EDDY THERMAL FEEDBACK.

summer NAO extremes increase

Under global warming, the occurrence of the summer NAO extremes increases for both positive and negative phases — evidence of increased summer NAO variability on daily timescales (Figure. 12a). Such increases are consistent with the increasing occurrence of their precursors. The anticyclonic Rossby wave breaking at the equator flank of the jet stream is the precursor of the positive summer NAO extremes. The cyclonic Rossby wave breaking at the poleward flank of the jet stream is the precursor of the negative summer NAO extremes. Under global warming, the occurrence of both anticyclonic Rossby wave breaking events and the cyclonic Rossby wave breaking at high latitudes increases with simulated global warming (Figure. 12b).

variability of eddy forcing increases

Consistent with changes in the Rossby wave breaking events, the associated eddy momentum forcing exhibits a strong increase in its variability: the standard deviation of the eddy momentum forcing from transient eddies enhances with global warming (Figure. 12c). This non-linear enhancement can be traced to changes in the lower-level baroclinicity. I show that the variability of the lower-level thermal feedback of the baroclinicity indeed displays a similar non-linear increase in its variability (compare lines in Figure. 12c with the dashed line in Figure. 12d).

land-ocean contrast increases

Finally, why does the eddy thermal forcing by quasi-stationary eddies becomes more variable? Although the near surface temperature increases everywhere, the pattern of change is not spatially uniform. One dominant feature of this heterogeneity is a stronger warming over land than over ocean. As a result, when a zonally uniform warming signal is removed, the land-ocean temperature contrast is found to be enhanced by global warming [44]. Since the quasi-stationary eddies are forced by the land-ocean thermal contrast, together with topographic forcing, such an enhancement may be associated with the enhanced variability of the eddy thermal forcing by quasi-stationary eddies. Nevertheless, this hypothesis requires further investigation.

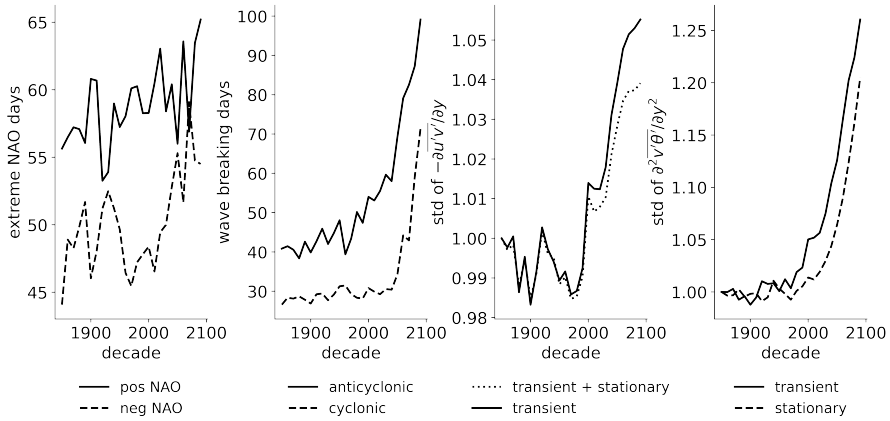

Figure 12: **Changes in the eddy forcing due to global warming increase the occurrence of the summer NAO extremes. a**, The occurrence of the summer NAO extremes. **b** The occurrence of both anticyclonic and cyclonic wave breaking events. The lines show the spatial mean of the occurrence of wave breaking events over [-90, 40, 50, 70 °N]. **c**, Changes in the standard deviation of the eddy momentum forcing averaged over [-180, 180, 50, 70 °N] at 250 hPa. **d**, Changes in standard deviation of the eddy thermal forcing averaged over [-180, 180, 50, 70 °N] at 850 hPa. All the standard deviations are calculated across all the ensembles within each decade, and then scaled by the value in the first decade (1850-1859).

4

SUMMARY AND CONCLUSION

4.1 HOW DOES THE SUMMER NAO RESPOND TO GLOBAL WARMING?

From my first study, it becomes clear that changes in the summer NAO in response to global warming can be partitioned into two distinct aspects: (i) the mean state of the summer NAO becomes more positive, and (ii) the variability and extremes of the summer NAO are increasing.

changes in the mean state

Similar to its winter counterpart, the summer NAO index exhibits a positive trend in it its mean state in climate projections. One of the mechanisms behind this change is the northward shift of the zonal jet stream winds [29, 49, 98]. All the SMILEs used in our study support such a positive trend in the summer NAO index.

changes in the variability

Superimposed on this positive trend, my study identifies a secondary summer NAO response to global warming — an enhancement in its variability. Evidence for this enhancement include a widening in the summer NAO index distribution and an increase in the occurrence of both positive and negative summer NAO extremes. This enhancement is statistically robust in MPI_GE in three different greenhouse gas-driven transient scenarios: a moderate warming scenario (RCP4.5), a strong warming scenario (RCP 8.5), and an idealized scenario in which the CO_2 concentration in the atmosphere increases by 1% per year.

changes in the impact

Not only does the occurrence of the summer NAO extremes increase, but the average impact of these extremes on European surface temperature is also amplified. All the climate models predict an amplified impact of NAO extremes on European temperature in summer. This amplification is significant over northwestern Europe, i.e., an amplified warming during positive summer NAO extremes, and an amplified cooling during negative summer NAO extremes.

robustness of the findings

The findings of an enhanced summer NAO variability and amplified impacts of summer NAO extremes are robust to various configurations of approaches used. They are supported by the NAO index generated by both the EOF analysis and the box-difference based method. They are predicted by multiple climate models. The enhanced summer NAO variability was not limited to a specific altitude in the troposphere, but was evident at almost all altitudes. This equivalent-barotropic response indicates the importance of interactions between eddies and the mean flow, as is later shown in my second study.

emergence in the historical period

Furthermore, I show that such an enhanced summer NAO variability and an amplified impact of the summer NAO extremes are likely emerging in the historical period. The 20CR dataset also indicates an amplified warming effect during negative summer NAO extremes over the Mediterranean, a concerning feature absent in the SMILEs.

4.2 WHAT ARE THE PHYSICAL PROCESSES DRIVING CHANGES IN SUMMER NAO EXTREMES IN RESPONSE TO GLOBAL WARMING?

In my second study, I provide a physical interpretation for the increase in the occurrence of the summer NAO extremes from a perspective of "eddy-mean-flow" interactions. I show that the eddy forcing of the summer NAO variability comprises upper-level momentum forcing and lower-level thermal forcing. These two components consist of contributions from transient eddies and quasi-stationary eddies. The upper-level momentum forcing is dominated by the transient eddies, and the lower-level thermal forcing is primarily driven by quasi-stationary eddies.

role of upper-level momentum forcing

The eddy momentum forcing at upper levels, specifically the convergence of the eddy momentum flux, alters the latitudinal position of the subpolar jet stream, which is associated with the phase of the summer NAO. I show that the occurrence of the positive summer NAO extremes is driven by a continuous positive anomaly of this momentum forcing beginning around 10 days prior to its onset. Conversely, the occurrence of the negative summer NAO extremes is driven by a negative anomaly.

role of lower-level thermal forcing

The eddy thermal forcing at lower levels, specifically the second meridional derivative of the eddy heat flux, modulates the lower-level baroclinicity. This baroclinicity is the source of transient eddies such as high- and low-pressure systems. While the transient eddies provide a negative feedback to the lower-level baroclinicity, the quasi-stationary eddies reinforce the baroclinicity through a positive feedback. The positive summer NAO extremes are sustained by a positive anomaly of the thermal forcing by quasi-stationary eddies at high latitudes, whereas the negative summer NAO extremes are associated with a negative anomaly.

changes under global warming

I show that global warming modifies this eddy forcing of the summer NAO extremes. Specifically, the variability of eddy thermal forcing at lower-level increases, due to an enhanced land–ocean temperature contrast by global warming. The increase in the variability of the eddy thermal forcing leads to a more variable transient eddy generation and thus contributes to an enhancement of the variability of the eddy momentum forcing. Through eddy–mean-flow interactions, this chain of enhancement is translated into enhanced occurrence of summer NAO extremes.

4.3 HOW DOES THE FINDING ADVANCE THE FIELD?

Our understanding of the atmospheric response to a transient warming climate is crucial for effective risk management, as it helps assess whether rates of adaptation can keep pace with worsening extreme weather [32]. But this response remains obscured due to strong internal variability [28, 80, 100]. Over the North Atlantic, previous studies have shown that the anthropogenic forced signal in the atmosphere projects strongly onto the internally generated pattern of the NAO [12, 20, 34, 63]. Therefore, the NAO index exhibits a long-term trend in its mean state [5, 36, 50, 52].

implications of the first study

My first study demonstrates that global warming affects not only the mean state of the summer NAO, but also enhances its variability. While a positive trend in the mean state of the summer NAO index suggests an increased probability of positive NAO extremes, the enhanced summer NAO variability suggests an increased probability of both positive and negative NAO extremes. As a consequence, contrasting severe weather events are becoming more likely under global warming. Changes in the variability of the summer NAO also provide insights into changes in the jet stream and blocking under global warming. Our study suggests that both the “fast-gets-faster" response [76] (corresponding to enhanced positive NAO extremes) and the “wave-get-wavier" response [13, 56, 77] (corresponding to enhanced negative NAO extremes) in jet stream winds are likely to occur in a transient warming climate.

implications of the second study

My second study provides a physical interpretation of the enhanced summer NAO variability under global warming. Based on composite analysis, I show that summer NAO variability is a direct response to the anomalous convergence of momentum flux carried by transient eddies at the upper level, which is associated with Rossby wave breaking. This mechanism, identified in the SMILEs, is consistent with a simple dynamical model [90]. The transient eddies originate from the lower-level baroclinic instability [38, 89]. Although transient eddies act to reduce baroclinicity in the process, I find that quasi-stationary eddies tend to maintain it during prolonged summer NAO extremes. This positive eddy feedback from quasi-stationary eddies supports the assumption, based on a simplified quasi-geostropic atmospheric model [102], that eddies of different frequencies play distinct roles in modulating baroclinicity. In particular, I show that changes in the statistics of the eddy forcing contribute to the increase in the occurrence of the summer NAO extremes.

summary of the contribution

My finding and interpretation advance our understanding of the large-scale atmospheric response to global warming through two key aspects. First, an extension of the study object: from the change in the temporal mean states—certainly an important aspect—to the change in the variability and extreme states, which directly govern the sur-

face weather. Second, a complementary dynamical framework used to interpret the atmospheric response: moving beyond the thermal wind balance—based on changes in the meridional temperature gradient (e.g., [45, 76])—to "eddy-mean-flow" interactions, which is based on changes in the eddy fluxes of momentum and heat.

outlook

Looking ahead, how atmospheric variability responds to global warming remains a challenging scientific question. One reason for this is that the atmospheric variability covers a very wide range of frequencies. The relative high frequency variability, such as the synoptic to sub-season variability of the summer NAO studied in this thesis, is generated internally within the atmosphere via interactions across processes with different scales. The relative low frequency variability, on the other hand, arise from coupling between the atmosphere and more slowly varying components like deep ocean and sea ice, and is beyond the scope of this study. For the high-frequency component, I have shown that their changes are associated with changes in the Rossby wave breaking, which can be traced to changes in the lower-level baroclincity. However, other aspects, such as changes in the background jet stream, may also contribute. Another open question is how changes in atmospheric variability and extreme events in a transient warming climate will inform the local adaptation decision-making. High-resolution global models, now reaching kilometer-scale resolution, opens new opportunities to tackle these challenges [75, 79].

Part II

APPENDIX

A

MORE EXTREME SUMMERTIME NORTH ATLANTIC OSCILLATION UNDER CLIMATE CHANGE

The attached manuscript has been publish as:

Liu, Q., Bader, J., Jungclaus, J.H., Matei, D. More extreme summertime North Atlantic Oscillation under climate change. Commun Earth Environ 6, 474 (2025). https://doi.org/10.1038/s43247-025-02422-x

Quan Liu[1,2], *Jürgen Bader*[3], *Johann H. Jungclaus*[1], *Daniela Matei*[1]

[1]Climate Variability Department, Max Planck Institute for Meteorology, Hamburg, Germany
[2]International Max Planck Research School on Earth System Modelling, Hamburg, Germany
[3]Institute of Oceanography, Center for Earth System Research and Sustainability (CEN), Universität Hamburg, Germany

Corresponding author: *Quan Liu*, quan.liu@mpimet.mpg.de

ABSTRACT

Extreme states of the North Atlantic Oscillation in summer can lead to severe weather events such as heatwaves and floods in Europe. But how these extremes evolve in response to climate change remains unexplored. Here we show that the statistical distribution of the summer North Atlantic Oscillation index grows wider with increasing global warming in large ensembles of climate change simulations as well as reanalysis data. Such an amplified variability of the summer North Atlantic Oscillation caused by global warming leads to a higher probability of summer North Atlantic Oscillation extremes — for both positive and negative phases — accompanied by an amplification of their impacts on surface temperature over northwestern Europe. Changes in summer North Atlantic Oscillation extremes highlight the effects of climate change on the transient behaviour of the atmosphere, and thus have important implications for extreme weather attribution.

A.1 INTRODUCTION

Some severe European weather events in summer, such as heatwaves, droughts, and floods, have been linked to extreme states of the North Atlantic Oscillation (NAO) [22–24, 34, 46, 84], the leading mode of atmospheric variability over the North Atlantic sector [36, 92]. The NAO represents a large-scale seesaw pattern in the atmospheric pressure anomaly. Its positive phase reflects an enhanced south-north pressure gradient associated with stronger zonal jet stream winds, and its negative phase reflects a reduced pressure gradient associated with weaker zonal jet stream winds. The probability of severe summer weather in Europe has increased disproportionately compared to the rest of Northern Hemisphere midlatitudes over the past 40 years [69, 91]. This amplified probability raises the concern that global warming could influence the summer NAO extremes, enhancing the likelihood of heat extremes over Europe. However, previous studies addressing changes in the summer NAO have focused on changes in the mean — particularly the long-term trends under global warming [27, 31]. To date, no study has examined changes in the variability, particularly the extreme states of the summer NAO, in response to global warming. To fill this gap is the purpose of this paper.

Long-term trends in the NAO index reveals the response of the mean state of the NAO to global warming and have been extensively studied, mostly for winter. In winter, the state-of-the-art climate models in the frame of the sixth phase of the Coupled Model Intercomparison Project (CMIP6) show a large spread in the trends of the NAO [14, 52], with most models agreeing on a positive trend til late 21 century (2080–2099) under the Representative Concentration Pathway (RCP) 8.5 scenario [52]. This positive NAO trend in winter

is intimately linked to adjustments of the jet stream: the models predict a strengthening and a poleward shift of the zonal jet in response to global warming [29, 49, 50, 61, 76]. Although an accelerating jet stream is also emerging in observations [96], a robust long-term trend in the winter NAO remains virtually undetectable [4, 64, 82]. In summer, climate models tend to simulate a positive trend in the NAO in the historical period, which is also subject to a large model dispersion and deviation from observations [5, 27, 37]. The large uncertainty in the trend of the NAO arises from the fact that different models respond differently to the same radiative forcing [83], trends predicted by models are biased from observations over the North Atlantic sector [4, 61, 96], and the NAO exhibits strong internal variability.

As a consequence of the positive trend, a previous study has reported more positive extreme states of the NAO in winter under simulated global warming [53]. This is expected as the fast upper-level zonal jet stream winds increase more than the average zonal jet stream winds under climate change [76]. While an upward trend in the mean state of the NAO would increase the likelihood of positive NAO extremes, an enhancement in the variability of the NAO would increase the likelihood of both positive and negative NAO extremes. A potential changes in the NAO variability is suggested by recent advances in seasonal forecasting. The predictive skill of the NAO variability is beyond the deterministic timescales of weather forecasts [25, 72]. This skillful prediction suggests that some fraction of the NAO variability are driven by predictive boundary conditions, such as sea surface temperature that changes with external forcing [61]. Indeed, a major source of the predictive skill for the NAO variability in the late 20 century is external forcing [43]. In addition, a study has shown that global warming will expand the spatial footprint of some internal atmospheric variability mode in winter [62]. Both the prediction and the climate impact studies suggest that the variability of the NAO may be altered by global warming, and the probability of both — the positive NAO extremes corresponding to enhanced zonal winds and the negative NAO extremes corresponding to enhanced blocking [15, 98, 99] — would increase.

The increasing likelihood of NAO extremes would raise a particular concern in summer, given their close association with the occurrence of temperature and precipitation extremes. For summer, studies have reported changes in both zonal and blocked atmospheric flows in response to global warming. For instance, the zonal component of the jet stream over North Atlantic sector exhibits a poleward shift and acceleration, especially over higher altitudes [45, 49, 76]. Meanwhile, Greenland blocking appear to be enhanced in the last 40 years [9, 13, 45, 65, 82]. Overall, changes in atmospheric flows represent a closely balanced tug-of-war between tropical warming over upper-tropospheric [49] and polar warming close the surface [13, 45, 82],

but which effect will dominate remains inconclusive [61]. It is plausible that both the zonal flow and blocked flow will change in summer under global warming. Given that the NAO variability is associated with transitions between the zonal and the blocked flows [98], changes in both, due to global warming, would suggest changes in summer NAO variability. However, examining such changes in the NAO variability is difficult because a small number of realizations of climate change simulations, e.g, from Coupled Model Intercomparison Project (CMIP), do not allow the internal variability to be properly diagnosed [16, 17, 95] and multi-model ensembles suffer from the additional structural uncertainty between models [18, 83].

Instead, a large ensemble of simulations with a single model allows the changing internal variability in a transient climate to be determined. The ensemble spread of such "initial-condition large ensembles (LEs)" is an expression of the internal variability at each individual time step [21, 54]. Temporal changes in the ensemble spread of the transient LEs under historical and future radiative forcing scenarios thus reveal changes in the internal variability — beyond the change in the mean state — against global warming [54, 62]. Using a collection of such LEs from various Earth system models further ensures the robustness of the results by accounting for the bias of each model [18]. It is also possible, albeit with large uncertainties, to isolate the internal variability in reanalysis data. In this case, temporal variability over a relatively short time window is usually taken as the internal variability (e.g. ref [31]). In this study, we use five LEs under historical condition and the Representative Concentration Pathway (RCP) 8.5 future scenarios [18], one LEs under 1% CO_2 scenario, one LEs under RCP 4.5 scenario [51], and the 20CR data [81]. We examine changes in the summer NAO between the first 10 years and the last 10 years of the LEs, which respectively represents the pre-industrial climate and a simulated $\sim$ 4K warmer climate. In particular, we investigate the occurrence of summer NAO extremes every non-overlapping ten years in LEs. The findings from LEs are compared with the 20CR in historical periods.

A.2 RESULTS

A.2.1 *Increased summer NAO variability and extreme states under global warming*

We begin by investigating the summer NAO response to global warming at 500 hPa in LEs. The summer NAO is decomposed from 500 hPa geopotential height (Z500) data by applying the Empirical Orthogonal Function (EOF) analysis along ensemble dimension (Methods). The LEs largely reproduce the spatial pattern of the summer NAO as a seesaw pattern for both the pre-industrial climate and the sim-

ulated ~ 4K warmer climate (Fig A1a for Max Planck Institute for Meteorology Grand Ensemble (MPI_GE), and Supplementary Figure. A1 for other LEs). In contrast to the apparent northward shift of the jet stream (contours, Supplementary Figure. A3c), the spatial pattern of the summer NAO changes only slightly under global warming (Supplementary Figure. A3i). We show that the resilience of the summer NAO pattern to global warming is consistent with a local enhancement, rather than a spatial shift, of the variability of the jet stream and Z500 (Supplementary Figure. A3f). This enhancement largely overlaps with the southern center of actions of the summer NAO, leading to the increase in the explained variance of the summer NAO from 18% to 24 % (Figure. A1a). Since the NAO dominates the weather over much of Europe, a more relevant question would be how global warming affects the strength of the NAO, i.e. the NAO index.

Changes in the NAO index due to global warming can be partitioned into two parts: 1) changes in the mean state of the NAO that is reflected by the shift in the mean of the NAO index distribution, and 2) changes in the variability of the NAO that is reflected by changes in the shape of the NAO index distribution. The changes in the mean state is evident when the NAO index is generated using the Z500 without removing the ensemble mean (Supplementary Figure. A4a) — all LEs used in this study agree on a positive long-term trend in the summer NAO index til the end of the 21 century (Supplementary Figure. A5). Given the evidence described in the introduction, we also examine changes in the variability of the NAO after removing the mean-state change (Methods). Our analysis provides strong evidence for a secondary summer NAO response to anthropogenic forcing: we find significant widening in the distributions of the summer NAO index in MPI_GE (Figure. A1b). Such an enhanced summer NAO variability is also seen in the NAO index generated by the classical method — difference between Iceland and the Azores (Supplementary Figure. A6a). The response of the summer NAO variability to global warming, superimposed on the mean state change, is projected by all Earth system models used in this study (Supplementary Figure. A2).

The enhanced variability would manifest itself in higher probabilities of both positive and negative NAO extremes. In this study, we define the summer NAO index above 1.5 standard deviation as positive NAO extremes, and those below -1.5 standard deviation as negative NAO extremes. We extract such NAO extremes every non-overlapping ten-years throughout the time span of the LEs (Methods). The MPI_GE, forced by historical and RCP8.5 future scenarios, shows continuous increases in the occurrence of both positive and negative summer NAO extremes at 500 hPa pressure level, either the NAO index is generated via EOF (Figure. A1c, d) or box difference based methods (Supplementary Figure. A6b, c). The MPI_GE_onepct,

same as MPI_GE but driven by a stronger anthropogenic forcing — the CO_2 concentration increases by 1% per year — shows more pronounced increases in the occurrences of positive and negative extremes (red lines, Figure. A1c, d). The MPI_GE forced by a more moderate warming scenario, RCP 4.5, shows weaker but still statistically significant increases (Supplementary Figure. A7).

The increase in the occurrence of the summer NAO extremes at 500 hPa is fairly consistent across different LEs (Figure. A2), indicating that such an increase is not due to model biases. Community Earth System Model (CESM1_CAM5) (blue lines, Figure. A2) and Commonwealth Scientific and Industrial Research Organization MK3.6 model (MK3.6) (green lines, Figure. A2) show increases in the occurrence of both positive and negative extremes. Two other models, Geophysical Fluid Dynamics Laboratory's Coupled Model (GFDL_CM3) and Canadian Earth System Model (CanESM2) behave differently from MPI_GE in terms of positive NAO extremes, either with varying NAO patterns (yellow and purple lines, Figure. A2) or a fixed NAO pattern (yellow and purple lines, Supplementary Figure. A10) (Methods). The different behavior of the GFDL_CM3 seems to be due to its 5 times smaller ensemble size compared to MPI_GE, so that the prediction is overwhelmed by the decadal variability. Indeed, if 20 ensemble members are randomly selected from 100 ensemble members of MPI_GE, the increase in the positive NAO extremes does not significantly emerge (compare filled yellow bar with unfilled orange bar, Figure. A2c). The different behavior of CanESM2 in terms of positive NAO extremes will be explained in section A.2.3 with respect to the representation of flow regimes.

Hints of the increasing probability of NAO extremes in summer are emerging in the historical periods. We extract the internal variability of the summer NAO in the historical periods from the 20CR (Methods). The 20CR data are used because, compared with other reanalysis data, it assimilates only sea-level pressure and sea surface temperature fields rather than utilizing all available observations in the troposphere, making it less sensitive to temporal inhomogeneities in the observations [7] and less constrained so that it includes some of the variability due to internal atmospheric processes [81]. The distribution of the summer NAO index in the last 40 years (1976-2015) is wider than in the first 40 years (1850-1889) of the record (Figure. A1f). For comparison, the widening is also evident when all the ensemble members of the 20CR (20CR_ens) are used to isolate the internal variability (Methods). Based on a threshold of 1.5 standard deviation of the first 40 years, the occurrence of the NAO extremes increases in the last 40 years (Figure. A1g, h). Assessing the significance of the increase appears to be difficult in the reanalysis data. Bootstrapping-based methods show that the increase in 20CR is insignificant and that in 20CR_ens is significant (error bar, Figure. A1g, h). This un-

certainty is partly due to the fact that bootstrapping requires a large sample size, and underlies the difficulty of extracting internal variability from reanalysis data (Methods). Nevertheless, the uncontroversial results between the 20CR and the LEs enhance our confidence that increasing probability of both positive and negative summer NAO extremes is likely to emerge in the historical periods.

The increasing occurrence of the summer NAO extremes is shown not only at 500hPa, but throughout most of the troposphere. Except for the near-surface altitudes, the rise in the occurrence of NAO extremes due to global warming appears to be significant up to 200 hPa, either under the 1% CO_2 scenario (Figure. A3a, b), or the Historical and RCP8.5 scenarios (Supplementary Figure. A11a, b) in MPI_GE. The vertically consistent changes are also evident in the 20CR (Figure. A3c, d) and 20CR_ens (Supplementary Figure. A11c, d). Note that the 20CR doesn't show obvious changes in the occurrence of summer NAO extremes at the upper troposphere (200 hPa). This is consistent with a recent study showing that upper atmospheric response to global warming would not emerge until 2050 [76]. Bootstrap based methods show that the increase in the 20CR is insignificant, and that in 20CR_ens is significant. Again, sample size may contribute to this uncertainty.

A.2.2 *Increased climate impacts of summer NAO extremes over northwestern Europe*

The large sample size of the extremes in LEs allows us to investigate changes in the climate impacts of the summer NAO extremes under global warming. To do so, we firstly remove long-term trend by removing the ensemble mean from each ensemble member, and then calculate composite mean of surface temperature and precipitation during these summer NAO extremes (Methods). A positive extreme summer NAO event has a warming effect over northwestern Europe and central North America, and a cooling effect over Greenland and the Mediterranean, a pattern that is consistent across different models and reanalysis data under pre-industrial climate (Figure. A4a-f). However, under the simulated ~ 4K warmer climate, the warming effect over Northwest Europe is increased and expanded (Figure. A4g-k). Such an amplification is statistically significant and consistent across different models (Figure. A4m-q). The opposite change — increased cooling over north-western Europe — occurs during negative summer NAO extremes (Figure. A5).

The amplified impact of summer NAO extremes on the surface temperature is also evident in the 20CR_ens (Figure. A4 and A5 r). The magnitude of the changes is smaller in the reanalysis data than in the LEs (Figure. A4r), because the background climate warmed by less than 1.5K in historical periods, compared to ~ 4K at the end of the

RCP8.5 runs of the LEs. The 20CR_ens additionally shows an apparent amplification of the warming effect over the Mediterranean basin during the negative NAO extremes under a warmer background climate (Figure. A5l). Such an amplification is also seen in the MPI_GE (Figure. A5m), CESM1_CAM5 (Figure. A5i), and GFDL_CM3 (Figure. A5k), but it is mostly insignificant, whereas changes of the opposite sign are shown in the CanESM2 and MK3.6. This highlights the challenge for climate models to project the regional climate change — uncertainty from both the strong internal variability and model difference [28, 100].

The temperature dipole pattern in Figure. A4 and Figure. A5 may be induced by other factors, such as variability of the soil moisture. However, an analysis based on Singular Value Decomposition (SVD) (Methods) shows that a dipole pattern of soil moisture over Europe can not induce a temperature pattern as strong as the summer NAO at the same time scale (Supplementary Figure. A14 and A17). To further ensure that the temperature dipole patterns shown in Figure. A4 and Figure. A5 are effects of the summer NAO extremes and not vice versa, we perform SVD analysis with time lead/lag. When the NAO is leading the surface temperature by one month, the surface temperature resembles the dipole pattern shown in Figure. A4 (Supplementary Figure. A15), whereas when the NAO is lagging the surface temperature, the temperature pattern is distinct (Supplementary Figure. A16). This difference confirms that the summer NAO extremes induce the temperature dipole pattern, rather than the temperature dipole pattern induces the summer NAO extremes.

In addition to surface temperature, we also examined changes in the effect of summer NAO extremes on precipitation (Supplementary Figure. A12 and A13). Similar to surface temperature, all models show consistence in the impact of the summer NAO extremes on precipitation. Under global warming, this pattern is amplified for both positive and negative summer NAO extremes. However, none of the models show that this amplification is statistically significant based on bootstrapping (Methods).

A.2.3 *Changes in the summer NAO extremes are associated with changes in the atmospheric flow regimes*

Atmospheric circulation exhibits multiple flow regimes [8], and transitions between them over the North Atlantic sector are associated with the summer NAO variability [98, 99]. Therefore, investigating changes in the flow regimes would provide a different perspective to changes in the summer NAO extremes, and enhance the robustness of the finding. In this study, because we use monthly data, the eddy-driven jet stream location [97] is used as a proxy for the strength of

the zonal flow regime, and the Greenland blocking index [30] is used as a proxy for the frequency of the blocked flow regime (Methods).

Changes in the two flow regimes over time are shown in Figure. A6a, b. We observe both an obvious poleward shift of the eddy-driven jet (black line, Figure. A6a) and an enhancement of the Greenland blocking (black line, Figure. A6b) under climate change. The northward shift of the mean-state of the eddy-driven jet stream would suggest more extreme episodes of eddy-driven jet being located further north; and the increased time-mean state of the the Greenland blocking index would suggest more extreme episodes of the eddy-driven jet stream being located south and merged with the subtropical jet [99]. Indeed, if we focus on the frequency of extreme states of the two regimes, the increases are more prominent (red lines, Figure. A6a, b).

Changes in both flow regimes are associated not only with the positive trend of the summer NAO (Supplementary Figure. A4c, d), but also with the increase in the summer NAO extremes (Figure. A6c). Under the pre-industrial climate, the negative and positive phases of the summer NAO extremes lie correspondingly in the second and fourth quadrant of the coordinate plane defined by the eddy-driven jet stream location and the Greenland blocking index (blue lines, Figure. A6c), confirming the close link between two flow regimes and the occurrence of positive and negative summer NAO extremes. Under the simulated ~ 4K warmer climate, the zonal flow shifts northward, and the Greenland blocking enhances (from blue dashed lines to orange dashed lines, Figure. A6c). Meanwhile, the occurrence of summer NAO extremes increases (compare orange contours with blue contours, Figure. A6c). We further show that increasing negative summer NAO extremes are linked with increasing number of extreme episodes of Greenland blocking, while increasing positive summer NAO extremes are linked with increasing extreme episodes of both northward diverting eddy-driven jet and Greenland blocking (Figure. A6d).

Finally, other models that show similar changes in the summer NAO extremes as MPI_GE show similar changes in the zonal and blocked flow regimes (Supplementary Figure. A22). The different behavior of CanESM2 with respect to the positive NAO extremes (Figure. A2c) compared to the other LEs is also evident in the flow regimes: the link between northward shifts of the eddy-driven jet stream location and the increase in the positive NAO extremes is weak (Supplementary Figure. A22g). This is probably because the location of the climatological eddy-driven jet stream in this model is more northerly than in the other models (dashed lines, Supplementary Figure. A22b).

A.3 CONCLUSION

It is well established that the mean state of the summer NAO changes in response to global warming. The mechanisms for such a change include changes in the zonal jet stream winds [29, 49, 50]. All LEs used in this study support a positive trend in the mean state of the summer NAO under global warming.

Here, we argue for a secondary response of the summer NAO to global warming — an increase in its variability. This increase is consistent with the implications of a simple conceptual Lorenz model [63]. The enhanced variability causes the extreme states of the summer NAO — for both positive and negative phases — to become more frequent and their impact over Northwestern Europe to increase. The increased occurrence of the summer NAO extremes is vertically consistent throughout most of the troposphere. The enhanced impact of these extremes over northwestern Europe is consistent with the slight strengthening of the NAO pattern over this region (Supplementary Figure. A3i). Such an enhanced impact of the NAO extremes in summer under global warming is consistent with its winter counterpart [62]. The increased occurrence and impacts of the summer NAO extremes are supported by most of the state-of-the-art LEs under consideration. Notwithstanding the differences in the production of ensemble members between simulations and reanalysis data, the 20CR reanalysis data suggests that increasing probability of the summer NAO extremes is emerging in the historical period.

The increasing occurrence and impact of the summer NAO extremes is robust to various configurations of the approach we used. For instance, the NAO index from both EOF and box difference methods supports the increasing occurrence; the analysis based on both composite mean and SVD supports the enhanced impact. Overall, the increase in the NAO extremes is more robust for the negative phase than the positive phase. A stronger increase in the negative summer NAO extremes is consistent with the enhancement of the jet variability particularly over the southern flank of the mean jet (Supplementary Figure. A3f). Nevertheless, as the mean state of the summer NAO becomes more positive under global warming, a small increase in the positive summer NAO extremes would still have a considerable effect.

The changes in both phases of summer NAO extremes are consistent with enhanced likelihood of poleward diverts of the eddy-driven jet stream and of intensified Greenland blocking episodes by global warming. While the increasing negative NAO extremes is dominated by enhanced Greenland blocking, the increasing positive NAO is linked to variations in both flow regimes. Our results thus suggest that both the 'fast gets faster' response [76] (corresponding to enhanced positive NAO extremes) and the 'wave gets wavier' response

[13, 56, 78] (corresponding to enhanced negative NAO extremes) in jet stream winds are likely to occur in transient warming climate, rather than one being dominant.

A.4 METHODS

A.4.1 *Data*

Historical and RCP8.5 runs of five Single Model Initial-condition Large Ensemble simulations (SMILEs) from the 'Multi-Model Large Ensemble Archive' (MMLEA)[18], one SMILEs forced by RCP4.5 scenario, and an experiment of 1% CO_2 run with Max Planck Institute Grand Ensemble (MPI_GE_onepct) [51] are used. The results from climate simulations are compared with that of the 20CR data [81]. The 20CR has 80 ensemble members. These ensemble members are generated using the Ensemble Kalman Filter [11], and are designed to reflect observational uncertainty. From the Monte Carlo aspect of the Ensemble Kalman Filter theory, each member is equally likely. By only assimilating the surface pressure and sea surface temperature, and using the coupled atmosphere–land model, the ensemble spread includes some of the uncertainty from the internal dynamics of the atmospheric circulation [11]. Therefore, the analysis of 20CR is also tested with all the ensemble members of the 20CR (20CR_ens). All the data are monthly and confined to boreal summer (June-July-August).

A.4.2 *Generating summer NAO index*

The NAO is decomposed from geopotential height data at all available levels in troposphere over the domain [20–80°N and 90°*W*–40°E] using Empirical Orthogonal Function (EOF) analysis. For each level, the geopotential height data are first weighted by cosine of the latitude. The NAO index is identified as the first principle coefficients (PCs) of the EOF analysis, and is standardized by dividing the index with the spatial standard deviation of the eigenvector instead of the usual way of being multiplied by the temporal standard deviation of itself. Since the EOF is applied independently for each ten-year interval (see section A.4.3), this way of standardization ensures that the index generated from different eigenvectors are comparable, and the multiplication of the index and the corresponding eigenvector still gives an estimate of the geopotential height field. We have also tried with a fixed spatial pattern for all different warming stages, the results are included in the Supplementary and do not change the main conclusion. The spatial pattern of the NAO is then obtained by projecting the geopotential field onto the standardized index, showing the change in the geopotential height field corresponding to the change in the NAO index of one standard deviation.

For comparison, NAO index using the difference between two boxes ($25°W-5°E, 45°N-55°N$) and ($52-22°W, 60°N-70°N$) [24] is also investigated for MPI_GE.

A.4.3 *Extracting internal variability of the NAO in SMILEs*

In SMILEs, the ensemble members differ only slightly in their initial conditions. The considerable ensemble spread during the simulation is then mainly due to internal variability of the climate system. The internal variability of the NAO is then extracted by applying the EOF analysis along the ensemble dimension of the SMILEs, after removing the ensemble mean from each of the ensemble members as previous studies [54, 62]. Note that the ability for the ensemble spread to estimate internal variability differs across different Earth System Models. MPI-GE provides the best representation of internal variability according to ref [85], partly due to its large ensemble size. Therefore, the ensemble size of all the SMILEs is expanded by concatenating all the ensemble members and all the summer months (June, July and August) within a ten-year interval. We refer to this combined dimension as 'pseudo ensemble'.

To examine the temporal evolution of summer NAO variability in SMILEs, the EOF along the pseudo ensemble dimension is conducted separately over each non-overlapping decade. This allows the spatial patterns of the NAO to vary across different warming periods. This is expected, as variations in the spatial structure of the NAO can lead to different impacts [6], and contribute to its response to global warming [24, 98]. As a reference, the decomposition using a fixed pattern (Supplementary Figure. A8) instead of the temporally varying patterns is also applied (Supplementary Figure. A9, Supplementary Figure. A10). In this case, the magnitude of the increase reduced for both positive and negative NAO extremes compared to that with the varying pattern. So that the increase in the occurrence of positive NAO extremes in CESM1_CAM5 does not significantly emerge.

The full NAO response, that includes changes in the variability and the mean state of the NAO for MPI_GE is given in Supplementary Figure. A4. The index for full NAO response are generated by projecting the Z500, without removing ensemble mean, to the NAO pattern of the first10 years of the simulation.

A.4.4 *Extracting internal variability of the NAO in 20CR*

The internal variability in the 20CR are extracted with two different methods, 1) with the ensemble mean only and 2) with all the ensemble members. The first method follows the typical use of the 20CR data. In this case, a quadratic fit of the single realization is taken as a representation of the externally forced signal. After removing the

quadratic fit from the time series at each pixel, the residuals are taken as a representation of the internal variability. The second method uses all the ensemble members of the 20CR. Different from SMILEs, the spread of the 20CR is not designed to measure the internal variability, and the the ensemble mean includes both the externally forced signal and the internal variability. Therefore, same as the first method, the quadratic fit of the ensemble mean is used to represent the externally forced signal, and is removed from all the ensemble members at each pixel.

Both methods have short-comes in extracting the internal variability in the 20CR. For the first method, single realization would underestimate the internal variability, and the small sample size would limit the use of bootstrapping. For the second method, although up to 80 ensemble members are available, the ensemble spread is much narrower than that of the MPI_GE, and shows clear decadal variability (Supplementary Figure. A20), indicating that the ensemble spread of the 20CR strongly underestimates the internal variability if it is treated the same as SMILEs. To minimize effects of the above limitations, the NAO from 20CR data are decomposed differently from the SMILEs. First, the full length of the data is used to decompose NAO spatial pattern. This is because the leading mode decomposed from 40 years of data do not fully resemble the typical summer NAO pattern (Supplementary Fig.A1f). Second, 40 years instead of 10 years are used as a window to compare changes in the internally generated NAO extremes.

A.4.5 *The occurrence of the summer NAO extremes*

1.5 standard deviation of the NAO index in the first period (first 10 years in SMILEs and first 40 years in 20CR) is used as a threshold to extract the NAO extremes for positive phase (above the threshold) and negative phase (below -1 times threshold). Although the standard deviation based threshold assumes Gaussian distributions, the results should be very similar if percentile based threshold is used. The advantage of the percentile based threshold is that it allows possible asymmetry of the NAO index. However, in MPI_GE, 1.5 standard deviation roughly corresponds to 93% percentile of the index, and -1.5 standard deviation to 7% of the index in LEs (Supplementary Figure. A21a). If 90th and 10th percentile are used as the thresholds, the corresponding value in standard deviation are roughly 1.3 and -1.3. Therefore, the NAO index in the first 10 years of the MPI_GE is actually symmetric. Other LEs show similar results as MPI_GE(Supplementary Figure. A21). As a reference, such positive NAO extremes occur 1.6 times per decade, and such negative NAO extremes occur 0.9 times per decade in 20CR based on Extreme Value Theory.

In the SMILEs and 20CR_ens, the summer NAO extremes in each period are counted from all the ensemble members and all the months within each period, and then divided by the ensemble size. The linear trend of the occurrence in SMILEs is calculated between 1950-2099, where all the models have an output. The rate of increase per decade is then represented by dividing the linear slope by the occurrence in the first 10 years and expressed as a percentage. For the ensemble mean of the 20CR, the summer NAO extremes are counted from all the months within each 40-year period, and the rate of increase per decade is estimated simply by $(O_{last40} - O_{first40})/(2015 - 1889) \times 10$, and represented as percentage by dividing this value with the occurrence in the first 40 years

A.4.6 *Climate impacts of the summer NAO extremes*

The impacts of summer NAO extremes on the surface temperature, the sea level pressure, and precipitation are examined using the composite analysis. The impact on the surface temperature in MPI_GE is verified with Singular Vector Decomposition (SVD). In both methods, the background changes are removed by removing the ensemble mean in all SMILEs, and the quadratic fit in the 20CR_ens.

For composite analysis, the pre-processed data in the months and ensemble members where the NAO indexes are identified as positive (or negative) extremes are averaged. As the occurrence of the NAO extremes differs between different warming stages, the same number of most extreme cases as in the pre-industrial climate are included. The composite analysis using all the extreme cases in the first interval and the last interval (rather than the same number of extreme cases) gives very similar results (plots not shown).

For SVD analysis, the variabiles are firstly normalized by their mean and standard deviation across all ensemble members and each decade. Then the pre-processed surface temperature and the Z500 are fed into the SVD. For comparison, same analysis is performed for the surface temperature and the soil moisture. To examine the causal relationship, the SVD with time lead/lag of one month is performed.

A.4.7 *Eddy-driven jet stream location and Greenland blocking index*

Because we use monthly data, the eddy-driven jet stream location and Greenland blocking can not be measured directly. Instead, we use two proxies on monthly data, which represent the statistical frequency of the occurrence of each regime in transient atmospheric flow. Following Woollings, et.al [99], the eddy-driven jet stream are identified as zonal wind averaged between levels of 925 hPa and 700 hPa. The location of the eddy-driven jet is defined as the latitude where the zonally averaged jet stream winds over a longitudinal sector ($0 - 60°W$ for the

North Atlantic) is in its maximum. Following Hanna, et. al [30], the Greenland blocking is simply estimated as the mean 500 hPa geopotential height for the [60–80°N and 20°–80°W] region.

A.4.8 *Statistical significance test*

Bootstrap-based methods are used to test the statistical significance of the widening of the NAO index distribution at the 95% level, and determine the 5% – 95% confidence interval of the occurrence of NAO extremes under different warming stages. Specifically, for testing the significance of the widening of the NAO index distribution, the NAO index of the first interval and the last interval are randomly resampled separately with replacement, and the difference between the standard deviations of the two generated samples are calculated. Such resampling and calculation are repeated for 1000 times. If 0 is outside of the 5% – 95% percentile of these differences, changes in the shape of the distribution is considered as significant. For the 5% – 95% confidence interval of the occurrence of NAO extremes, at each 10-year (40-year for the 20CR) intervals, the NAO index is randomly resampled for 1000 times with replacement. The occurrences of the extreme cases in these generated samples are counted in the same way as the original index. The 2.5% – 97.5% quantile of these occurrences is identified as the 5% – 95% confidence interval for the occurrence of NAO extremes.

Bootstrap method is also used to check whether the difference of the impact of the extreme NAO between the first interval and the last interval is statistically significant at the 95% confidence level. Specifically, 1000 samples of NAO index are generated by resampling with replacement. For each of the generated NAO time series, extract the extreme cases, and examine their impacts on surface temperature using composite analysis as orignal NAO index, separately for the first internal and the last interval. And then calculate the difference between impacts of these two intervals. Such calculations are repeated for all the generated NAO time series. After getting the whole 1000 temperature differences, the 2.5% – 97.5% quantile of these differences is calculated. if 0 is not in the range, the difference of the composite mean temperature field between the last interval and the first interval is considered as significant.

The 5% – 95% confidence interval of the linear trend of the evolution of extreme NAO occurrence is obtained using student's t test.

DATA AVAILABILITY The model data used in the study are available online at https://www.earthsystemgrid.org/dataset/ucar.cgd.ccsm4.CLIVAR$_$LE.html (for CanESM2 [42], CESM1_CAM5 [41], MK3.6 [39], GFDL_CM3 [86]) and at https://esgf-data.dkrz.de/projects/

mpi-ge/ (for MPI_GE [51]). The 20CR data set can be found at https://psl.noaa.gov/data/gridded/data.20thC$_$ReanV3.html (ref [81]).

CODE AVAILABILITY The codes used in the manuscript are available at https://doi.org/10.5281/zenodo.15363373 (ref [66]).

ACKNOWLEDGMENTS This project has received funding from the JPI Climate & JPI Oceans NextG-Climate Science-ROADMAP project (01LP2002A) and the European Union's Horizon Europe Impetus4Change project (101081555). We thank the US CLIVAR Working Group on Large Ensembles and NSF AGS-0856145 Amendment 87 for supporting the Multi-Model Large Ensemble Archive. We also thank the US National Oceanic and Atmospheric Administration Physical Sciences Laboratory for archiving the 20CR data and providing access. We thank the German Climate Computing Center (DKRZ) for providing the necessary computational resources. We thank Prof. Dr. Jochem Marotzke and Prof. Dr. Tiffany A. Shaw for their constructive comments on our manuscript. We would like to thank Dr. Albert Ossó and two other anonymous reviewers for their constructive comments.

COMPETING INTERESTS The authors declare no competing interests.

AUTHOR CONTRIBUTIONS Quan Liu analyzed the data, made the plots, and wrote the manuscript. Jürgen Bader, Johann H. Jungclaus, and Daniela Matei initiated the project. All authors discussed the results, and finalized the manuscript.

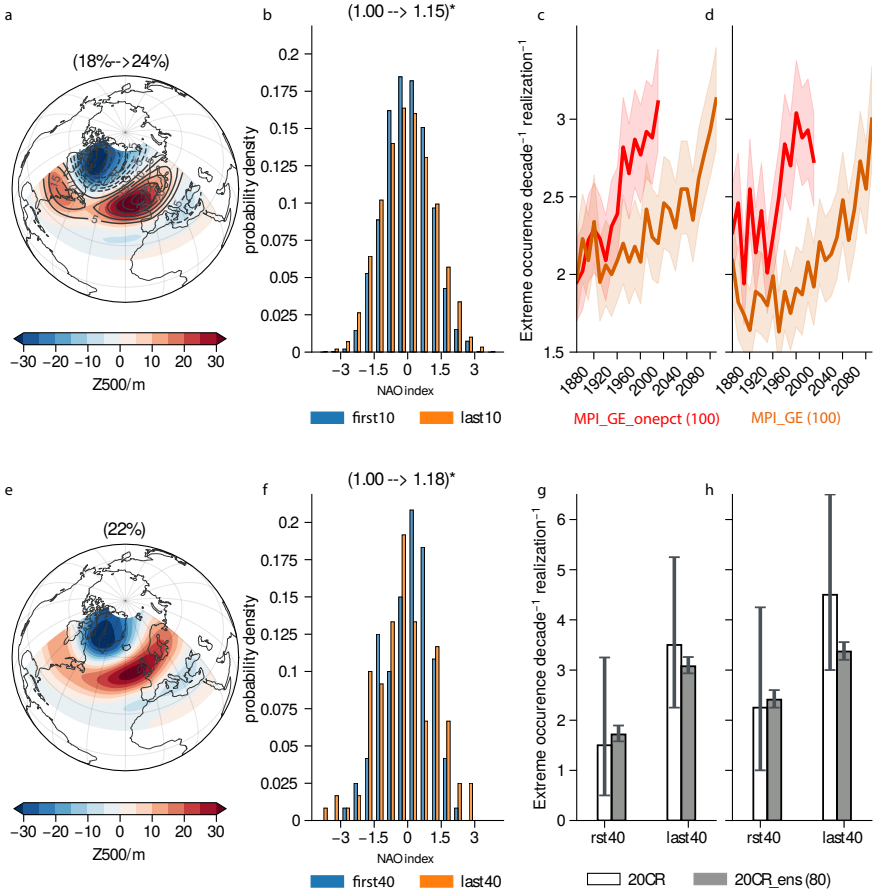

Figure A1: **The occurrence of summer NAO extremes at** 500 **hPa increases under global warming. a,** Spatial patterns of the summer NAO in the first 10 years (1850-1859, shading) and the last 10 years (2090-2099, contour) of the Max Planck Institute Grand Ensemble (MPI_GE) historical and RCP8.5 runs. The percentages in the top parentheses indicate changes in the explained variance. **b,** The distribution of the NAO index widens under the simulated global warming in the MPI_GE. Numbers in the top parentheses indicate changes in the standard deviation, with asterisk indicating significance at the 95% confidence level based on bootstrapping. **c,** Evolution of the occurrence of the positive NAO extremes every non-overlapping 10 years in the MPI_GE and MPI_GE_onepct. MPI_GE_onepct runs for 100 years with the initial condition of 1850, and forced by 1% CO_2 increase per-year. Shading represents the 5% – 95% confidence interval based on bootstrapping. Numbers in the legend show the ensemble size. **d,** Same as (**c**) but for negative NAO extremes. **e,** Spatial pattern of the NAO in the NOAA-CIRES-DOE 20th Century Reanalysis (20CR) data during (1850-2015). The percentage in the top parentheses indicates the explained variance. **f,** Distribution of the NAO index in the 20CR. The first 40 years represent (1850-1889) and the last 40 years represent (1976-2015). Numbers in the top parentheses indicate changes in the standard deviation, with asterisk indicating significance at the 95% confidence level. **g,** The occurrence of positive NAO extremes in the 20CR. 20CR_ens represent the 20CR with all the ensemble members. Error bars represent the 5% – 95% confidence interval based on bootstrapping. **h,** Same as (**g**), but for negative NAO extremes.

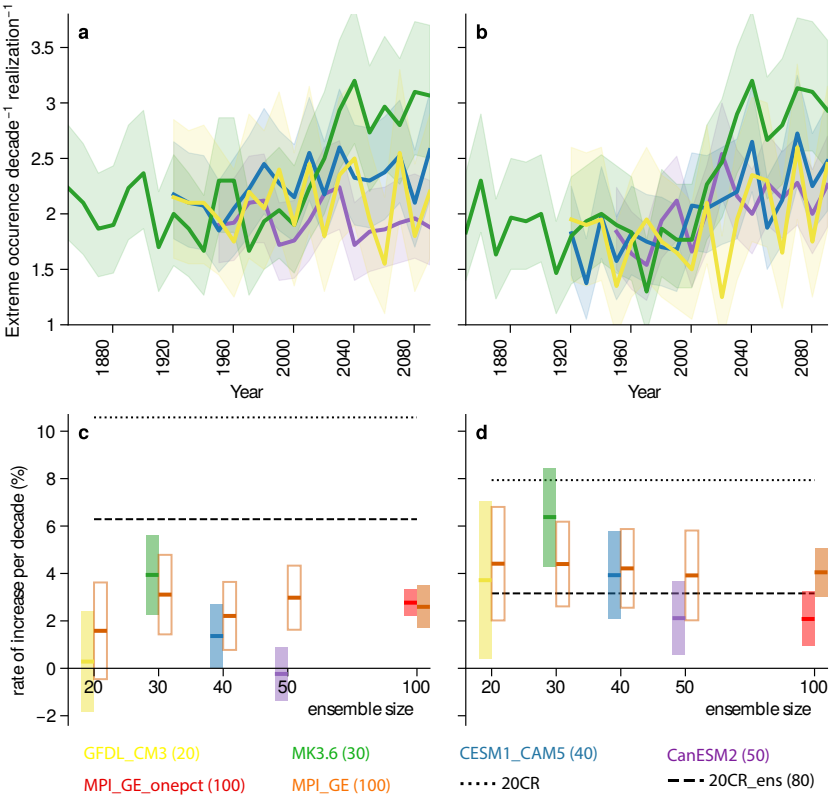

Figure A2: **Upward trend in the occurrence of summer NAO extremes at** 500 **hPa across different Earth System Models.** **a,** Evolution of the occurrence of positive NAO extremes per decade. Shadings represent 5% – 95% confidence interval based on bootstrapping. **b,** Same as (**a**), but for negative extremes. **c,** The rate of increase in the occurrence of positive summer NAO extremes per decade during 1950-2100, shown as a solid line for each model. Filled bars represent the 5% – 95% confidence interval by student-t test. Unfilled bars represent the 5% – 95% confidence interval by student-t test of resampled historical and RCP8.5 runs of Max Planck Institute Grand Ensemble (MPI_GE). **d,** Same as (**c**) but for the negative summer NAO extremes. Numbers in the brackets of the legend indicate ensemble size.

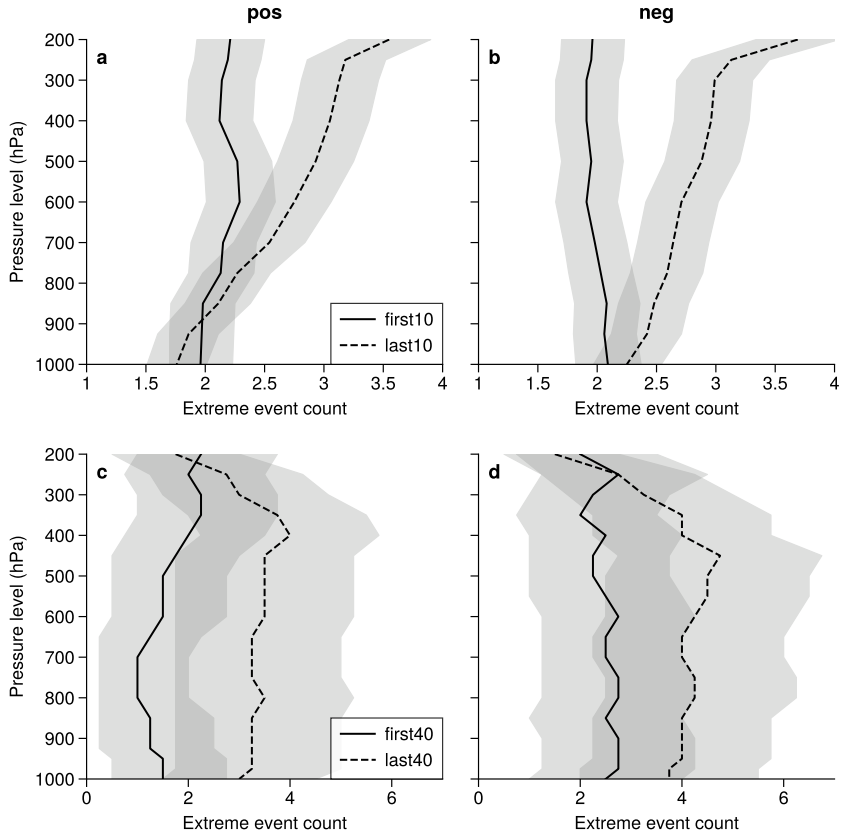

Figure A3: **The occurrence of summer NAO extremes increases throughout most of the troposphere. a,** Profile of the occurrence of the positive summer NAO extremes in Max Planck Institute Grand Ensemble 1% CO_2 run (MPI_GE_onepct). **b,** Same as (**a**), but for negative summer NAO extremes. **c,** Profile of the occurrence of the positive summer NAO extremes in the first-40 years (1850-1889) and the last-40 years (1976-2015) in the NOAA-CIRES-DOE 20th Century Reanalysis (20CR). **d,** Same as (**c**), but for negative NAO extremes. Shading represents $5\% - 95\%$ confidence intervals based on bootstrapping.

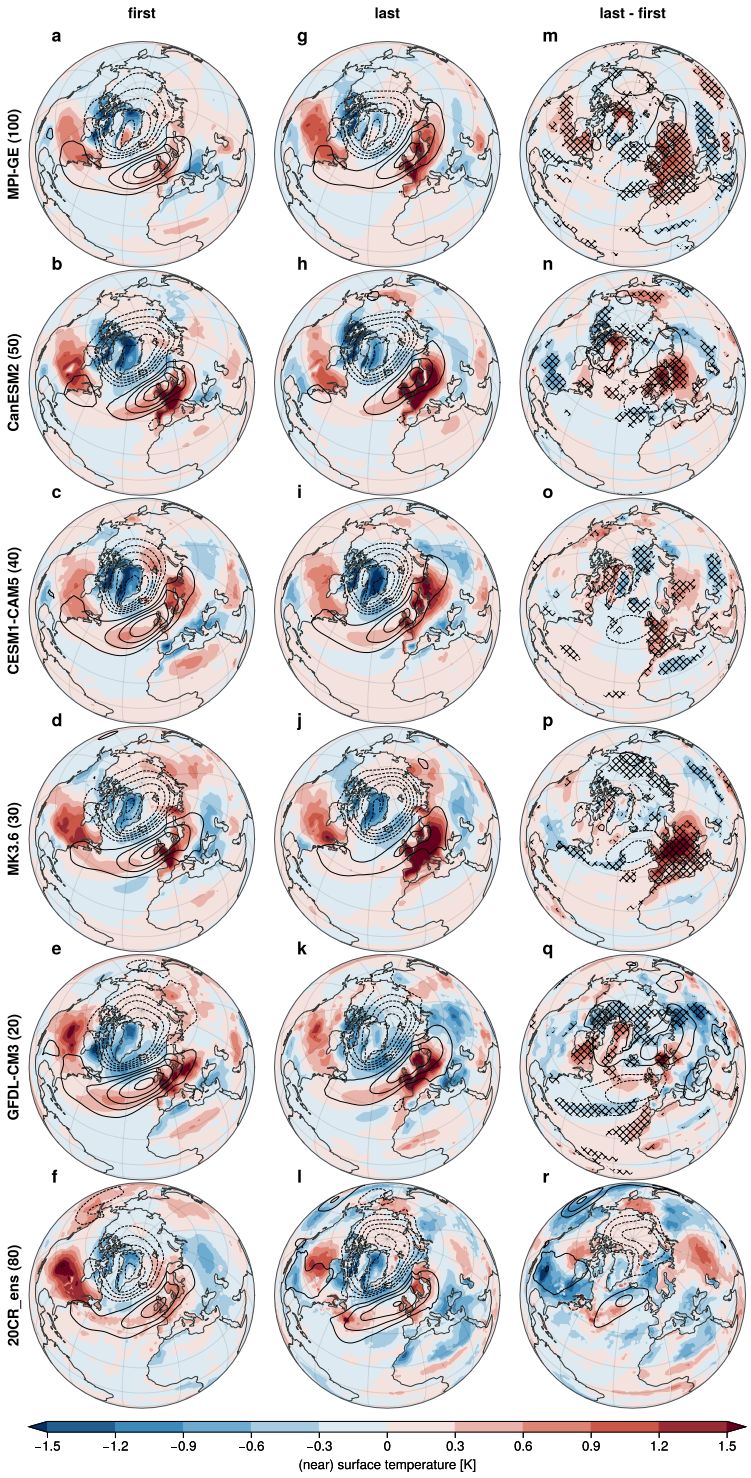

Figure A4: **The impact of positive summer NAO extremes on (near) surface temperature amplifies over the northwestern Europe in a warmer climate. a-f,** The impact of positive NAO extremes on surface temperature (shading) and sea level pressure (contours) in the first 10 years of simulations (**f** for the first 40 years of 20CR) from different Earth System Models. Contours are drawn at intervals of 1 hPa, ranging from -5 hPa to 5 hPa, excluding the 0 hPa contour. **g-k,** Same as (**a-e**), but for the last 10 years of the simulations (**l** for the first 40 years of 20CR). **m-r**, The difference between the last 10 years and the first 10 years (**r** for the last 40 years first 40 years of the 20CR). Crossed patches represent areas where the difference is significant at 95% confidence level based on bootstrapping.

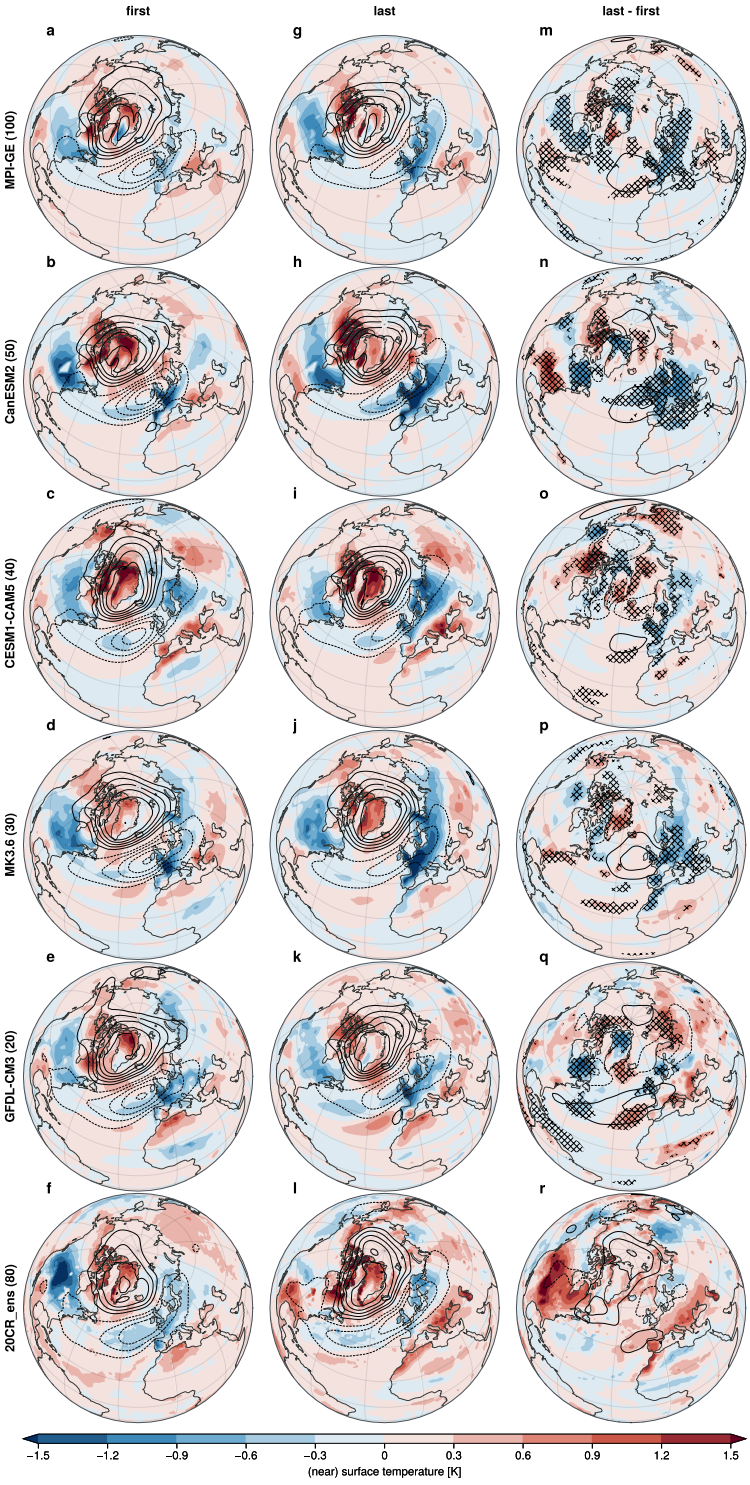

Figure A5: same as Figure. A4 but for negative summer NAO extremes.

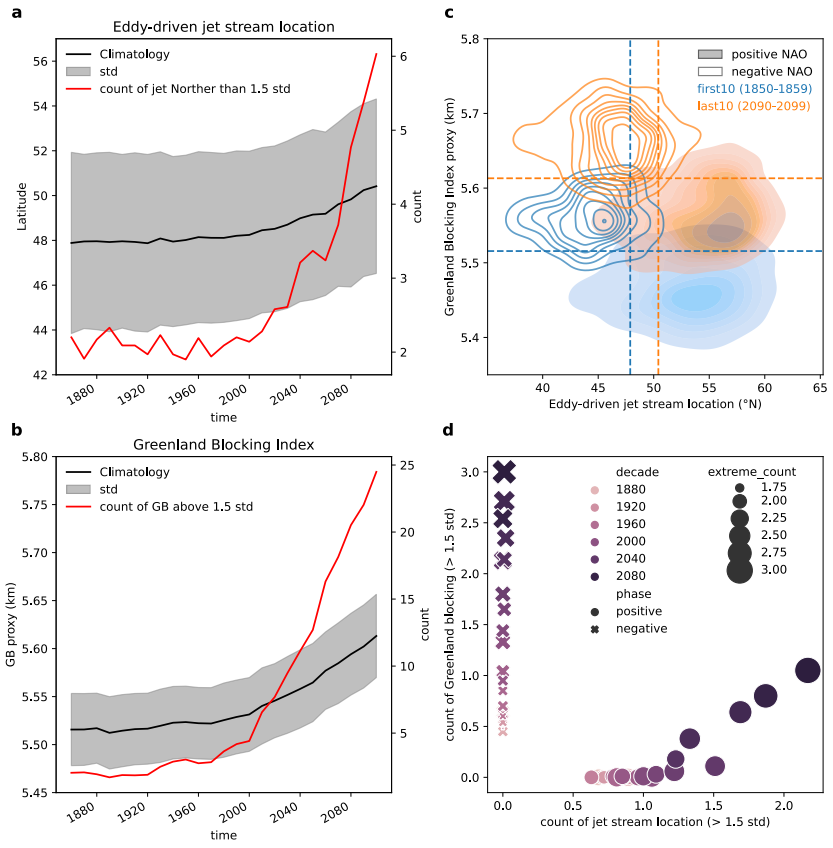

Figure A6: **Changes in the frequency of flow regimes coincide with changes in the summer NAO extremes. a,** Temporal evolution the eddy-driven jet stream location per non-overlapping decade. Shading shows 1 standard deviation along time and ensemble dimension for each decade. **b,** same as **a** but for the Greenland blocking index. **c,** Density plot of occurrence of summer NAO extremes as a function of eddy-driven jet stream location and Greenland blocking index. Contours represent the negative summer NAO extremes, and shadings represent the positive summer NAO extremes. Blue colors represent the extreme events in the first 10 years, and orange colors the last 10 years. Dashed lines represent the climatology of the eddy-driven jet location (vertical dashed lines) and the Greenland blocking index (horizontal dashed lines), respectively for the first 10 (blue dashed lines) and the last 10 years (orange dashed lines). **d,** Scatter plot of occurrence of summer NAO extremes as a function of counts of eddy-driven jet stream location more north than 1.5 standard deviation of the first 10 years and counts of Greenland blocking index higher than 1.5 standard deviation of the first 10 years. Counts correspond to per decade per member. All plots are shown for historical and RCP8.5 runs of the MPI_GE. Definitions of eddy-driven jet and Greenland blocking can be found in Methods.

SUPPLEMENTARY INFORMATION FOR APPENDIX A

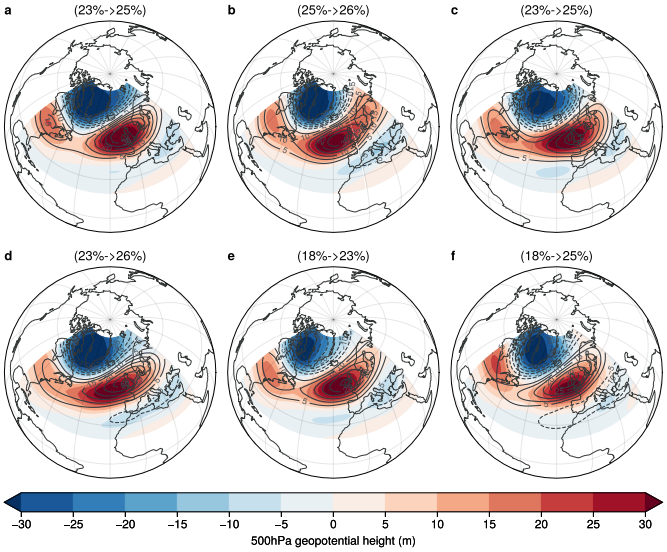

Supplementary Figure. A1: **NAO spatial patterns of all the SMILEs from MMLEA.** Spatial patterns of the NAO in the first (shading) and the last (contour) 10 years of the simulations in (**a**) CanESM2, (**b**) CESM-CAM5, (**c**) MK3.6, (**d**) GFDL_CM3, (**e**) MPI_GE_onepct, and (**f**) the first (shading) and the last (contour) 40 years in the 20CR with all ensemble members. The percentage in the brackets shows the explained variance change.

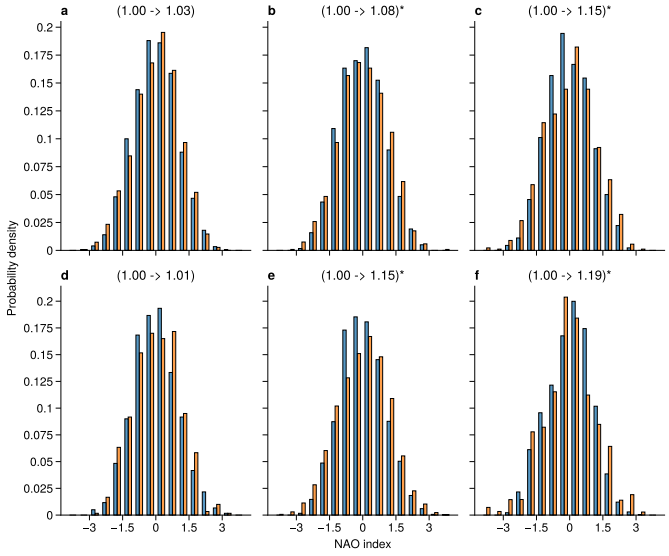

Supplementary Figure. A2: Summer NAO index distribution of all the SMILEs from MMLEA corresponding to the spatial pattern in Supplementary Fig A1, correspondingly for (**a**) CanESM2, (**b**) CESM-CAM5, (**c**) MK3.6, (**d**) GFDL_CM3, (**e**) MPI_GE_onepct and (**f**) 20CR with all ensemble members. The numbers in the brackets show changes in the standard deviation. Blue bars for the first 10 (40) years, orange for the last 10 (40) years. The asterisk indicates that the change is statistically significant at the 95% confidence level based on bootstrapping.

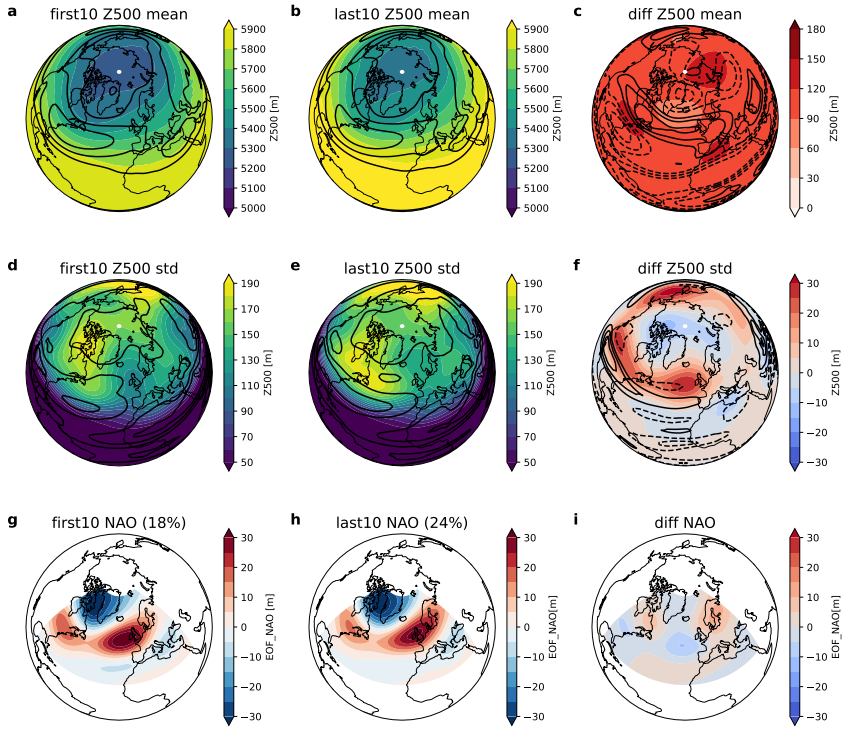

Supplementary Figure. A3: **Atmospheric response to global warming at 500 hPa over the North Atlantic sector. a,** Shading shows the mean of the 500 hPa geopotential height during 1850-1859 in MPI_GE. Contours show the mean of the zonal wind (u) at 500 hPa pressure level during 1850-1859 in MPI_GE. Contours are drawn at intervals of 5 m/s, ranging from $0 - 20$ m/s, excluding the 0 m/s contour. **b,** Same as (**a**), but for 2090-2099. **c,** The difference between **b** and **a**. Contours are drawn at intervals of 0.5 m/s, ranging from $-1.5 - 1.5$ m/s, excluding the $0m/s$ contour. **d,** Shading shows the standard deviation of the 500 hPa geopotential height during 1850-1859 in MPI_GE. Contours show the standard deviation of the zonal wind (u) at 500 hPa pressure level during 1850-1859 in MPI_GE. Contours are drawn at intervals of 2 m/s, ranging from $0 - 10$ m/s. **e,** Same as (**d**), but for 2090-2099. **f,** The difference between **e** and **d**. Contours are drawn the same as **c**. **g**, The spatial pattern of the NAO during 1850-1859 in MPI_GE. The percentage in the brackets shows the explained variance. **h**, Same as **g**, but for 2090-2099. **i**, The difference between **h** and **g**.

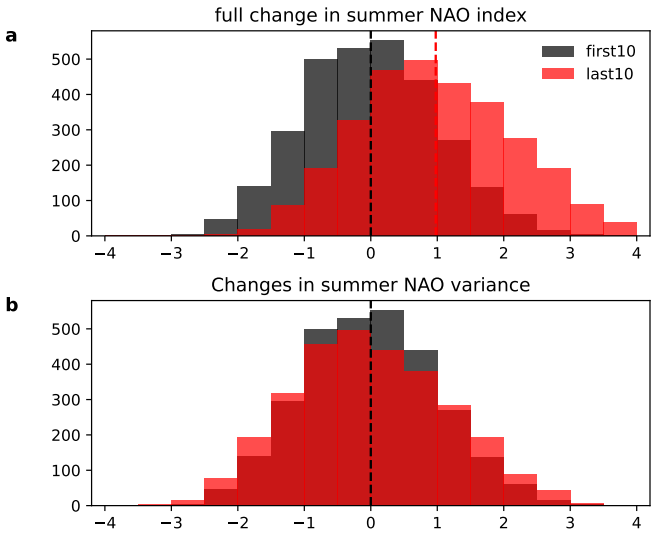

Supplementary Figure. A4: **Full response of the summer NAO to global warming in MPI_GE**. **a** Changes in the summer NAO index that is generated by 500 hPa geopotential height data without removing the ensemble mean. Dashed lines show the climatology for the first 10 (black) and last 10 years (red) of the simulations. **b** As is **a**, but with the mean of the NAO index removed. **c**, as **a**, but for the NAO index during which the eddy-driven jet stream is more northly than the climatology of the first 10 years. **d**, same as **c**, but for Greenland blocking index.

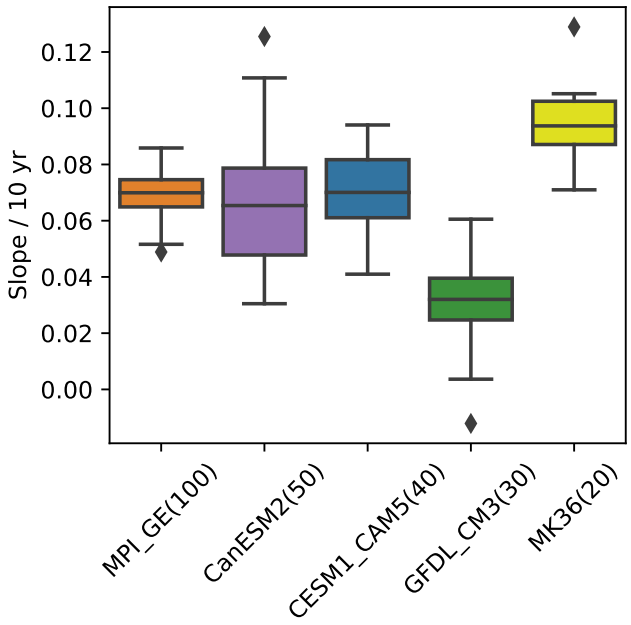

Supplementary Figure. A5: **Positive trends in the time-mean state of the summer NAO index** Slope on the y-axis represents the linear trend across the whole time span. Spread of the box plot indicate the range of the responses across different ensemble members. The box extends from the first quartile to the third quartile of the data, with a line at the median. The whiskers extend from the box to the farthest data point lying within 1.5x the inter-quartile range from the box. Diamonds represent outliers.

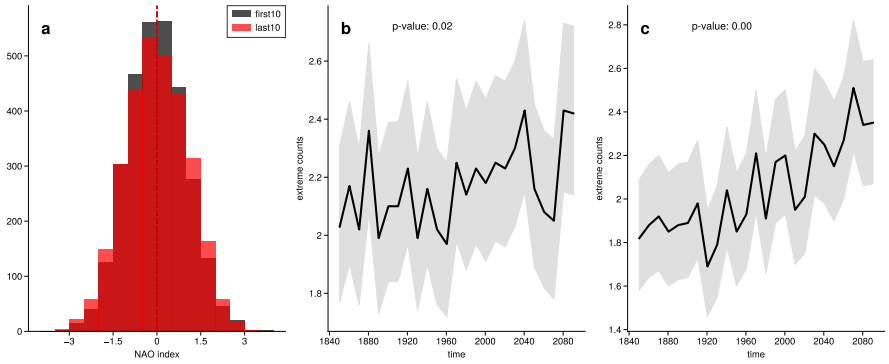

Supplementary Figure. A6: **Increasing summer NAO extremes from NAO index using the difference between two boxes (**$25°W - 5°E, 45°N - 55°N$**) and (**$52 - 22°W, 60°N - 70°N$**) [dunstone2023SNAOpredict_supply].** **a** NAO index distribution of the pre-industrial climate (1850-1859) and (2090-2099). Shading shows the 5-95% confidence interval based on bootstrapping. **b** Evolution of the occurrence of positive summer NAO extremes. **c**, as **a**, but for negative summer NAO extremes.

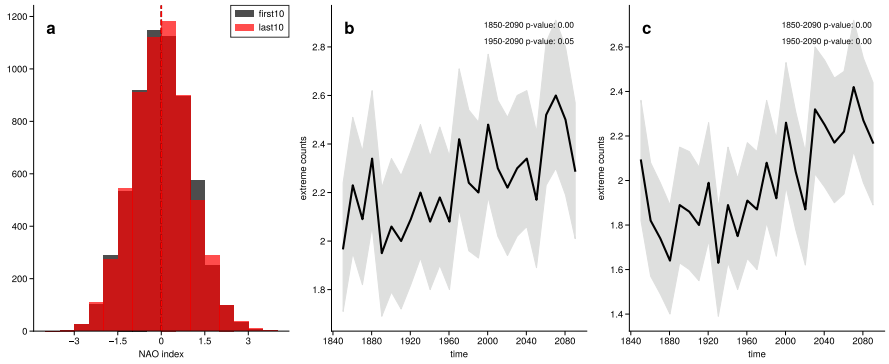

Supplementary Figure. A7: **Increasing occurrence of summer NAO extremes in a moderate warming scenario.** **a**, The NAO index in the historical and Representative Concentration Pathway (RCP) 4.5 scenario of MPI_GE. **b**, The evolution of the occurrence of the positive NAO extremes every non-overlapping 10 years. Shading represents the $5\% - 95\%$ confidence interval based on bootstrapping, see Methods. **c**, As is **b**, but for negative summer NAO extremes. P-values $\leqslant 0.05$ indicate statistical significance at 5% level.

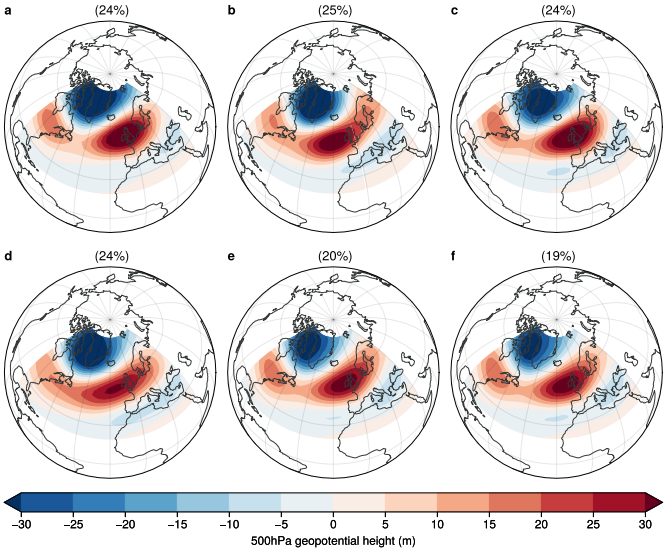

Supplementary Figure. A8: **The spatial patterns of the NAO when all the data (all the summer months and all the ensemble members) are used.** The spatial patterns of the NAO in (**a**) CanESM2, (**b**) CESM-CAM5, (**c**) MK3.6, (**d**) GFDL_CM3, (**e**) MPI_GE_onepct, and (**f**) MPI_GE. The percentage in the brackes shows the explained variance.

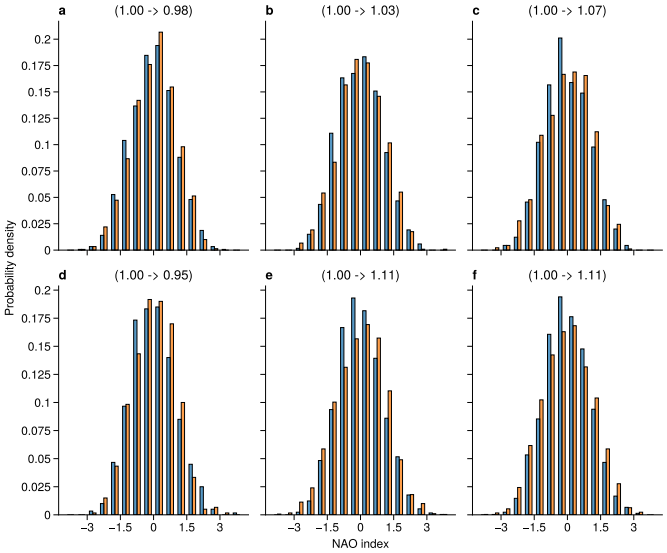

Supplementary Figure. A9: The distribution of the NAO using the fixed spatial patterns from Supplementary Figure. A8, correspondingly for (**a**) CanESM2, (**b**) CESM-CAM5, (**c**) MK3.6, (**d**) GFDL_CM3, (**e**) MPI_GE_onepct, and (**f**) MPI_GE. The numbers in brackets show the changes in the standard deviation. Significance tests were not implemented here due to the high computational load.

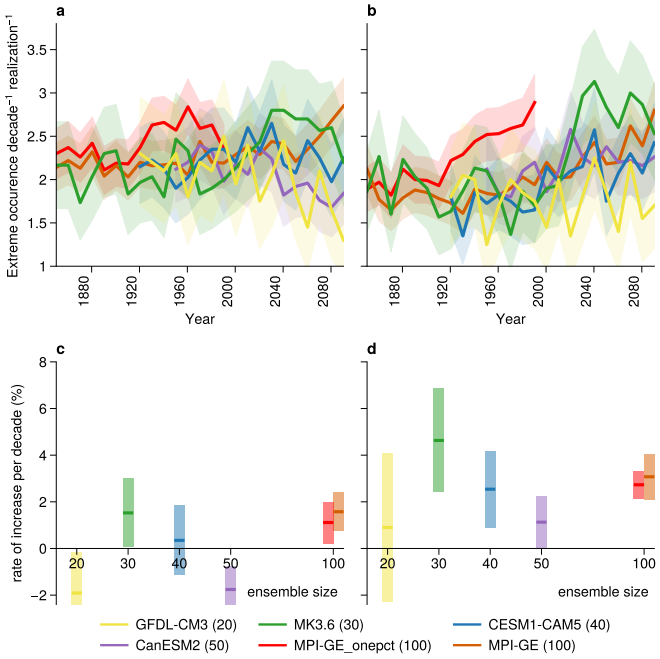

Supplementary Figure. A10: **Changes in the extreme NAO occurrence when the fixed spatial pattern is used to generated the NAO index.** The temporal evolution of the extreme NAO occurrence for positive phase (**a**) and for negative phase (**b**). Shading represent 5% – 95% confidence interval based on bootstrapping. The increase rate per decade in the extreme NAO occurrence for positive phase (**c**) and for negative phase (**d**). Shading represent 5% – 95% confidence interval based on student-t test.

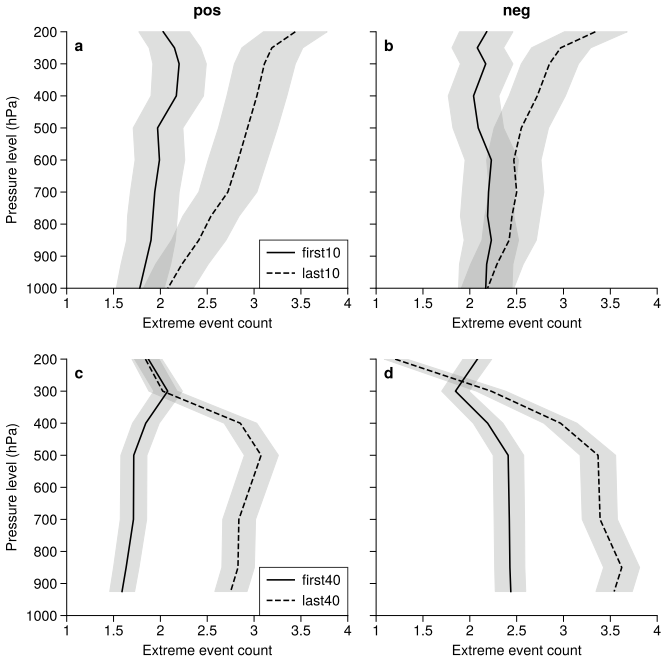

Supplementary Figure. A11: **The increased occurrence of extreme summer NAO events in troposphere in simulations in MPI_GE and all ensemble members of 20CR.** **a,** Profile of the increase in the occurrence of the positive extreme NAO events in MPI_GE. **b,** Same as (**a**), but for negative extreme NAO events. **c,** Profile of the increase in the occurrence of the positive extreme NAO events in all ensemble members of 20CR. **d,** Same as (**c**), but for negative extreme NAO events. Shaded areas represent $5\% - 95\%$ confidence interval based on bootstrapping.

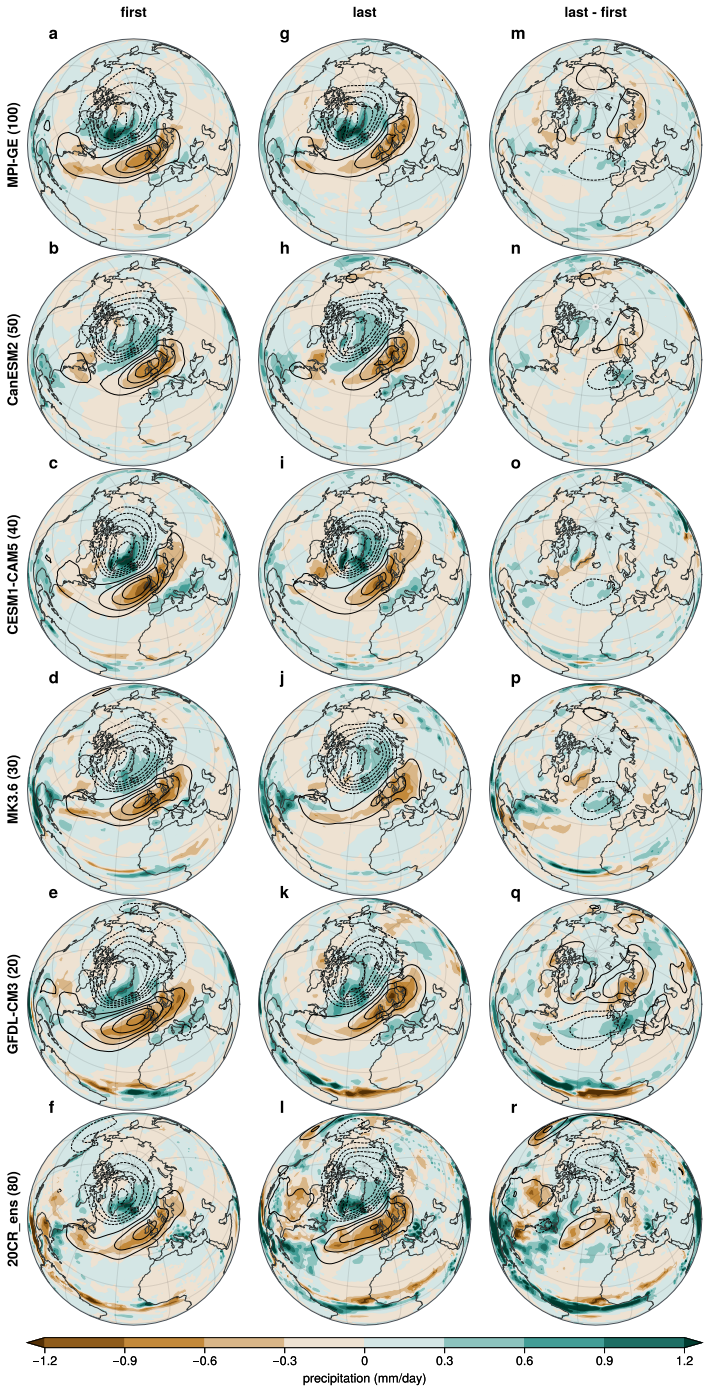

Supplementary Figure. A12: **The impact of positive summer NAO extremes on precipitation and sea level pressure. a-e,** The impact of positive NAO extremes on precipitation (colors) and sea level pressure (lines) in the first 10 years of simulations from different Earth System Models. Contours are drawn at intervals of 1 hPa, ranging from -5 hPa to 5 hPa, excluding the 0 hPa contour. **g-k,** Same as (**a-e**), but for the last 10 years of the simulations. **m-q,** The difference between the last 10 years and the first 10 years. **f**, The impact of positive NAO extremes on the precipitation in the first 40 years (1850-1889) of 20CR with all ensemble members. **l**, Same as (**f**) but for the last 40 years (1976-2015). **r**, The difference between the last 40 years and the first 40 years in the 20CR_ens. None of the differences are statistically significant.

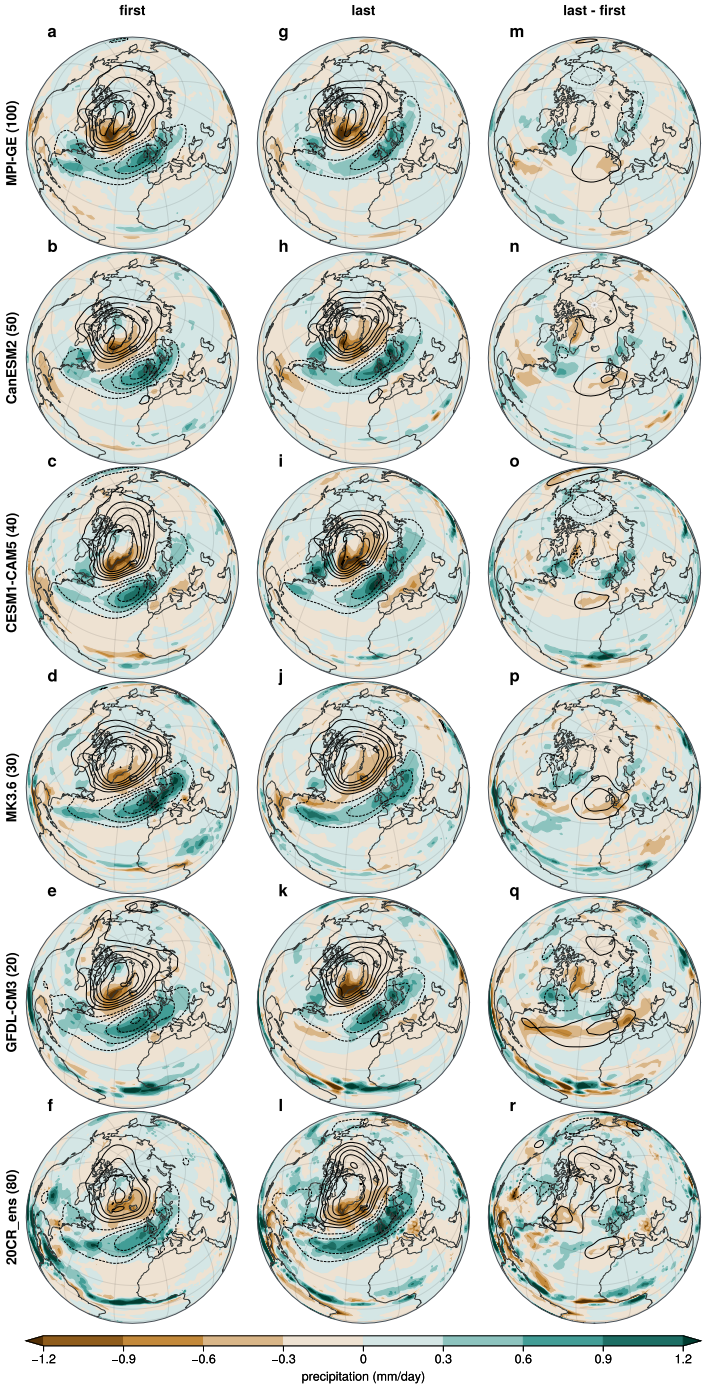

Supplementary Figure. A13: Same as Figure. A4 but for negative summer NAO extremes.

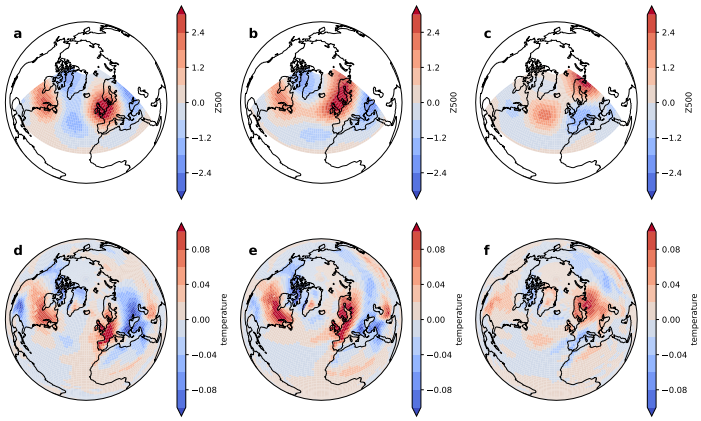

Supplementary Figure. A14: **Singular Value Decomposition (SVD) between 500 hPa geopotential height (Z500) and surface temperature in MPI_GE. a,** The left SVD mode pattern, corresponding to the summer NAO pattern, in 1850-1859. **b,** Same as (**a**), but for the 2090-2099. **c,** The difference between the **b** and **a**. **d**, The right SVD mode pattern, corresponding to the surface temperature, in 1850-1859 of MPI_GE. **e**, Same as (**d**) but for 2090-2099. **f**, The difference between **e** and **d**. All values are normalized with their mean and standard deviation.

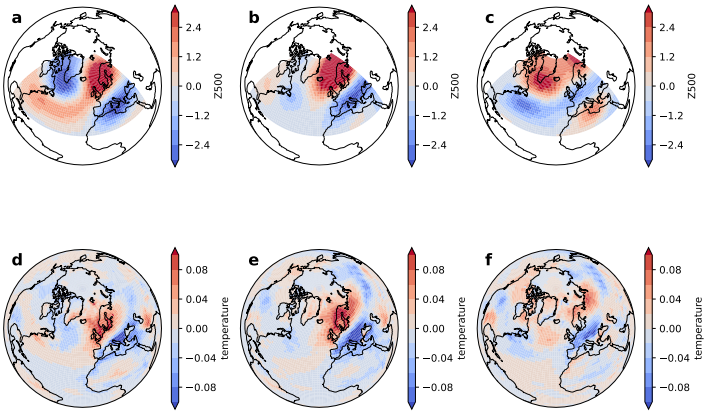

Supplementary Figure. A15: Same as Figure. A14 but the Z500 is one month leading the surface temperature.

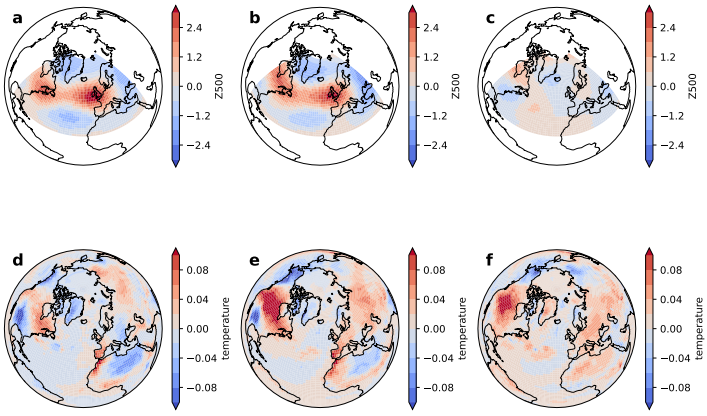

Supplementary Figure. A16: Same as Figure. A14 but the Z500 is one month lagging the surface temperature.

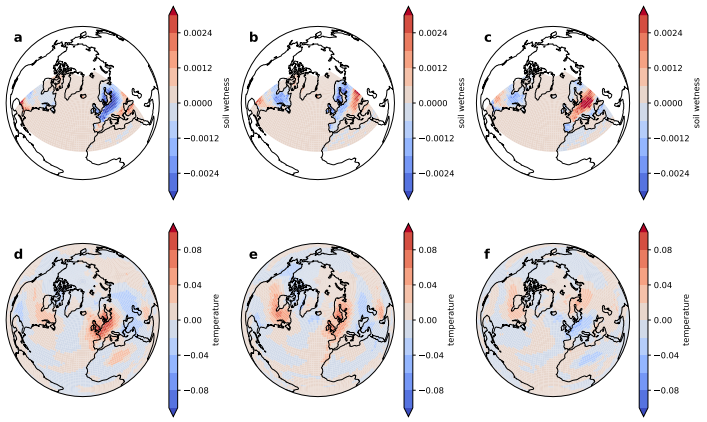

Supplementary Figure. A17: **Singular Value Decomposition (SVD) between soil wetness and surface temperature in MPI_GE. a,** The left SVD mode pattern, corresponding to soil wetness, in 1850-1859. **b,** Same as (**a**), but for the 2090-2099. **c,** The difference between the **b** and **a**. **d**, The right eof mode pattern of the SVD, corresponding to surface temperature, in 1850-1859 of MPI_GE. **e**, Same as (**d**) but for 2090-2099. **f**, The difference between **e** and **d**. All values are normalized with their mean and standard deviation.

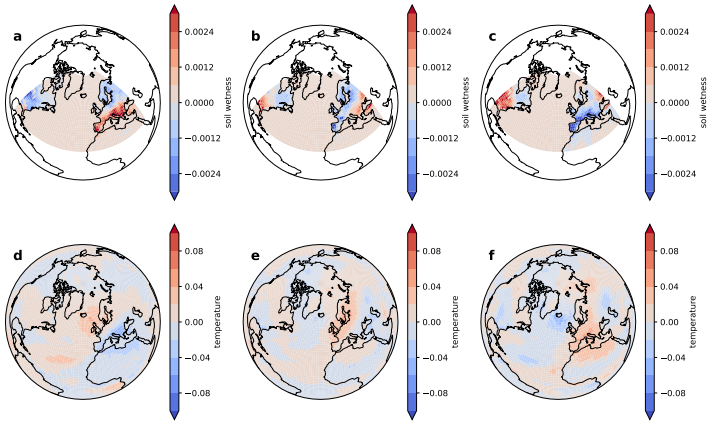

Supplementary Figure. A18: Same as Figure. A17 but the soil wetness is one month leading the surface temperature.

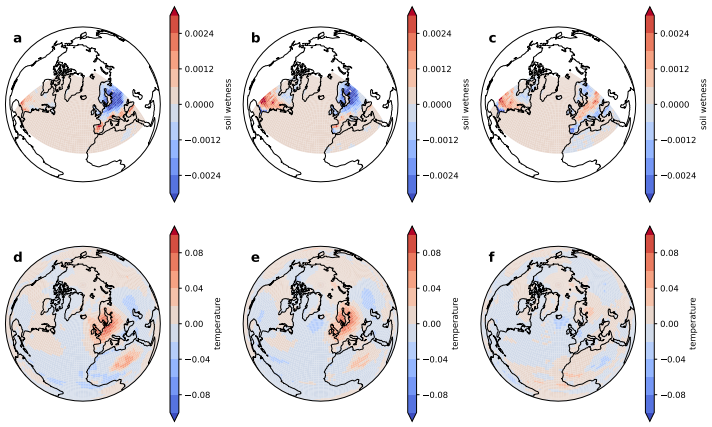

Supplementary Figure. A19: Same as Figure. A17 but the soil wetness is one month lagging the surface temperature.

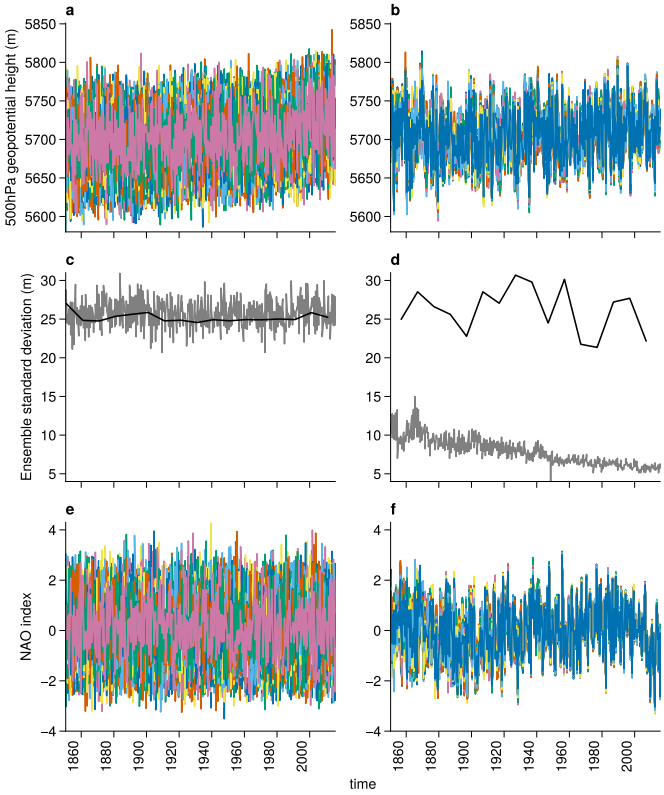

Supplementary Figure. A20: **The 20CR can not fully represent the NAO variability along the ensemble dimension. a** The evolution of the average 500 hPa geopotential height over the south center of action of the NAO ([-30, 10, 40,60]) for all the ensemble members in the MPI_GE during the historical period (1850-2015). Each colored line represents one realization. **b** Same as **a** but for the 20CR. **c** The evolution of the standard deviation of all ensemble members for every ten years (black line) and every year (grey line) in the MPI_GE. **d** Same as **c** but for the 20CR. **e** The evolution of the NAO index in all the ensemble members for the MPI_GE. **f** Same as **e** but for the 20CR.

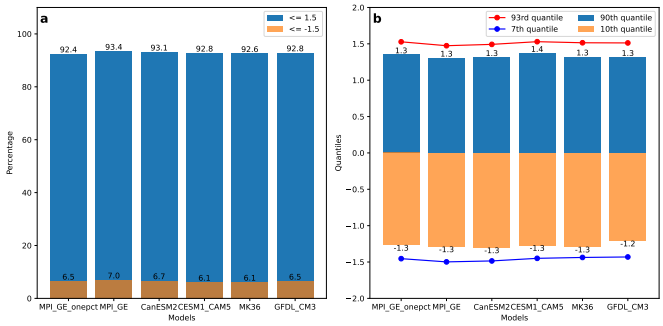

Supplementary Figure. A21: **Thresholds based on standard deviation versus those based on percentage.** **a** The corresponding percentile-based thresholds for 1.5 standard deviation and -1.5 standard deviation for all the simulations. **b** The 90th and 10th quantiles of the summer NAO index in the first 10 years of the simulations are shown as bars, and the 93rd and 7th quantiles of the summer NOA index in the first 10 years of the simulations, which roughly correspond to 1.5 standard deviations, are shown as lines.

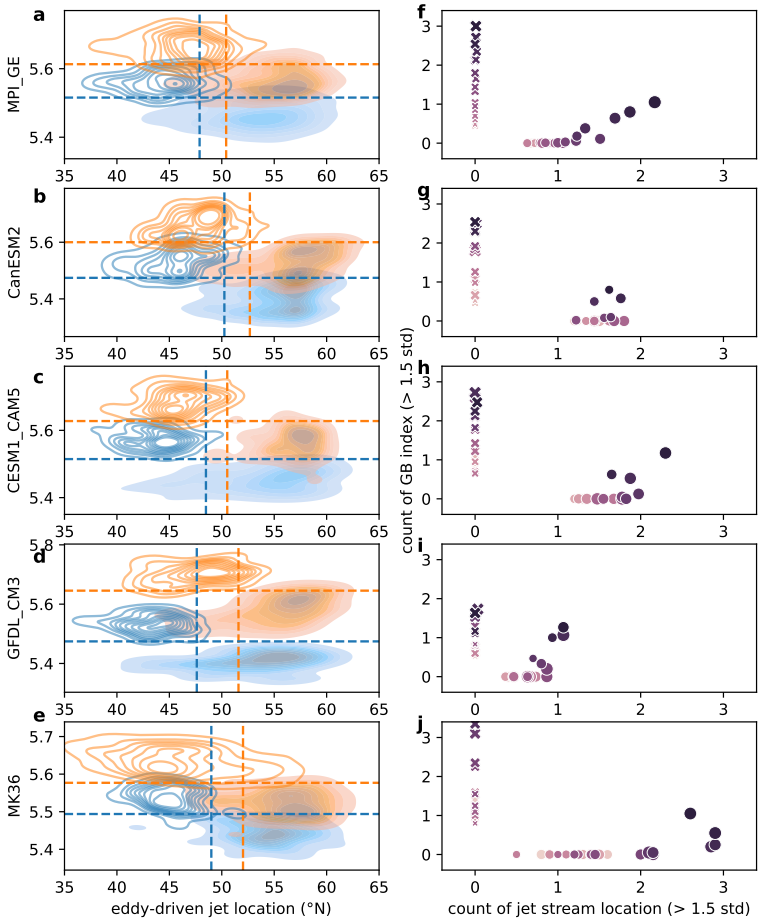

Supplementary Figure. A22: **Changes in flow regimes and NAO extremes for other LEs.** Density plot for occurrence of NAO extremes as a function of eddy-driven jet location (x-axis) and Greenland blocking index (y-axis), correspondingly for MPI_GE (**a**), CanESM2 (**b**), CESM1_CAM5 (**c**), GFDL_CM3 (**d**), and MK36 (**e**). **f-j**, same order as **a-e**, but shown as the occurrence of the NAO extremes as a function of count of jet stream location more northly than 1.5 standard deviation of the first 10 years (x-axis) and count of Greenland blocking index higher than 1.5 standard deviation of the first 10 years (y-axis). The counts are divided by the corresponding ensemble size. Legends are the same as the Main text Figure. A6e

B

CHANGES IN ATMOSPHERIC EDDIES BY GLOBAL WARMING CONTRIBUTE TO MORE SUMMER NORTH ATLANTIC OSCILLATION EXTREMES

The attached manuscript is a work in preparation:

Liu, Q., Bader, J., Jungclaus, J.H., Matei, D. Changes in atmospheric eddies contribute to more summertime North Atlantic Oscillation extremes. Manuscript in preparation. 2025.

Quan Liu[1,2], *Jürgen Bader*[3], *Johann H. Jungclaus*[1], *Daniela Matei*[1]

[1]Climate Variability Department, Max Planck Institute for Meteorology, Hamburg, Germany
[2]International Max Planck Research School on Earth System Modelling, Hamburg, Germany
[3]Institute of Oceanography, Center for Earth System Research and Sustainability (CEN), Universität Hamburg, Germany

ABSTRACT

The occurrence of the summer North Atlantic Oscillation increase in a transient warming climate. This enhancement would causes more contrasting severe weather over different parts of Europe, but the driving mechanism is yet to be understood. We conduct composite analysis that is physically motivated by “eddy-mean-flow" interactions using daily output of one large ensemble climate change simulations. We show that transient eddies directly drive the summer NAO variability through momentum forcing at upper-level. These transient eddies arise from lower-level baroclinicity, which is sustained by a positive thermal feedback from quasi-stationary eddies. Under global warming, the variability of the thermal feedback by quasi-stationary eddies increase, likely in response to an enhanced land-ocean temperature contrast, ultimately leading to the increase in the summer NAO extremes. Our study underscores the role of eddy fluxes in explaining the atmospheric response to global warming.

B.1 INTRODUCTION

The regional atmospheric response to global warming remains a major source of uncertainty in climate projection [28, 75, 79, 80, 100]. Over the North Atlantic, the anthropogenic forced changes in the atmospheric circulation appear to project strongly onto the internally generated mode of North Atlantic Oscillation (NAO) [21, 63, 80]. Such a NAO-like response manifests itself as a long-term trend in the NAO index [27, 37, 48, 52, 64]. However, in a transient warming climate, the summertime NAO index further shows an enhancement in its variability[48]. Such a secondary NAO response to global warming would have profound impacts on Europe, leading to less reliable weather forecast and higher probability of contrasting severe weather over different regions. Although the enhanced summer NAO variability is consistently predicted by different climate models [48], an understanding of the driving mechanism is missing.

Previous studies have shown that the thermal wind balance can be used to explain the changes in the upper-level zonal jet stream winds [45, 76], but it cannot be used to explain changes in the variability of the summer NAO. This is because the thermal wind balance is built on the equilibrium states rather than transient states. Studies based on simple dynamic models suggest that the variability of the NAO arise from “eddy-mean-flow" interactions [68, 90, 102]. The enhancement in the summer NAO variability, therefore, may be interpreted through changes in its eddy forcing.

Eddies with different frequencies play different roles in sustaining atmospheric variability mode [58, 102]. Generally, the eddies can be characterized by (i) transient eddies with temporal periods of less

than 12 days and with wavenumber typically larger than 6, and (ii) quasi-stationary eddies with normally smaller wave numbers. These two types of eddies rise from different processes. The transient eddies rise from the lower-level baroclinic instability, while the quasi-stationary eddies rise from the asymmetric distribution of the thermal feedback, such as land-ocean contrast [38]. The North Atlantic sector experiences both a maximum of the transient eddy kinetic energy (Supplementary Figure. B1a) and a trough of quasi-stationary eddies with wave number 3 (Supplementary Figure. B1b).

In this study, we investigate the eddy forcing of the summer NAO variability by both types of eddies. Moreover, we investigate how changes in this eddy forcing by global warming lead to more summer NAO extreme events. Using daily output from the Coupled Model Intercomparison Project Phase 6 version of the Max Planck Institute for meteorology Grand Ensemble (MPI_GE_CMIP6), we extract the prolonged summer NAO extremes as periods when the index exceeds ± 1.5 standard deviations for more than five consecutive days—above 1.5 for the positive phase and below –1.5 for the negative phase. We obtain the transient eddies by applying band-filter of 2-12 days along time dimension, and the quasi-stationary eddies as zonal anomaly of the 30-day running mean of the daily data.

B.2 RESULTS

B.2.1 *Summer NAO variability, upper-level jet, and lower-level baroclinicity.*

we begin by showing that the summer NAO is associated with the zonal jet stream winds at upper-level. During positive summer NAO extremes, the subpolar jet stream tilts northeast-southwest towards Northern Europe, separating from the subtropical jet (Figure. B1a). Conversely, during negative summer NAO extremes, the subpolar jet merges with the subtropical jet, forming a continuous zonal belt of a single jet stream (Figure. B1b). Therefore, consistent with its winter counterpart [98], the variability of the summer NAO is essentially linked to the meridional displacement of upper-level subpolar jet (Figure. B1c).

Similarly, the summer NAO is associated with the baroclinicity at lower-level. Here, the lower level baroclinicity is approximated with the Eady growth rate at 850 hPa (Methods) [35]. During positive NAO extremes, there is a local maximum of the Eady growth rate over North America continent between [50 - 70 °N] (Figure. B1d), coinciding with the local maximum of the zonal jet stream wind at upper level (Figure. B1d). Conversely, during negative summer NAO extremes, the Eady growth rate over high latitudes of the North America decreases, and that over North Europe between [40-60 °N] in-

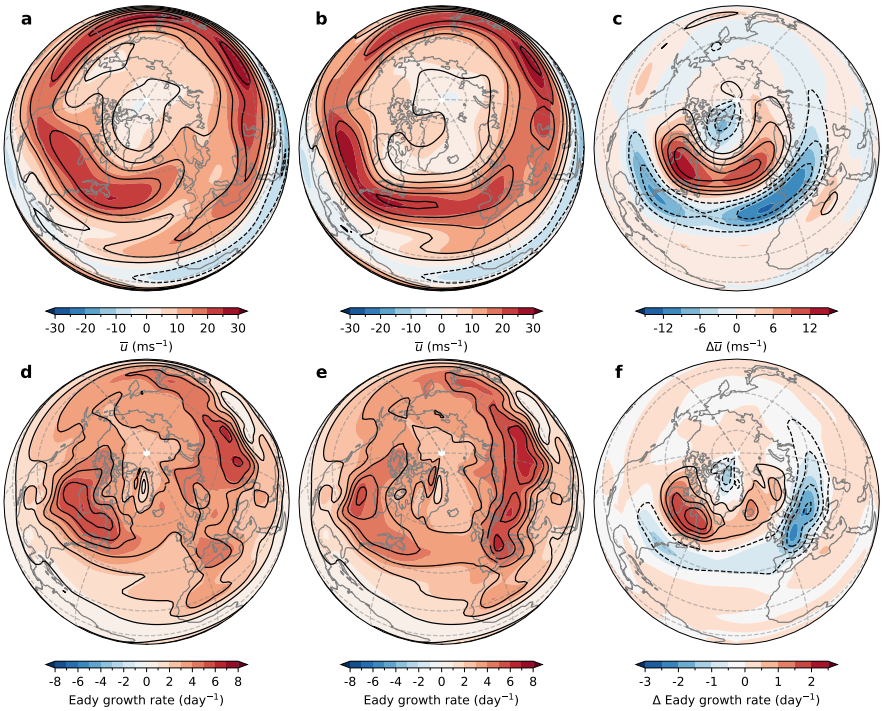

Figure. B1: **The variability of the summer NAO is associated with the variability of the upper-level jet and lower-level baroclinicity.** **a**, Composite mean of the zonal wind (unit: ms^{-1}) at 250 hPa for the positive summer NAO extremes. Shadings show the first 10 years (1850-1859), contours show the last 10 years (2090-2099). Contours share the same intervals as the shadings, eliminating 0 m/s. **b**, Composite mean of the zonal wind at 250 hPa for the negative summer NAO extremes. **c**, The difference between **b** and **a**. **d**, Composite mean of the Eady growth rate (unit: day^{-1}) at 850 hPa for the positive summer NAO extremes. shadings for the first 10 years, and contours for the last 10 years. Contours share the same intervals as the shadings, eliminating 0 day^{-1}. **e**, Composite mean of the Eady growth rate at 850 hPa for the negative summer NAO extremes. **f**, Difference between **e** and **d**.

creases (Figure. B1e), coinciding with the extension of the zonal jet stream at the upper level (Figure. B1e). Therefore, the NAO variability is also linked to the fluctuations in the lower-level baroclinicity (Figure. B1f).

Connections to both the upper-level jet and the lower-level baroclinicity underscore different aspects of the eddy forcing of the summer NAO variability. The associated upper-level jet variability highlights the effect of the eddy momentum forcing, because it is driven by the anomalous convergence of eddy momentum flux $\overline{u'v'}$, as is shown in the zonal momentum equation for a non divergent (quasi-geostrophic) flow:

$$\frac{\partial \overline{u}}{\partial t} = f_0 \overline{v} - \frac{\partial}{\partial y} \overline{u'v'} + \overline{F} \tag{5}$$

where (u, v) are the horizontal velocity, $\overline{F}$ represents frictional term. Hats and primes denote respectively the mean and eddy components of the flow. Meanwhile, the associated fluctuation of the lower-baroclincity highlights the eddy heat forcing, because it is related to eddy heat flux $\overline{v'\theta'}$, as is shown in the meridional derivative of the zonal-mean thermodynamic equation [38, 58]:

$$\frac{\partial}{\partial t}\left(-\frac{\partial \overline{\theta}}{\partial y}\right) = \frac{\partial^2}{\partial y^2}\overline{v'\theta'} - \frac{\partial}{\partial y}\left(\Gamma\,\overline{\omega}\right) - \mathcal{R} \tag{6}$$

where $\Gamma = -T\dfrac{\partial \ln \theta}{\partial p}$ is the static stability parameter; ω represents vertical velocity; $\mathcal{R}$ represents diabatic heating.

Therefore, the eddy forcing of the summer NAO variability can be partitioned into upper-level momentum forcing, and the lower-level thermal feedback. These two aspects are not distinct, as the lower-level baroclinicity is the source of the transient eddies that propagate upwards [38, 60]. These generated transient eddies, which are associated with lows and highs, transport warm air poleward and cold air equator. Therefore, they act to weaken the meridional temperature gradient and the baroclinicity, limiting the further eddy generation—a negative eddy feedback [68, 102]. However, during summer NAO extremes—which, by definition, are prolonged—baroclinicity must be sustained. In the following, we show the different roles of the transient eddies and quasi-stationary eddies in exerting the eddy forcing.

B.2.2 *upper-level eddy momentum forcing of the summer NAO*

The eddy momentum forcing is quantified by the convergence of the eddy momentum flux (the second term on the right hand side of equation 5). The composite means of the anomalous eddy momentum forcing across different phases of summer NAO extremes exhibit dipolar-like patterns in their zonal means (Figure. B2). At high latitudes, the positive summer NAO extremes are associated with an anomalous convergence of the eddy momentum flux (Figure. B2a), while the negative summer NAO extremes are associated with an anomalous divergence (Figure. B2d). We then decompose this momentum forcing into that from transient eddies and that from quasi-stationary eddies. At upper level, the eddy momentum forcing of the summer NAO extremes is dominated by transient eddies (Figure. B2b, e), while that from quasi-stationary eddies plays a secondary role (Figure. B2c, f).

To establish the casual link between the anomalous eddy momentum forcing and the occurrence of the summer NAO extremes, we

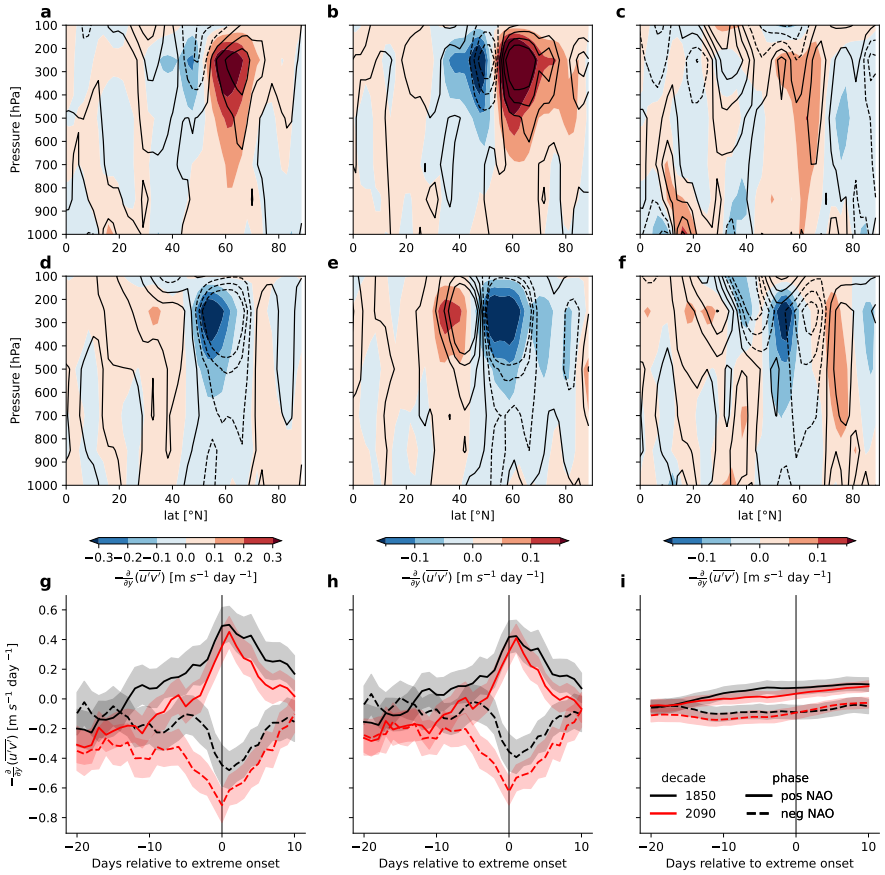

Figure. B2: **Dipolar-like pattern in anomalous eddy momentum forcing is causing occurrence of summer NAO extremes. a**, Zonal average of the composite mean of the anomalous convergence of the total (transient eddies and quasi-stationary eddies) eddy momentum flux for the positive summer NAO extremes. The composite mean is calculated as an average over a time window of (-10, 5) days relative to the onset of all the identified extreme events. Colors for the first 10 years (1850-1859) and contours for the last 10 years (2090-2099) of the simulations. **b**, Same as **a**, but only for the transient eddies. **c**, Same as **a**, but only for the quasi-stationary eddies. **d-f**, Same as **a-c**, but for the negative summer NAO extremes. **g**, The anomalous convergence of the total eddy momentum flux at 250 hPa zonally averaged over [50 - 70 °N] as a function of time relative to the onset of the summer NAO extremes. **h**, Same as **g**, but only for the transient eddies. **i**, Same as **g**, but only for the quasi-stationary eddies.

plot its spatial average over high latitudes ([50 - 70 ° N]) as a function of time relative to the onset of the summer NAO extremes (Figure. B2g-i). The latitudes are chosen to encompass the northern center of actions of the dipolar-like pattern identified in Figure. B2b. The eddy momentum forcing is indeed a driving factor in the occurrence of summer NAO extremes, as it begins to diverge from its climatological state roughly 10 days before the onset of the positive and negative

phases (Figure. B2g). Consistent with the profile of the composite mean (Figure. B2a-f), the transient eddies are playing a leading role, and the quasi-stationary eddies are playing a secondary role.

B.2.3 *lower-level eddy thermal feedback of the summer NAO*

The eddies also modulate the summer NAO variability by changing the lower-level baroclinicity through eddy thermal feedback. The eddy thermal feedback is represented by the second meridional derivative of the eddy heat flux (the first term on the right hand side of equation 6). However, we present the zonal mean of the composite anomalous first derivative instead since the second derivative is very noisy (Figure. B3a-f). The second derivative can be inferred from the locations where the sign of the first derivative flips. To illustrate that the eddy thermal feedback is an driving effect in the occurrence of the summer NAO extremes, we plot the zonal mean value of the second derivative averaged between [50-70 °N] as a function of time relative to the onset of the summer NAO extremes (Figure. B3g-i), consistent with the region used for the momentum forcing analysis.

Transient eddies indeed exert a negative feedback. During the development of positive summer NAO extremes, they transport warm air poleward, weakening the lower-level baroclinicity and thus acting as a negative forcing on the positive extreme event (solid lines, Figure B3h). Conversely, during negative NAO extremes, the baroclinicity shifts equatorward (Figure B2f). Transient eddies respond by transporting cold air equatorward, enhancing the baroclinicity at higher latitudes and pushing it poleward, thereby also exerting a negative feedback on the negative extreme event (dashed lines, Figure B3h).

To support a sustained generation of transient eddies during the prolonged summer NAO extremes, the baroclinicity must be maintained. We show that it is the quasi-stationary eddies that fulfill this role. 15 days or so prior to the onset of the positive summer NAO extremes, the quasi-stationary eddies start to exert a positive forcing to the mean flow, enhancing the lower-level baroclinicity (solid lines, Figure. B3i). The anomalous positive forcing by the quasi-stationary eddies offsets the anomalous negative forcing from the transient eddies. As a result, there is a net positive anomaly of the eddy thermal feedback prior to the onset of the positive summer NAO extremes (solid line, Figure. B3g), that maintains the lower level baroclinicity. Conversely, for negative phase of the summer NAO extremes, the upper-level jet weakens and shifts equatorward, due to a reduced convergence of the eddy momentum flux (Figure. B2d-f). This reduced eddy generation is mainly caused by an anomalous negative thermal feedback to the baroclinicity by quasi-stationary eddies at high latitudes, which begins 15 days or so prior to the onset (Figure. B3i).

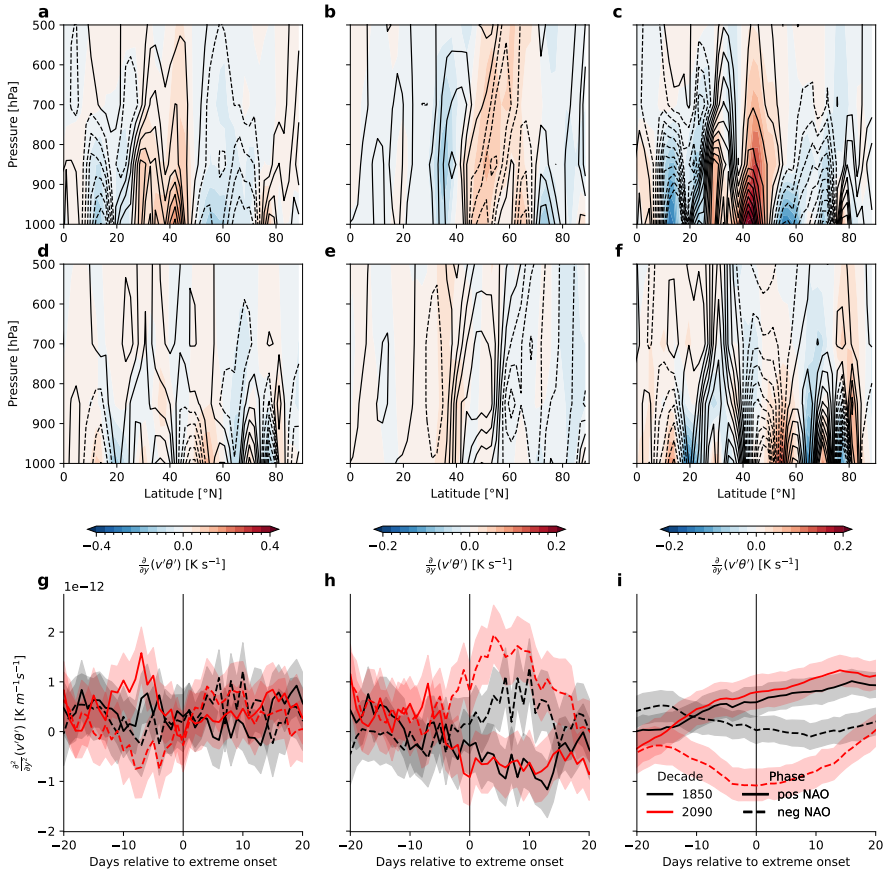

Figure. B3: **Lower-level eddy thermal feedback is primarily contributed by quasi-stationary eddies. a**, Zonal average of the composite mean of the anomalous convergence of the total (transient eddies and quasi-stationary eddies) eddy heat flux for the positive summer NAO extremes. The composite mean is calculated as an average over a time window of (-10, 5) days relative to the onset of all the identified extreme events. Colors for the first 10 years (1850-1859) and contours for the last 10 years (2090-2099) of the simulations. **b**, Same as **a**, but only for the transient eddies. **c**, Same as **a**, but only for the quasi-stationary eddies. **d**-**f**, Same as **a**-**c**, but for the negative summer NAO extremes. **g**, The anomalous convergence of the total eddy heat flux at 850 hPa zonally averaged over [40 - 60 °N] as a function of time relative to the onset of the summer NAO extremes. **h**, Same as **g**, but only for the transient eddies. **i**, Same as **g**, but only for the quasi-stationary eddies.

B.2.4 *Changes in the eddy forcing of summer NAO under global warming*

So far, we have shown that the summer NAO variability is associated with the meridional displacement of the upper-level zonal jet, which is primarily driven by anomalous eddy momentum forcing from the transient eddies. These eddies arise from the lower-level baroclinic instability, which is mainly sustained by the quasi-stationary eddies.

The fact that different types of eddies play different roles in modulating the summer NAO variability provides a basis for understanding the projected enhancement in the variability of the summer NAO.

Under global warming, the occurrence of the summer NAO extremes increases for both the positive and negative phases — an evidence of enhanced summer NAO variability on daily timescale (Figure. B4a). This increase is also supported by changes in the wave breaking events—precursors of the summer NAO extremes [67]. The anticyclonic wave breaking events occurring at the south flank of the jet over the east side of the North Atlantic region are precursors of the positive summer NAO extremes (Supplementary Figure. B2a-c). The cyclonic wave breaking occurring at the west side of the North Atlantic region are precursors of negative summer NAO extremes (Supplementary Figure. B2d-f). Under global warming, the occurrence of both the anticyclonic and cyclonic wave breaking events at high latitudes increases (Figure. B4b, Supplementary Figure. B3).

The increase in the summer NAO extremes can be traced to the increase in the variability of their eddy forcing. Under global warming, the variability of the upper-level eddy momentum forcing, especially that from the transient eddies, exhibits a strong non-linear increase (Figure. B4c). This increase is attributable to the non-linear increase in the variability of the lower-level eddy thermal feedback (Figure. B4d), which, via modulating the baroclinicity, determines the variability of the transient eddy generation. As has been shown in the previous section, the thermal feedback by quasi-stationary eddies is more important than the transient eddies.

Lastly, why does the eddy thermal feedback by quasi-stationary eddies become more variable under global warming? Although the near surface temperature increases everywhere, the pattern of change is not spatially uniform. One dominant feature of this heterogeneity is stronger warming over land than over ocean (Supplementary Figure. B4). As a result, when a zonally uniform warming signal is removed, the land-ocean temperature contrast is found to increase under climate change (Figure. B5a, b). This enhanced asymmetry modify the quasi-stationary eddies (Figure. B5c) and lead to changes in the eddy heat flux they carry (Figure. B4d).

B.3 CONCLUSION AND DISCUSSION

Using composite analysis that is physically motivated by eddy-mean-flow interactions, we show that the transient eddies and the quasi-stationary eddies are jointly driving the occurrence of the summer NAO extremes. Transient eddies forces the NAO variability through upper-level momentum flux convergence, while quasi-stationary eddies modulate it via lower-level heat flux. The different roles of the transient eddies and the quasi-stationary eddies in driving the sum-

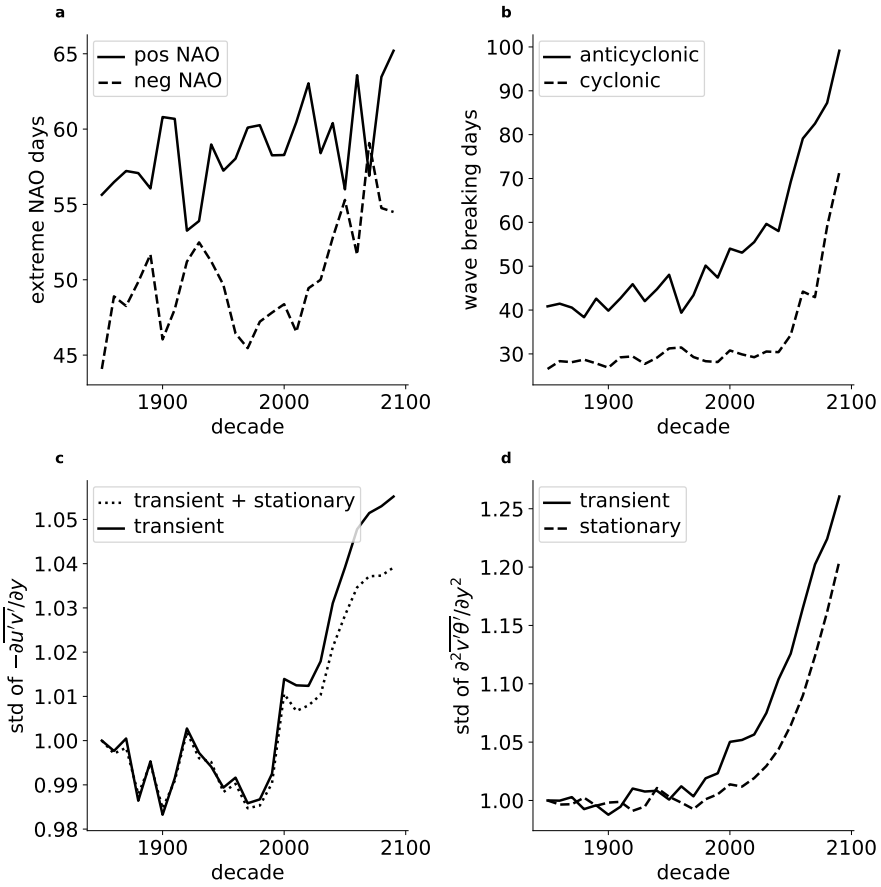

Figure. B4: **Changes in the eddy forcing due to global warming increase the occurrence of the summer NAO extremes. a**, The occurrence of the summer NAO extremes. **b** The occurrence of both anticyclonic and cyclonic wave breaking events. The events are counted from the spatial mean over ([-90, 40, 50, 70 °N]). **c**, Changes in the standard deviation of the eddy momentum forcing averaged over [-180, 180, 50, 70 °N] at 250 hPa. **d**, Changes in standard deviation of the eddy thermal feedback averaged over [-180, 180, 50, 70 °N] at 850 hPa. All the standard deviations are calculated across all the ensembles within each decade, and then scaled by the value in the first decade (1850-1859).

mer NAO variability were suggested by simple dynamic models [90, 102].

Moreover, we provide a chain of reasoning about why the summer NAO variability increases with global warming. We show that this enhancement can be traced back to the enhanced variability of the thermal feedback by quasi-stationary eddies, which is a direct response to the increased land-ocean temperature contrast under global warming. My interpretation advances our understanding of the large-scale atmospheric response to global warming: in addition to the traditional explanation based on changes in the meridional temperature gradient via thermal wind balance (e.g., [45, 76]), it highlights "eddy–mean-

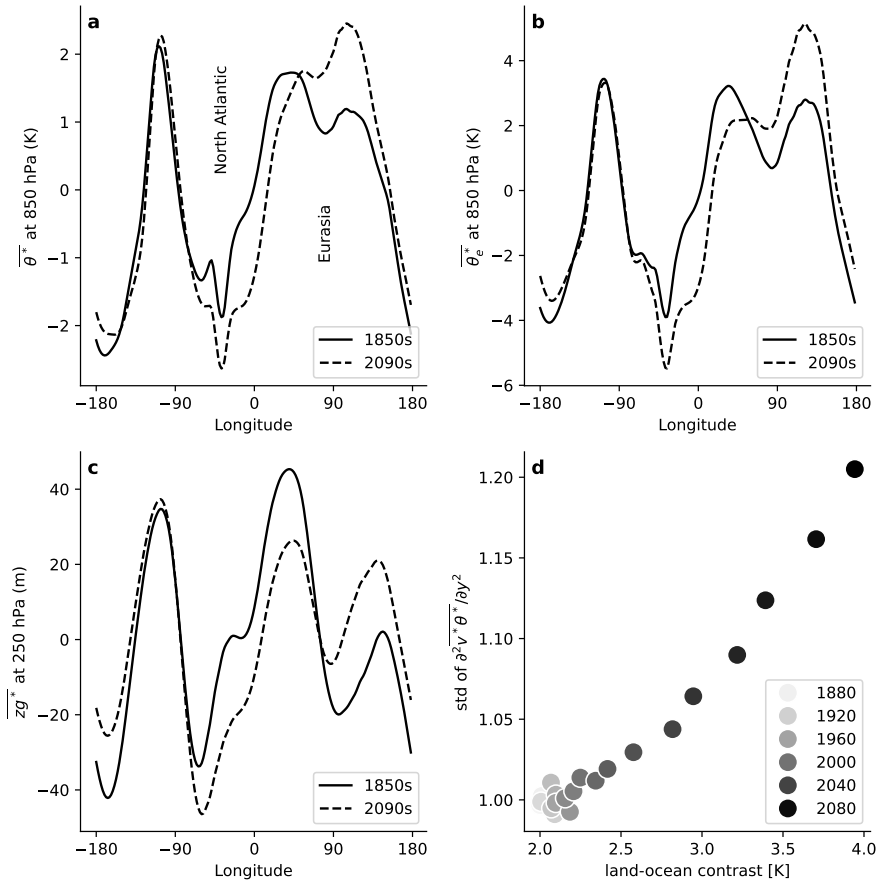

Figure. B5: **Increase in the land-ocean contrast under global warming induces changes in the quasi-stationary eddies. a**, Meridional mean of the zonal anomaly of the potential temperature ($\overline{\theta^*}$). **a**, Meridional mean of the zonal anomaly of the equivalent potential temperature ($\overline{\theta_e^*}$). **c**, Meridional mean of the zonal anomaly of the 250 hPa geopoential height ($\overline{zg^*}$), which shows quasi-stationary eddies with wavenumber 3. Overline represents meridional mean between [50-70 °N]. Asterisk represents zonal anomaly. The plots show the climatology during both decades across all ensemble members.

flow" interactions—specifically changes in the eddy fluxes of momentum and heat—as a fundamental dynamical framework.

B.4 METHODS

B.4.1 *Data*

We use daily output of CMIP6 version of the Max Planck Institute for Meteorology Large ensemble simulations (MPI_GE_CMIP6), forced by historical and further scenario of Shared Socioeconomic Pathways 585 (SSP585). We extracted NAO extremes that persist during June, July, and August. The jet stream and baroclinicity are calculated at

250 hPa and 850 hPa, respectively. The eddy fluxes of momentum and heat are calculated for the whole troposphere (1000 hPa - 100 hPa).

B.4.2 *NAO extreme events*

The pattern of the NAO is decomposed by applying the Empirical Orthogonal Functions (EOF) along the ensemble dimension of the monthly 500 hPa geopotential height data. The detailed process can be found in ref [48]. To obtain daily NAO index, we firstly subtract a varying seasonal cycle, which is a monthly mean over all ensemble members and every ten years, from the original daily data of the geopotential height. Then this daily anomalous geopotential data is projected onto the monthly NAO pattern to get the daily NAO index. Extreme events of the NAO are extracted when the value is above 1.5 standard deviations or below 1.5 standard deviations for the positive and negative phases, respectively, and lasts for at least 5 days, excluding a single exceptional day.

B.4.3 *Upper-level jet and lower-level baroclinicity*

The upper-level jet is represented with the climatology of the zonal wind at 250 hPa during each decade in all ensemble members. The baroclinicity is approximated by the Eady growth rate [35], which is defined as:

$$\sigma_E \approx 0.31 \cdot \frac{f}{N} \left| \frac{\partial \mathbf{v}}{\partial z} \right| \tag{7}$$

where σ_E is the Eady growth rate, f is the Coriolis parameter, N is the Brunt–Väisälä frequency, defined as $N = \sqrt{\frac{g}{\theta}\frac{\partial \theta}{\partial z}}$, where g is gravitational acceleration and θ is the potential temperature, $\frac{\partial \mathbf{v}}{\partial z}$ is the vertical shear of the wind, z is the vertical height, $\mathbf{v}$ is the horizontal wind. In this study, since we focus on the effects of the zonal mean of the eddy thermal feedback, only the vertical shear of the zonal wind ($\frac{\partial u}{\partial z}$) is used in the calculation. The low-level baroclinicity is represented as the Eady growth rate at 850 hPa.

B.4.4 *The transient eddies and the quasi-stationary eddies*

The prime terms (e.g., u', v', θ') for the transient eddies are calculated by applying band-pass filter of 2-12 days on the corresponding daily variable [67]. The prime terms for the quasi-stationary eddies are calculated by first applying a 30-day running mean to the original daily variable and then subtracting the zonal mean of the ensemble

mean of the filtered data from the filtered data themselves [47]. To account for the influence of water vapor transported by eddies, we use equivalent potential temperature instead of potential temperature in the calculation of eddy heat flux, following the approach used in the moist Eliassen–Palm (EP) flux formulation. [26, 101].

B.4.5 *Wave breaking events*

Wave breaking events are identified from the potential vorticity field on the 330 K isentropic surface [40, 94]. Only events with at least 50 % of their area located north of 40°N are retained to ensure their relevance to the subpolar jet. They are classified into anticyclonic wave breaking and cyclonic wave breaking, based on the sign of the eddy momentum flux by transient eddies [67].

SUPPLEMENTARY INFORMATION FOR APPENDIX B

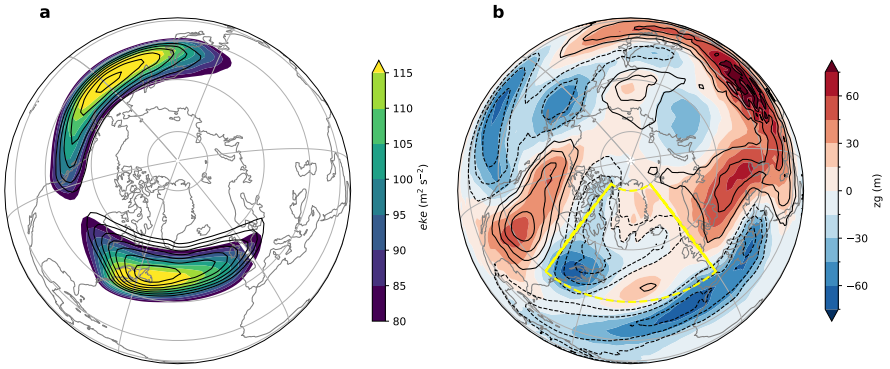

Supplementary Figure. B1: **Transient eddies and quasi-stationary eddies over the North Atlantic sector. a,** The climatology of the eddy kinetic energy of the transient eddies at 250 hPa. Data show the climate change simulations by MPI_GE_CMIP6 forced by histroical and SSP585 scenarios. Colors for first 10 years of the simulations (1850-1859), contours for the last 10 years of simulations (2090-2099). **b**, The zonal anomaly of geopotentail height shows a wavenumber 3 quasi-stationary eddy at 250 hPa. Colors for the first 10 years of simulations (1850-1859), contours for the last 10 years of simulations (2090-2099), with 0 line excluded. Yellow dashed line outlines the North Atlantic sector.

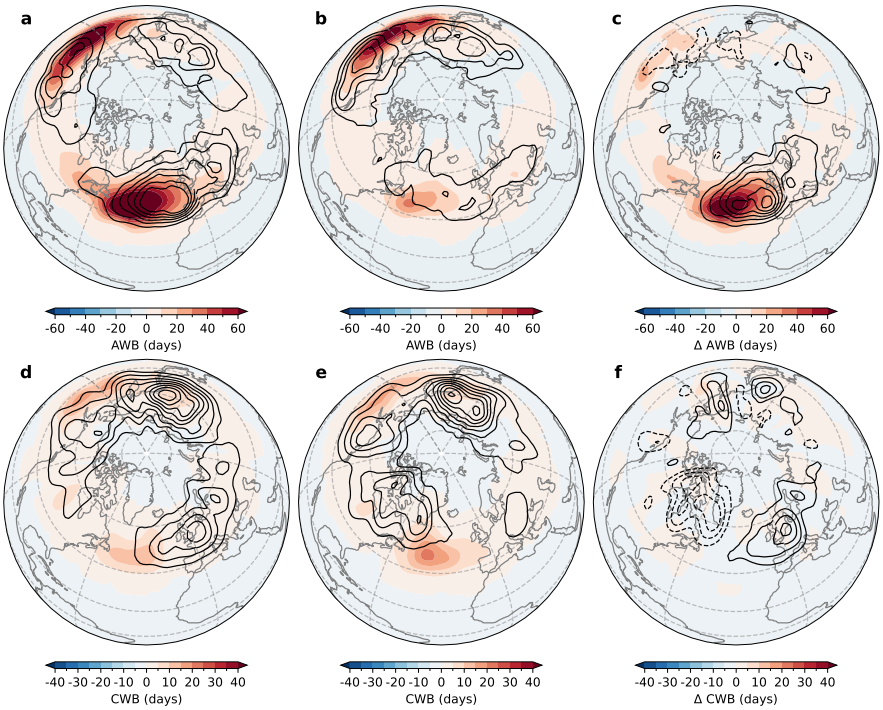

Supplementary Figure. B2: **Wave breaking events as precursors of the summer NAO extremes. a**, Sum of the occurrence of the anticyclonic wave breaking during [-10, 5] days relative to the positive summer NAO extremes. Shades for the first 10 years of the simulations (1850-1859), contours for the last 10 years of the simulations (2090-2099). **b**, Same as **a**, but for the negative summer NAO extremes. **c**, The difference between the **b** and **a**. **d**-**f**, Same as **a**-**c**, but for the cyclonic wave breaking.

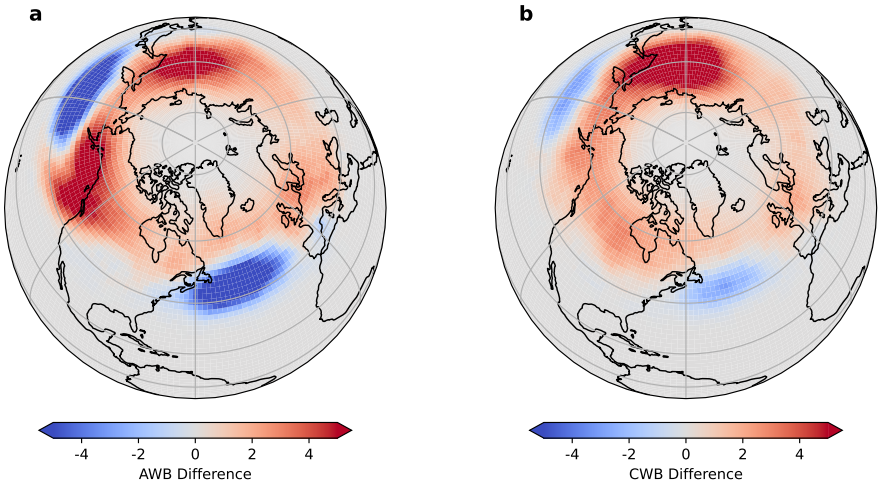

Supplementary Figure. B3: **Changes in the wave breaking events under global warming. a,** Difference of the occurrence of the anticlcylonic wave breaking between the last 10 years of the simulations (2090-2099) and the first 10 years of the simulations (1850-1859). **b**, Same as **a**, but for the cyclonic wave breaking.

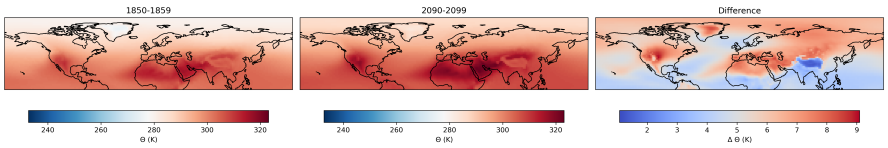

Supplementary Figure. B4: **Global warming enhances land-ocean temperature contrast. a,** The potential temperature at 850 hPa in the first 10 years of simulations (1850-1859). **b**, The potential temperature at 850 hPa in the last 10 years of simulations (2090-2099). **c**, the different between **b** and **a**. Data come from MPI_GE_CMIP6 forced by historical and SSP585 scenario.

BIBLIOGRAPHY

[1] Panos J Athanasiadis and Maarten HP Ambaum. "Linear contributions of different time scales to teleconnectivity." In: *Journal of Climate* 22.13 (2009), pp. 3720–3728.

[2] Anthony G Barnston and Robert E Livezey. "Classification, seasonality and persistence of low-frequency atmospheric circulation patterns." In: *Monthly weather review* 115.6 (1987), pp. 1083–1126.

[3] Maurice L Blackmon, YH Lee, and John M Wallace. "Horizontal structure of 500 mb height fluctuations with long, intermediate and short time scales." In: *Journal of Atmospheric Sciences* 41.6 (1984), pp. 961–980.

[4] Russell Blackport and James A Screen. "Weakened evidence for mid-latitude impacts of Arctic warming." In: *Nature Climate Change* 10.12 (2020), pp. 1065–1066.

[5] Ileana Bladé, Brant Liebmann, Didac Fortuny, and Geert Jan van Oldenborgh. "Observed and simulated impacts of the summer NAO in Europe: implications for projected drying in the Mediterranean region." In: *Climate dynamics* 39 (2012), pp. 709–727.

[6] Florian Börgel, Claudia Frauen, Thomas Neumann, and HE Markus Meier. "The Atlantic Multidecadal Oscillation controls the impact of the North Atlantic Oscillation on North European climate." In: *Environmental research letters* 15.10 (2020), p. 104025.

[7] Savin S Chand, Kevin JE Walsh, Suzana J Camargo, James P Kossin, Kevin J Tory, Michael F Wehner, Johnny CL Chan, Philip J Klotzbach, Andrew J Dowdy, Samuel S Bell, et al. "Declining tropical cyclone frequency under global warming." In: *Nature Climate Change* 12.7 (2022), pp. 655–661.

[8] Jule G Charney and John G DeVore. "Multiple flow equilibria in the atmosphere and blocking." In: *Journal of the atmospheric sciences* 36.7 (1979), pp. 1205–1216.

[9] Rei Chemke and Dim Coumou. "Human influence on the recent weakening of storm tracks in boreal summer." In: *npj Climate and Atmospheric Science* 7.1 (2024), p. 86.

[10] Bo Christiansen, Shuting Yang, and Dominic Matte. "The Forced Response and Decadal Predictability of the North Atlantic Oscillation: Nonstationary and Fragile Skills." In: *Journal of Climate* 35.18 (2022), pp. 5869–5882. DOI: 10.1175/JCLI-D-21-0807.1.

[11] Gilbert P Compo, Jeffrey S Whitaker, Prashant D Sardeshmukh, Nobuki Matsui, Robert J Allan, Xungang Yin, Byron E Gleason, Russell S Vose, Glenn Rutledge, Pierre Bessemoulin, et al. "The twentieth century reanalysis project." In: *Quarterly Journal of the Royal Meteorological Society* 137.654 (2011), pp. 1–28.

[12] Susanna Corti, Franco Molteni, and TN Palmer. "Signature of recent climate change in frequencies of natural atmospheric circulation regimes." In: *Nature* 398.6730 (1999), pp. 799–802.

[13] Dim Coumou, Jascha Lehmann, and Johanna Beckmann. "The weakening summer circulation in the Northern Hemisphere mid-latitudes." In: *Science* 348.6232 (2015), pp. 324–327.

[14] Eleonora Cusinato, Angelo Rubino, and Davide Zanchettin. "Winter Euro-Atlantic climate modes: Future scenarios from a CMIP6 multi-model ensemble." In: *Geophysical Research Letters* 48.19 (2021), e2021GL094532.

[15] Paolo Davini, Chiara Cagnazzo, Richard Neale, and Joe Tribbia. "Coupling between Greenland blocking and the North Atlantic Oscillation pattern." In: *Geophysical Research Letters* 39.14 (2012).

[16] Paolo Davini and Fabio D'Andrea. "Northern Hemisphere atmospheric blocking representation in global climate models: twenty years of improvements?" In: *Journal of Climate* 29.24 (2016), pp. 8823–8840.

[17] Paolo Davini and Fabio D'Andrea. "From CMIP3 to CMIP6: Northern Hemisphere Atmospheric Blocking Simulation in Present and Future Climate." In: *Journal of Climate* 33.23 (2020), pp. 10021–10038. DOI: 10.1175/JCLI-D-19-0862.1.

[18] Clara Deser, Flavio Lehner, Keith B Rodgers, Toby Ault, Thomas L Delworth, Pedro N DiNezio, Arlene Fiore, Claude Frankignoul, John C Fyfe, Daniel E Horton, et al. "Insights from Earth system model initial-condition large ensembles and future prospects." In: *Nature Climate Change* 10.4 (2020), pp. 277–286.

[19] Clara Deser and Adam S Phillips. "A range of outcomes: the combined effects of internal variability and anthropogenic forcing on regional climate trends over Europe." In: *Nonlinear Processes in Geophysics* 30.1 (2023), pp. 63–84.

[20] Clara Deser, Adam S Phillips, Michael A Alexander, and Brian V Smoliak. "Projecting North American climate over the next 50 years: Uncertainty due to internal variability." In: *Journal of Climate* 27.6 (2014), pp. 2271–2296.

[21] Clara Deser, Adam Phillips, Vincent Bourdette, and Haiyan Teng. "Uncertainty in climate change projections: the role of internal variability." In: *Climate dynamics* 38 (2012), pp. 527–546.

[22] Giorgia Di Capua, S Sparrow, Kai Kornhuber, Eftychia Rousi, S Osprey, D Wallom, B van den Hurk, and Dim Coumou. "Drivers behind the summer 2010 wave train leading to Russian heatwave and Pakistan flooding." In: *npj Climate and Atmospheric Science* 4.1 (2021), p. 55.

[23] Marie Drouard, Kai Kornhuber, and Tim Woollings. "Disentangling Dynamic Contributions to Summer 2018 Anomalous Weather Over Europe." In: *Geophysical Research Letters* 46.21 (2019), pp. 12537–12546. DOI: https://doi.org/10.1029/2019GL084601.

[24] Nick Dunstone, Doug M Smith, Steven C Hardiman, Leon Hermanson, Sarah Ineson, Gillian Kay, Chaofan Li, Julia F Lockwood, Adam A Scaife, Hazel Thornton, et al. "Skilful predictions of the Summer North Atlantic Oscillation." In: *Communications Earth & Environment* 4.1 (2023), p. 409.

[25] Nick Dunstone, Doug Smith, Adam Scaife, Leon Hermanson, Rosie Eade, Niall Robinson, Martin Andrews, and Jeff Knight. "Skilful predictions of the winter North Atlantic Oscillation one year ahead." In: *Nature Geoscience* 9.11 (2016), pp. 809–814.

[26] John G Dwyer and Paul A O'Gorman. "Moist formulations of the Eliassen–Palm flux and their connection to the surface westerlies." In: *Journal of the Atmospheric Sciences* 74.2 (2017), pp. 513–530.

[27] Chris K Folland, Jeff Knight, Hans W Linderholm, David Fereday, Sarah Ineson, and James W Hurrell. "The summer North Atlantic Oscillation: past, present, and future." In: *Journal of Climate* 22.5 (2009), pp. 1082–1103.

[28] Alex Hall. "Projecting regional change." In: *Science* 346.6216 (2014), pp. 1461–1462.

[29] Nicholas MJ Hall, Brian J Hoskins, Paul J Valdes, and Catherine A Senior. "Storm tracks in a high-resolution GCM with doubled carbon dioxide." In: *Quarterly Journal of the Royal Meteorological Society* 120.519 (1994), pp. 1209–1230.

[30] Edward Hanna, Thomas E Cropper, Richard J Hall, and John Cappelen. "Greenland Blocking Index 1851–2015: a regional climate change signal." In: *International Journal of Climatology* 36.15 (2016), pp. 4847–4861.

[31] Edward Hanna, Thomas E Cropper, Philip D Jones, Adam A Scaife, and Rob Allan. "Recent seasonal asymmetric changes in the NAO (a marked summer decline and increased winter variability) and associated changes in the AO and Greenland Blocking Index." In: *International Journal of Climatology* 35.9 (2015), pp. 2540–2554.

[32] Luke J Harrington, Kristie L Ebi, David J Frame, and Friederike EL Otto. "Integrating attribution with adaptation for unprecedented future heatwaves." In: *Climatic Change* 172.1 (2022), p. 2.

[33] Hans Hersbach, Bill Bell, Paul Berrisford, Shoji Hirahara, András Horányi, Joaquín Muñoz-Sabater, Julien Nicolas, Carole Peubey, Raluca Radu, Dinand Schepers, et al. "The ERA5 global reanalysis." In: *Quarterly journal of the royal meteorological society* 146.730 (2020), pp. 1999–2049.

[34] Daniel E Horton, Nathaniel C Johnson, Deepti Singh, Daniel L Swain, Bala Rajaratnam, and Noah S Diffenbaugh. "Contribution of changes in atmospheric circulation patterns to extreme temperature trends." In: *Nature* 522.7557 (2015), pp. 465–469.

[35] Brian J Hoskins and Paul J Valdes. "On the existence of storm-tracks." In: *Journal of Atmospheric Sciences* 47.15 (1990), pp. 1854–1864.

[36] James W Hurrell. "Decadal trends in the North Atlantic Oscillation: Regional temperatures and precipitation." In: *Science* 269.5224 (1995), pp. 676–679.

[37] IPCC. *Climate Change 2021: The Physical Science Basis. Contribution of Working Group I to the Sixth Assessment Report of the Intergovernmental Panel on Climate Change*. Ed. by V. Masson-Delmotte et al. Cambridge, UK and New York, NY, USA: Cambridge University Press, 2021. DOI: 10.1017/9781009157896.

[38] Ian N James and Ian N James. *Introduction to circulating atmospheres*. Cambridge University Press, 1995.

[39] Stephen Jeffrey, Leon Rotstayn, Mark Collier, Stacey Dravitzki, Carlo Hamalainen, Chris Moeseneder, Kenneth Wong, and Jozef Syktus. "Australia's CMIP5 submission usingthe CSIRO-Mk3. 6 model." In: *Australian Meteorological and Oceanographic Journal* 63.1 (2013), pp. 1–13.

[40] S Kaderli. *WaveBreaking-Detection, Classification and Tracking of Rossby Wave Breaking*. 2023.

[41] Jennifer E Kay, Clara Deser, A Phillips, A Mai, Cecile Hannay, Gary Strand, Julie Michelle Arblaster, SC Bates, Gokhan Danabasoglu, James Edwards, et al. "The Community Earth System Model (CESM) large ensemble project: A community resource for studying climate change in the presence of internal climate variability." In: *Bulletin of the American Meteorological Society* 96.8 (2015), pp. 1333–1349.

[42] Megan C Kirchmeier-Young, Francis W Zwiers, and Nathan P Gillett. "Attribution of extreme events in Arctic sea ice extent." In: *Journal of Climate* 30.2 (2017), pp. 553–571.

[43] Jeremy M Klavans, Mark A Cane, Amy C Clement, and Lisa N Murphy. "NAO predictability from external forcing in the late 20th century." In: *NPJ climate and atmospheric science* 4.1 (2021), p. 22.

[44] F Hugo Lambert and John CH Chiang. "Control of land-ocean temperature contrast by ocean heat uptake." In: *Geophysical research letters* 34.13 (2007).

[45] Simon H Lee, Paul D Williams, and Thomas HA Frame. "Increased shear in the North Atlantic upper-level jet stream over the past four decades." In: *Nature* 572.7771 (2019), pp. 639–642.

[46] Muyuan Li, Yao Yao, Ian Simmonds, Dehai Luo, Linhao Zhong, and Xiaodan Chen. "Collaborative impact of the NAO and atmospheric blocking on European heatwaves, with a focus on the hot summer of 2018." In: *Environmental Research Letters* 15.11 (2020), p. 114003.

[47] Varavut Limpasuvan and Dennis L Hartmann. "Wave-maintained annular modes of climate variability." In: *Journal of Climate* 13.24 (2000), pp. 4414–4429.

[48] Quan Liu, Jürgen Bader, Johann H Jungclaus, and Daniela Matei. "More extreme summertime North Atlantic Oscillation under climate change." In: *Communications Earth & Environment* 6.1 (2025), pp. 1–12.

[49] David J Lorenz and Eric T DeWeaver. "Tropopause height and zonal wind response to global warming in the IPCC scenario integrations." In: *Journal of Geophysical Research: Atmospheres* 112.D10 (2007).

[50] Dehai Luo, Tingting Gong, and Linhao Zhong. "Dynamical relationship between the phase of North Atlantic Oscillations and the meridional excursion of a preexisting jet: An analytical study." In: *Journal of the atmospheric sciences* 65.6 (2008), pp. 1838–1858.

[51] Nicola Maher, Sebastian Milinski, Laura Suarez-Gutierrez, Michael Botzet, Mikhail Dobrynin, Luis Kornblueh, Jürgen Kröger, Yohei Takano, Rohit Ghosh, Christopher Hedemann, et al. "The Max Planck Institute Grand Ensemble: enabling the exploration of climate system variability." In: *Journal of Advances in Modeling Earth Systems* 11.7 (2019), pp. 2050–2069.

[52] Christine M McKenna and AC Maycock. "Sources of uncertainty in multimodel large ensemble projections of the winter North Atlantic Oscillation." In: *Geophysical Research Letters* 48.14 (2021), e2021GL093258.

[53] Christine M McKenna and AC Maycock. "The role of the North Atlantic Oscillation for projections of winter mean precipitation in Europe." In: *Geophysical Research Letters* 49.19 (2022), e2022GL099083.

[54] Sebastian Milinski. "Internal variability in a changing climate: A large ensemble perspective on tropical Atlantic rainfall." PhD thesis. Universität Hamburg Hamburg, 2019.

[55] Ivan Mitevski, Simon H Lee, Gabriel Vecchi, Clara Orbe, and Lorenzo M Polvani. "More positive and less variable North Atlantic Oscillation at high CO2 forcing." In: *npj Climate and Atmospheric Science* 8.1 (2025), p. 171.

[56] Woosok Moon, Baek-Min Kim, Gun-Hwan Yang, and John S. Wettlaufer. "Wavier jet streams driven by zonally asymmetric surface thermal forcing." In: *Proceedings of the National Academy of Sciences* 119.38 (2022), e2200890119. DOI: 10.1073/pnas.2200890119.

[57] Ji Nie, Peng Wang, Wenchang Yang, and Benkui Tan. "Northern hemisphere storm tracks in strong AO anomaly winters." In: *Atmospheric Science Letters* 9.3 (2008), pp. 153–159.

[58] Yu Nie, Yang Zhang, Xiu-Qun Yang, and Gang Chen. "Baroclinic anomalies associated with the Southern Hemisphere Annular Mode: Roles of synoptic and low-frequency eddies." In: *Geophysical Research Letters* 40.10 (2013), pp. 2361–2366.

[59] Dirk Olonscheck, Laura Suarez-Gutierrez, Sebastian Milinski, Goratz Beobide-Arsuaga, Johanna Baehr, Friederike Fröb, Tatiana Ilyina, Christopher Kadow, Daniel Krieger, Hongmei Li, et al. "The new Max Planck Institute grand ensemble with CMIP6 forcing and high-frequency model output." In: *Journal of Advances in Modeling Earth Systems* 15.10 (2023), e2023MS003790.

[60] Isidoro Orlanski. "Bifurcation in eddy life cycles: Implications for storm track variability." In: *Journal of the atmospheric sciences* 60.8 (2003), pp. 993–1023.

[61] Albert Ossó, Ileana Bladé, Alexey Karpechko, Camille Li, Douglas Maraun, Olivia Romppainen-Martius, Len Shaffrey, Aiko Voigt, Tim Woollings, and Giuseppe Zappa. "Advancing Our Understanding of Eddy-driven Jet Stream Responses to Climate Change–A Roadmap." In: *Current Climate Change Reports* 11.1 (2024), p. 2.

[62] John P O'Brien and Clara Deser. "Quantifying and understanding forced changes to unforced modes of atmospheric circulation variability over the North Pacific in a coupled model large ensemble." In: *Journal of Climate* 36.1 (2023), pp. 19–37.

[63] Timothy N Palmer. "A nonlinear dynamical perspective on climate prediction." In: *Journal of Climate* 12.2 (1999), pp. 575–591.

[64] Joaquim G Pinto and Christoph C Raible. "Past and recent changes in the North Atlantic Oscillation." In: *Wiley Interdisciplinary Reviews: Climate Change* 3.1 (2012), pp. 79–90.

[65] Jonathon R Preece, Thomas L Mote, Judah Cohen, Lori J Wachowicz, John A Knox, Marco Tedesco, and Gabriel J Kooperman. "Summer atmospheric circulation over Greenland in response to Arctic amplification and diminished spring snow cover." In: *Nature Communications* 14.1 (2023), p. 3759.

[66] Liu Quan. *Decomposing North Atlantic Oscillation from Multi-Model Large Ensemble*. Zenodo. Version v1.0. May 2025. DOI: 10.5281/zenodo.15363374.

[67] G Rivière and Isidoro Orlanski. "Characteristics of the Atlantic storm-track eddy activity and its relation with the North Atlantic Oscillation." In: *Journal of the Atmospheric Sciences* 64.2 (2007), pp. 241–266.

[68] Walter A Robinson. "A baroclinic mechanism for the eddy feedback on the zonal index." In: *Journal of the Atmospheric Sciences* 57.3 (2000), pp. 415–422.

[69] Efi Rousi, Kai Kornhuber, Goratz Beobide-Arsuaga, Fei Luo, and Dim Coumou. "Accelerated western European heatwave trends linked to more-persistent double jets over Eurasia." In: *Nature communications* 13.1 (2022), p. 3851.

[70] Hans Egede Saabye and Georg Fries. *Greenland: Being Extracts from a Journal Kept in that Country in the Years 1770 to 1778*. London: Printed for Boosey and Sons, 1818.

[71] R Saravanan. "Atmospheric low-frequency variability and its relationship to midlatitude SST variability: Studies using the NCAR Climate System Model." In: *Journal of Climate* 11.6 (1998), pp. 1386–1404.

[72] AA Scaife, A Arribas, E Blockley, A Brookshaw, RT Clark, N Dunstone, R Eade, D Fereday, CK Folland, M Gordon, et al. "Skillful long-range prediction of European and North American winters." In: *Geophysical Research Letters* 41.7 (2014), pp. 2514–2519.

[73] Adam A Scaife, Chris K Folland, Lisa V Alexander, Anders Moberg, and Jeff R Knight. "European climate extremes and the North Atlantic Oscillation." In: *Journal of Climate* 21.1 (2008), pp. 72–83.

[74] Andrea Schneidereit, Silke Schubert, Pavel Vargin, Frank Lunkeit, Xiuhua Zhu, Dieter HW Peters, and Klaus Fraedrich. "Large-scale flow and the long-lasting blocking high over Russia: Summer 2010." In: *Monthly Weather Review* 140.9 (2012), pp. 2967–2981.

[75] Tiffany A Shaw, Julie M Arblaster, Thomas Birner, Amy H Butler, DIV Domeisen, Chaim I Garfinkel, Hella Garny, Kevin M Grise, and A Yu Karpechko. "Emerging climate change signals in atmospheric circulation." In: *AGU Advances* 5.6 (2024), e2024AV001297.

[76] Tiffany A Shaw and Osamu Miyawaki. "Fast upper-level jet stream winds get faster under climate change." In: *Nature Climate Change* 14.1 (2024), pp. 61–67.

[77] Tiffany A Shaw, Osamu Miyawaki, Hsing-Hung Chou, and Russell Blackport. "Fast-get-faster explains wavier upper-level jet stream under climate change." In: *Communications Earth & Environment* 5.1 (2024), p. 653.

[78] Tiffany A Shaw, Osamu Miyawaki, Hsing-Hung Chou, and Russell Blackport. "Fast-get-faster explains wavier upper-level jet stream under climate change." In: *Communications Earth & Environment* 5.1 (2024), p. 653.

[79] Tiffany A Shaw and Bjorn Stevens. "The other climate crisis." In: *Nature* 639.8056 (2025), pp. 877–887.

[80] Theodore G Shepherd. "Atmospheric circulation as a source of uncertainty in climate change projections." In: *Nature Geoscience* 7.10 (2014), pp. 703–708.

[81] Laura C Slivinski, Gilbert P Compo, Jeffrey S Whitaker, Prashant D Sardeshmukh, Benjamin S Giese, Chesley McColl, Rob Allan, Xungang Yin, Russell Vose, Holly Titchner, et al. "Towards a more reliable historical reanalysis: Improvements for version 3 of the Twentieth Century Reanalysis system." In: *Quarterly Journal of the Royal Meteorological Society* 145.724 (2019), pp. 2876–2908.

[82] Doug M Smith, Rosie Eade, MB Andrews, Holly Ayres, A Clark, S Chripko, Clara Deser, NJ Dunstone, Javier García-Serrano, Guillaume Gastineau, et al. "Robust but weak winter atmospheric circulation response to future Arctic sea ice loss." In: *Nature communications* 13.1 (2022), p. 727.

[83] Doug M Smith, Adam A Scaife, Rosie Eade, P Athanasiadis, Alessio Bellucci, I Bethke, R Bilbao, LF Borchert, L-P Caron, F Counillon, et al. "North Atlantic climate far more predictable than models imply." In: *Nature* 583.7818 (2020), pp. 796–800.

[84] Pedro M. Sousa, David Barriopedro, Alexandre M. Ramos, Ricardo García-Herrera, Fátima Espírito-Santo, and Ricardo M. Trigo. "Saharan air intrusions as a relevant mechanism for Iberian heatwaves: The record breaking events of August 2018 and June 2019." In: *Weather and Climate Extremes* 26 (2019), p. 100224. ISSN: 2212-0947.

[85] Laura Suarez-Gutierrez, Sebastian Milinski, and Nicola Maher. "Exploiting large ensembles for a better yet simpler climate model evaluation." In: *Climate Dynamics* 57.9-10 (2021), pp. 2557–2580.

[86] Lantao Sun, Michael Alexander, and Clara Deser. "Evolution of the global coupled climate response to Arctic sea ice loss during 1990–2090 and its contribution to climate change." In: *Journal of Climate* 31.19 (2018), pp. 7823–7843.

[87] Philip Sura. "Noise-induced transitions in a barotropic β-plane channel." In: *Journal of the atmospheric sciences* 59.1 (2002), pp. 97–110.

[88] Sakari M Uppala, PW Kållberg, Adrian J Simmons, U Andrae, V Da Costa Bechtold, M Fiorino, JK Gibson, J Haseler, A Hernandez, GA Kelly, et al. "The ERA-40 re-analysis." In: *Quarterly Journal of the Royal Meteorological Society: A journal of the atmospheric sciences, applied meteorology and physical oceanography* 131.612 (2005), pp. 2961–3012.

[89] Geoffrey K Vallis. *Atmospheric and oceanic fluid dynamics*. Cambridge University Press, 2017. ISBN: 9781107588417.

[90] Geoffrey K Vallis, Edwin P Gerber, Paul J Kushner, and Benjamin A Cash. "A mechanism and simple dynamical model of the North Atlantic Oscillation and annular modes." In: *Journal of the atmospheric sciences* 61.3 (2004), pp. 264–280.

[91] R Vautard, J Cattiaux, T Happé, J Singh, R Bonnet, C Cassou, D Coumou, F D'Andrea, Davide Faranda, E Fischer, et al. "Heat extremes in Western Europe are increasing faster than simulated due to missed atmospheric circulation trends." In: *Nature Communications* 14 (Oct. 2023), p. 6803. ISSN: 2041-1723.

[92] GT Walker and EW Bliss. "Memoirs of the royal meteorological society." In: *World weather V* 4 (1932), pp. 53–84.

[93] John M Wallace and David S Gutzler. "Teleconnections in the geopotential height field during the Northern Hemisphere winter." In: *Monthly weather review* 109.4 (1981), pp. 784–812.

[94] Heini Wernli and Michael Sprenger. "Identification and ERA-15 climatology of potential vorticity streamers and cutoffs near the extratropical tropopause." In: *Journal of the atmospheric sciences* 64.5 (2007), pp. 1569–1586.

[95] Tim Woollings, David Barriopedro, John Methven, Seok-Woo Son, Olivia Martius, Ben Harvey, Jana Sillmann, Anthony R Lupo, and Sonia Seneviratne. "Blocking and its response to climate change." In: *Current climate change reports* 4 (2018), pp. 287–300.

[96] Tim Woollings, Marie Drouard, Christopher H O'Reilly, David MH Sexton, and Carol McSweeney. "Trends in the atmospheric jet streams are emerging in observations and could be linked to tropical warming." In: *Communications Earth & Environment* 4.1 (2023), p. 125.

[97] Tim Woollings, Abdel Hannachi, and Brian Hoskins. "Variability of the North Atlantic eddy-driven jet stream." In: *Quarterly Journal of the Royal Meteorological Society* 136.649 (2010), pp. 856–868.

[98] Tim Woollings, Abdel Hannachi, Brian Hoskins, and Andrew Turner. "A regime view of the North Atlantic Oscillation and its response to anthropogenic forcing." In: *Journal of Climate* 23.6 (2010), pp. 1291–1307.

[99] Tim Woollings, Brian Hoskins, Mike Blackburn, and Paul Berrisford. "A new Rossby wave–breaking interpretation of the North Atlantic Oscillation." In: *Journal of the Atmospheric Sciences* 65.2 (2008), pp. 609–626.

[100] Shang-Ping Xie, Clara Deser, Gabriel A Vecchi, Matthew Collins, Thomas L Delworth, Alex Hall, Ed Hawkins, Nathaniel C Johnson, Christophe Cassou, Alessandra Giannini, et al. "Towards predictive understanding of regional climate change." In: *Nature Climate Change* 5.10 (2015), pp. 921–930.

[101] Ray Yamada and Olivier Pauluis. "Momentum balance and Eliassen–Palm flux on moist isentropic surfaces." In: *Journal of the Atmospheric Sciences* 73.3 (2016), pp. 1293–1314.

[102] Yang Zhang, Xiu-Qun Yang, Yu Nie, and Gang Chen. "Annular mode–like variation in a multilayer quasigeostrophic model." In: *Journal of the Atmospheric Sciences* 69.10 (2012), pp. 2940–2958.

ÜEBEREINSTIMMUNGSERKLÄRUNG | DECLARATION ON CONFORMITY

Ich versichere, dass dieses gebundene Exemplar der Dissertation und das in elektronischer Form eingereichte Dissertationsexemplar (über den Docata-Upload) sowohl das bei der Fakultät zur Archivierung eingereichte gedruckte gebundene Exemplar der Dissertationsschrift identisch sind.

I hereby confirm that this bound copy of the dissertation and the electronically submitted version (via the Docata upload) are identical to the printed bound copy of the dissertation submitted to the faculty for archiving.

Hamburg, August 2025

Quan Liu

EIDESSTATTLICHE VERSICHERUNG | DECLARATION ON OATH

Hiermit erkläre ich an Eides statt, dass ich die vorliegende Dissertationsschrift selbst verfasst und keine anderen als die angegebenen Quellen und Hilfsmittel benutzt habe. Sofern im Zuge der Erstellung der vorliegenden Dissertationsschrift generative Künstliche Intelligenz (gKI) basierte elektronische Hilfsmittel verwendet wurden, versichere ich, dass meine eigene Leistung im Vordergrund stand und dass eine vollständige Dokumentation aller verwendeten Hilfsmittel gemäß der Guten wissenschaftlichen Praxis vorliegt. Ich trage die Verantwortung für eventuell durch die gKI generierte fehlerhafte oder verzerrte Inhalte, fehlerhafte Referenzen, Verstöße gegen das Datenschutz- und Urheberrecht oder Plagiate.

Hamburg, August 2025

Quan Liu

Hinweis / Reference

Die gesamten Veröffentlichungen in der Publikationsreihe des MPI-M
„Berichte zur Erdsystemforschung / Reports on Earth System Science“,
ISSN 1614-1199

sind über die Internetseiten des Max-Planck-Instituts für Meteorologie erhältlich:
https://mpimet.mpg.de/forschung/publikationen

All the publications in the series of the MPI -M
„Berichte zur Erdsystemforschung / Reports on Earth System Science“,
ISSN 1614-1199

are available on the website of the Max Planck Institute for Meteorology:
https://mpimet.mpg.de/en/research/publications